Molecular Therapy
Original Article

Universal allogeneic CAR T cells engineered with *Sleeping Beauty* transposons and CRISPR-CAS9 for cancer immunotherapy

Jaitip Tipanee,[1] Ermira Samara-Kuko,[1] Thierry Gevaert,[3] Marinee K. Chuah,[1,2,4] and Thierry VandenDriessche[1,2,4]

[1]Department of Gene Therapy and Regenerative Medicine, Faculty of Medicine and Pharmacy, Vrije Universiteit Brussel, Building D, Room D365, Laarbeeklaan 103, 1090 Brussels, Belgium; [2]Center for Molecular and Vascular Biology, Department of Cardiovascular Sciences, University of Leuven, 3000 Leuven, Belgium; [3]Department of Radiotherapy, Oncology Centre University Hospital Brussels (Universitair Ziekenhuis (UZ) Brussel), Vrije Universiteit Brussel, Brussels, Belgium

Allogeneic CD19-specific chimeric antigen receptor (CAR) T cells with inactivated donor T cell receptor (TCR) expression can be used as an "off-the-shelf" therapeutic modality for lymphoid malignancies, thus offering an attractive alternative to autologous, patient-derived T cells. Current approaches for T cell engineering mainly rely on the use of viral vectors. Here, we optimized and validated a non-viral genetic modification platform based on *Sleeping Beauty* (SB) transposons delivered with minicircles to express CD19-28z.CAR and CRISPR-Cas9 ribonucleoparticles to inactivate allogeneic TCRs. Efficient TCR gene disruption was achieved with minimal cytotoxicity and with attainment of robust and stable CD19-28z.CAR expression. The CAR T cells were responsive to CD19+ tumor cells with antitumor activities that induced complete tumor remission in NALM6 tumor-bearing mice while significantly reducing TCR alloreactivity and GvHD development. Single CAR signaling induced the similar T cell signaling signatures in TCR-disrupted CAR T cells and control CAR T cells. In contrast, TCR disruption inhibited T cell signaling/protein phosphorylation compared with the control CAR T cells during dual CAR/TCR signaling. This non-viral SB transposon-CRISPR-Cas9 combination strategy serves as an alternative for generating next-generation CD19-specific CAR T while reducing GvHD risk and easing potential manufacturing constraints intrinsic to viral vectors.

INTRODUCTION

Chimeric antigen receptor (CAR) T cell adoptive immunotherapy has emerged as a promising therapeutic modality for lymphoid malignancies.[1,2] The US Food and Drug Administration and the European Medicines Agency have approved CAR T cell products for refractory cell precursor acute lymphoblastic leukemia and large B cell lymphoma.[3,4] Nevertheless, specific challenges hamper widespread use of CAR T cell therapy, including dependency on autologous patient-specific T cells and substantial inter-patient variability. Particularly for pediatric and heavily treated patients who previously received chemotherapies and/or stem cell transplantation, the resulting lymphopenic conditions may lead to inadequate T cell numbers, suboptimal CAR T cell functions, and unsuccessful CAR T cell production.[5–8] Although use of allogeneic CAR T cells could overcome some of the limitations of autologous, patient-specific CAR T cells,[9,10] allogeneic T cell transplantation triggers graft-versus-host disease (GvHD) because of HLA-mismatched α/β T cells.[11–15] Of note, depletion of α/β T cells alleviates GvHD effects,[16,17] and TCR ablation in T cells prevents GvHD in mice.[18–20]

Several strategies of endogenous TCR inactivation in allogeneic CAR T cells have been reported to augment the safety and efficacy of adoptive immunotherapy and minimize GvHD risk. The current approaches largely rely on the combination of clustered regularly interspaced short palindromic repeats (CRISPR)/CRISPR-associated protein 9 (Cas9) technology and viral vector transduction for TCR disruption and CAR expression in allogeneic T cells, respectively.[9,19,21,22] Despite the successes of CAR T cell manufacturing and therapeutic applications, there is an unmet need to overcome the limitations caused by viral vectors including complex large-scale manufacturing of viral vectors and rigorous biosafety testing to exclude the presence of replication-competent retroviruses.[23–26] As an alternative for gene delivery, the use of transposons offers a number of distinct advantages over viral vector-based approaches, including larger cargo capacity to deliver multiple transgenes, reliance on cost-effective non-viral transfection strategies and their relatively random integration profiles compared with the biased integration pattern of integrating viral vectors.[27–33] These advantages could greatly facilitate vector manufacturing and simplify regulatory approval on the path to clinical translation.[34] Nevertheless, to our knowledge, combining transposons with CRISPR-Cas9 technologies

Received 2 January 2022; accepted 7 June 2022;
https://doi.org/10.1016/j.ymthe.2022.06.006.

[4]Co-senior author

Correspondence: Thierry VandenDriessche, Department of Gene Therapy & Regenerative Medicine, Faculty of Medicine & Pharmacy, Vrije Universiteit Brussel (VUB), Building D, Room D365, Laarbeeklaan 103, B-1090 Brussels, Belgium.
E-mail: thierry.vandendriessche@vub.be
Correspondence: Marinee K. Chuah, Department of Gene Therapy & Regenerative Medicine, Faculty of Medicine and Pharmacy, Vrije Universiteit Brussel (VUB), Building D, Room D365, Laarbeeklaan 103, B-1090 Brussels, Belgium.
E-mail: marinee.chuah@vub.be

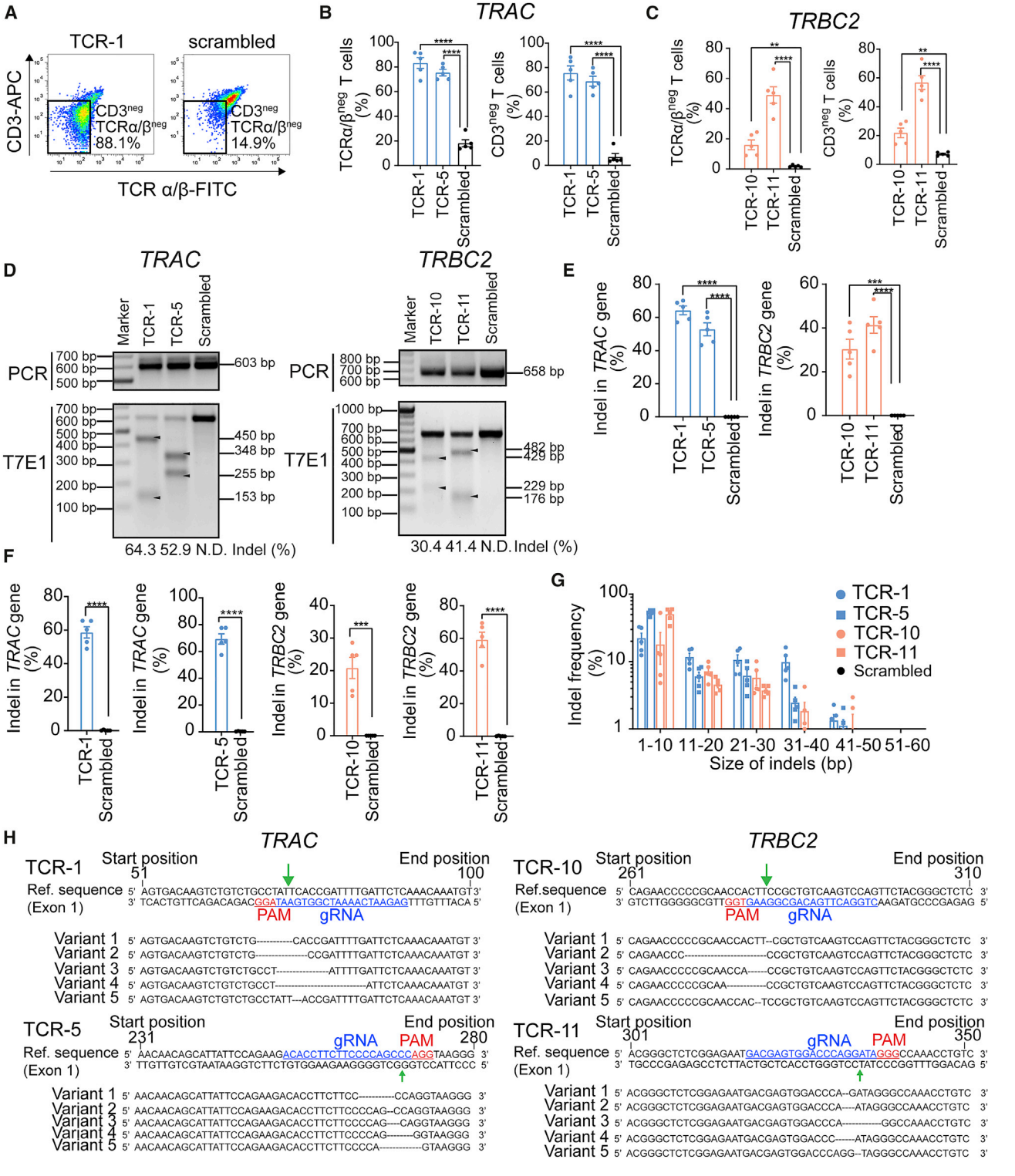

Figure 1. CRISIPR-Cas9-mediated single-gene KO in human CD8+ T cells using RNP particles

After 48 h post-CD3/CD28 stimulation, 5×10^5 human CD8+ T cells were subjected to nucleofection of 70 pmol *TRAC*- or *TRBC2*-targeting RNP particles (Cas9:sgRNA ratio of 1:1). (A) Schematic representation of TCRα/β and CD3 coexpression in *TRAC*-targeting TCR-1 (left) or scrambled control (right) RNP-transfected cells. (B) Percentages of TCRα/β^{neg} (left) and $CD3^{neg}$ (right) T cell population by flow cytometry after 48 h post-*TRAC*-targeting RNP nucleofection. (C) Percentages of TCRα/β^{neg} (left) and $CD3^{neg}$

(legend continued on next page)

for the manufacturing of allogeneic TCR knockout (TCR KO) CAR T cells has not yet been explored.[35]

Here, we describe the optimization and validation of non-viral system based on (1) *Sleeping Beauty* (SB) transposon[31,36]-mediated expression of CD19-targeted CAR and (2) targeted inactivation of endogenous TCR genes using CRISPR-Cas9-ribonucleoparticles (RNPs) for engineering human "off-the-shelf" CAR T cell devoid of endogenous TCR. The resulting CAR T cells are highly functional against CD19-expressing target cells and CD19+ tumor-bearing mice for tumor eradication with reduced TCR alloreactivity and GvHD development. Moreover, a comprehensive molecular analysis was performed to examine the downstream signaling effects in the TCR-disrupted CAR T cells.

RESULTS

CRISPR-Cas9 RNP for single- and dual-gene disruption in human T cells

We first screened different single-guide RNAs (sgRNAs) specifically designed to target the *TRAC* and *TRBC2* genes in the HEK293 cell line using a T7 endonuclease 1 assay (Tables S1 and S2). *TRAC* and *TRBC2* gene disruption was readily detectable in most TCR-targeted guide RNA (gRNA) groups (4/5 *TRAC*-targeting sgRNAs; 6/6 *TRBC2*-targeting sgRNAs) (Figure S1). The indel percentages of TCR-1 and TCR-5 gRNAs targeting the *TRAC* gene and TCR-8, TCR-9, TCR-10, and TCR-11 gRNAs targeting *TRBC2* gene were higher compared with those achieved using the other gRNAs (Figures S1C–S1D). We therefore selected the TCR-1, TCR-5, TCR-8, TCR-9, TCR-10, and TCR-11 gRNAs for subsequent TCR disruption in human CD8+ T cells.

CRISPR-Cas9 RNP complexes composed of TCR-targeting gRNA and purified Cas9 protein (TCR RNP) were nucleofected into T cells. *TRAC*-targeting TCR-1 and TCR-5 RNPs led to ~80% TCR-negative (TCR^{neg}) T cells (Figures 1A and 1B). *TRBC2*-targeting TCR-10 and TCR-11 RNPs unexpectedly outperformed TCR-8 and TCR-9 (in contrast to the results obtained in HEK293 cells) and resulted in ~20%–50% TCR^{neg} T cells for TCR-10/TCR-11 as opposed to 15%–38% for TCR-8/TCR-9 (Figures 1C and S2A). Loss of TCR expression after TCR disruption is consistent with a significant increase in CD3-negative ($CD3^{neg}$) T cells (Figures 1A–1C). TCR downregulation impairs TCR/CD3 complex formation, which in turn results in decreased CD3 expression.[37] The loss of TCR expression following TCR RNP delivery correlated with 50%–70% and ~30%–40% indel percentages in *TRAC* and *TRBC2* genes, respectively (Figures 1D, 1E, S2C, and S2D). Deep sequencing confirmed on-target TCR disruption, corresponding to 60%–70% and 20%–60% for *TRAC* and *TRBC2* targeting, respectively (Figure 1F). Most indels ranged from 1 to 10 nucleotides (Figures 1G and 1H), resulting in frameshift variants and in-frame deletions (Table S3). Overall cell viability was comparable among all conditions, indicating that TCR disruption after CRISPR-Cas9 RNP transfection did not lead to any discernable cytotoxicity (Figure S3).

To broaden the versatility of the approach, we investigated whether the CRISPR-Cas9 RNP platform allows for efficient simultaneous disruption of multiple target genes in human CD8+ T cells. Simultaneous targeting of both the *TRAC* and *TRBC2* loci did not significantly increase the percentages of TCR^{neg} or $CD3^{neg}$ T cells compared with using only a single TCR-11 RNP (Figure S4). Based on this finding, we used a single TCR-specific gRNA (TCR-1-targeting *TRAC*) for TCR gene inactivation in subsequent experiments.

Non-viral transfection of a transgene of interest in the TCR^{neg} cells

We subsequently optimized the platform to efficiently deliver any transgene of interest in the CRISPR-Cas9-modified TCR/$CD3^{neg}$ T cells. The commercially available pmaxGFP plasmid was selected for the platform optimization owing to its robust GFP reporter expression in a broad range of cells, including T cells, and its availability for instant use. The use of pmaxGFP described in previous studies highlights its convenience for platform optimization and serves as a benchmark to compare study outcomes by using the same standardized vector design and reporter gene.[38–41] The first strategy was based on a single co-transfection of CRISPR-Cas9 RNP and a GFP reporter plasmid (pmaxGFP) (Figure S5A, upper), which led to only ~8.3% ± 2.27% GFP+$CD3^{neg}$ T cells in the pmaxGFP/TCR-1 RNP-transfected group (Figure S5B, left). The total percentage of $CD3^{neg}$ T cells was not significantly different between the pmaxGFP/TCR-1 RNP-treated groups and TCR-1 RNP controls, suggesting that pmaxGFP co-transfection did not interfere with the efficiency of TCR-1 RNP-mediated gene disruption (Figure S5C, left). In contrast, the total GFP+ fraction in the pmaxGFP/scrambled RNP group was 5.4-fold greater than in the pmaxGFP/TCR-1 RNP group (Figure S5D, left), indicating that the TCR CRISPR-Cas9 components attenuated the efficacy of GFP transfection and/or expression during nucleofection.

Since the major difference between the TCR-1 and the scrambled gRNA is the targeting sequence (TCR-targeting versus non-targeting sequences), we tested the hypothesis of whether it is restricted to TCR-targeting gRNA or whether it represents a more general phenomenon, irrespective of the gRNA and its target sequence. Therefore, an

(right) T cell population by flow cytometry analysis 48 h post-nucleofection with *TRBC2* RNP. (D) Schematic representatives of indel mutation detected by T7 endonuclease 1 (T7E1) assay after 48 h of *TRAC*-targeting (left) or *TRBC2*-targeting (right) RNP nucleofection. The indel percentage values are the averages of five biologically independent donors. (E) Quantitative analysis of indel mutation percentage in *TRAC* (left) and *TRBC2* (right) genes detected by T7E1 assay after 48 h post-nucleofection. (F) Quantitative analysis of indel mutation percentage in *TRAC* and *TRBC2* genes detected by deep sequencing analysis after 48 h post-RNP nucleofection. (G) Indel mutation frequency relative to the size of indels in *TRAC* and *TRBC2* genes detected by deep sequencing analysis after 48 h post-nucleofection. Data are representative of five biologically independent donors. (H) Schematic representation of mutated DNA sequences in *TRAC* (left) and *TRBC2* (right) after TCR-targeting RNP nucleofection. Data are shown as means ± SEM (n = 5 biologically independent donors); Student's t test: $^{**}p < 0.01$, $^{***}p < 0.001$, $^{****}p < 0.0001$.

additional experiment was carried out by co-transfection of (1) 70 pmol *TRAC*-targeting TCR-1, programmed cell death protein 1 (PD1)-targeting PD1-5 (i.e., the PD1 KO activity was experimentally validated previously; representing a gene-targeting gRNA that is not relevant to TCR KO), or non-targeting scramble RNP (gRNA:Cas9 = 1:1), and (2) 500 ng of pmaxGFP into human T cells (Figures S6A–S6C). Forty-eight hours post-transfection, both PD1/pmaxGFP- and TCR/pmaxGFP-transfected cells revealed a pronounced decrease in total GFP+ population compared with the scrambled control/pmaxGFP group (Figures S6A and S6C). This indicates that the reduction of GFP transfection efficiency is not restricted to TCR targeting per se but may represent a more general phenomenon associated with CRISPR-Cas9-mediated gene targeting, irrespective of the gRNA and its target sequence. The exact reason is not clear and beyond the scope of this study but may be related to the cellular response following induction of dsDNA breaks.[42]

Then we investigated whether the Cas9 dosage titration can improve the GFP transfection efficiency while maintaining a relatively robust TCR KO efficiency (Figure S6D). Our result showed that a reduction of Cas9 to 35 and 17.5 pmol during a single nucleofection enhanced the total GFP+ population to ∼60% (Figure S6D, circular orange line) but inevitably compromised ∼20% of TCR gene disruption (Figure S6D, squared blue line).

The second strategy was based on sequential delivery of CRISPR-Cas9 RNP and pmaxGFP (24 h later) to generate GFP+TCR/CD3^{neg} T cells (Figure S5A, middle). This approach yielded 53.7% ± 5.49% GFP+CD3^{neg} T cells in the pmaxGFP/TCR-1 RNP-transfected group, which was 7.8-fold higher compared with the pmaxGFP/scrambled RNP-transfected group (Figure S5B, middle). Similar levels of total CD3^{neg} T cells (Figure S5C, middle) and total GFP+ T cells (Figure S5D, middle) were observed between the TCR-1 RNP/pmaxGFP and control groups. This pattern suggests that pmaxGFP transfection did not interfere with the efficiency of TCR-1 RNP-mediated gene disruption and vice versa.

To further increase the overall yield of GFP+TCR/CD3^{neg} T cell production, CD3^{neg} cells were specifically enriched by CD3+ T cell depletion using magnetic activated cell sorting (MACS) in TCR-1 RNP-transfected T cells before pmaxGFP transfection (Figure S5A, lower). Up to 80% GFP+CD3^{neg} T cells could be obtained following pmaxGFP/TCR-1 RNP transfection (Figure S5B, right). We also consistently observed equivalent percentages of total CD3+ T cells and GFP+ T cells between TCR-1 RNP/pmaxGFP and the corresponding control groups (Figures S5C, right and S5D, right). Depletion of CD3+ T cells led to a ∼1.5-fold increase in GFP+TCR/CD3^{neg} T cell purity compared with sequential transfection of the bulk heterogeneous CD3+/CD3^{neg} T cell population (Figures S5E and S5F). The overall transfection efficiency of pmaxGFP was unexpectedly enhanced ∼1.5-fold after CD3^{neg} enrichment (Figure S5G). Despite the comparable cell viability (Figure S7), a gradual decrease in total GFP+CD3^{neg} T cell numbers after CD3+ T cell depletion was apparent, indicating a loss of cells during cell processing (Figure S5H).

Rapid production of TCR KO CAR T cells targeting CD19 antigen for transient CAR expression

We employed the optimized sequential transfection approach to generate CD19-specific CAR T cells devoid of TCR expression (CD19-28z.CAR/TCR KO). For this purpose, we replaced the pmaxGFP plasmid with a minicircle (mc) DNA encoding a CD19-specific CAR fused to a GFP reporter gene via a T2A self-cleaving peptide, under the control of the hybrid elongation factor 1/human T cell leukemia virus promoter. The resulting mc plasmid, which was devoid of bacterial backbone DNA, was designated as mcCD19-28z.CAR (Figure 2A). The main advantages of mcDNA are its superior transfection efficiency and amelioration of the cellular toxicity caused by the bacterial backbone in conventional plasmids.[43] Due to the differences in DNA size, vector design, and/or promoter strength when comparing mcCD19-28z.CAR vector with pmaxGFP, a dose-dependent transfection study was therefore carried out to assess the optimal DNA amount of the mcCD19-28z.CAR vector for achieving high transfection efficiency (Figure S8A). The results showed that, to obtain similar transfection efficiencies as pmaxGFP (i.e., ∼60%), the mcCD19-28z.CAR vector required a 2-fold higher DNA dose compared with the amount of pmaxGFP plasmid used (i.e., 1 μg mcCD19-28z.CAR versus 500 ng pmaxGFP; Figure S8A, orange line). We therefore selected the dose of 1 μg mcCD19-28z.CAR vector per 5×10^5 T cells for CAR T cell manufacturing in the subsequent experiments. As expected, CAR expression correlated directly with GFP (Figure S8B), supporting use of GFP as a surrogate marker for CAR expression in the subsequent experiments.

Consistent with our result obtained from the platform optimization experiment using pmaxGFP plasmid (Figures S5B–S5D, left), the single nucleofection of mcCD19-28z.CAR/TCR-1 RNP components is relatively inefficient to generate the CD19-28z.CAR/TCR KO T cells (Figures S9A–S9C). This justifies the use of sequential nucleofection platform for robust CAR/TCR KO production in the subsequent experiments (Figure 2B). Sequential transfection of T cells with TCR-1 or scrambled control RNP followed by mcCD19-28z.CAR resulted in ∼60%–70% of the target cell population (i.e., CAR+CD3^{neg} population for mcCD19-28z.CAR/TCR-1 transfection; CAR+CD3+ population for mcCD19-28z.CAR/scrambled control transfection) (Figures 2C and 2D, left) and comparable amounts of total CAR T cells (both CD3^{neg} and CD3+) (Figure 2D, middle). Similar percentages of total CD3^{neg} T cells were obtained from the mcCD19-28z.CAR/TCR-1 RNP and mock/TCR-1 RNP control transfection, suggesting that TCR disruption was unaffected by mcCD19-28z.CAR DNA transfection (Figure 2D, right). Interestingly, in the CD19-28z.CAR/TCR KO T cells, which are mostly CD3^{neg}, the percentage of CAR expression gated in the CD3^{neg} fraction was significantly higher than that in the CD3+ fraction (Figure S9D). Conversely, in the CD19-28z.CAR/scrambled control T cells, which are predominately CD3+, a significant increase in CAR expression was observed in the CD3+ fraction compared with the CD3^{neg} fraction (Figure S9D). CAR T cells consisted mainly of the stem cell-like memory (Tscm) (CD45RA+CD45RO+/^{neg}CD62L+CD95+) subset, and less central memory (CD45RO+CD62L+CD95+), effector

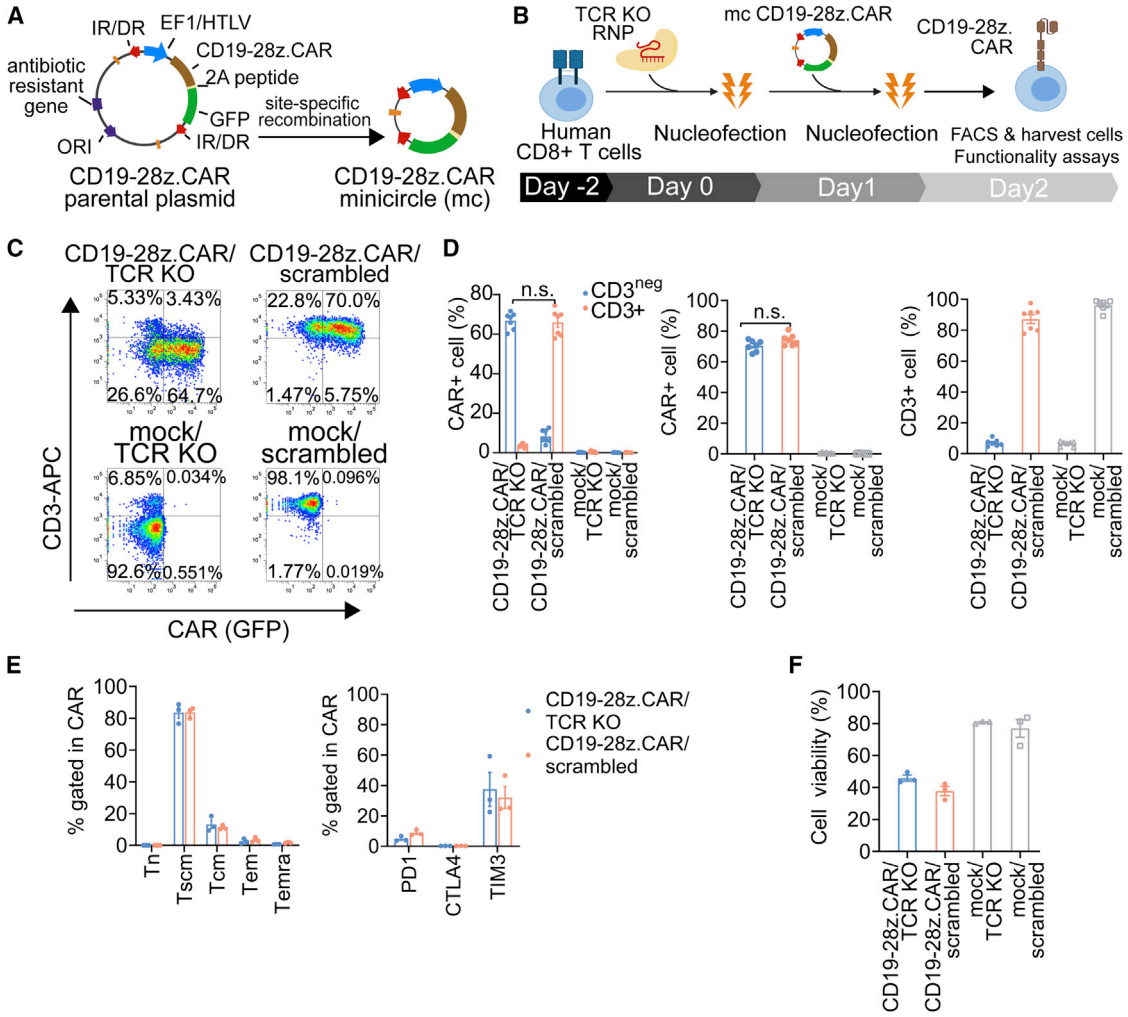

Figure 2. Production and characterization of CD19-specific CAR/TCR KO T cells using the non-viral CRISPR-Cas9 RNP-mc vector platform for transient CAR expression

(A) Schematic representation of the mcDNA vector generated from the parental plasmid via site-specific recombination, which further removed the bacterial backbone and minimized the overall vector size. Specifically, the mcCD19-28z.CAR vector contains a single multicistronic construct under the regulation of elongation factor 1 alpha-HTLV (EF1/HTLV). The CD19-28z.CAR and GFP reporter genes are linked via a self-cleavable 2A peptide. The expression cassette is flanked with IR/DR inverted repeats. (B) Schematic representation of the CAR T cell production method: 5×10^5 stimulated human CD8+ T cells were subjected to nucleofection of 70 pmol of TCR-1 RNP. Twenty-four hours later, the cells were electroporated with 1 μg of mcCD19-28z.CAR. Next day, the cells were harvested for flow cytometry analysis and functionality tests. (C) Schematic flow cytometric plot. (D) Percentages of (left) fractioned CAR/$CD3^{neg}$ and CAR/CD3+ cells, (middle) total CAR+ cells, and (right) total CD3+ cells in CD19-28z.CAR/TCR KO, CD19-28z.CAR/scrambled control, mock/TCR KO, and mock/scrambled control T cells analyzed by flow cytometry at 24 h post-transfection. (E) Immunophenotyping analysis of (left) T cell memory markers and (right) PD1, CTLA4, and TIM3 immune checkpoint markers in CD19-28z.CAR/TCR KO and CD19-28z.CAR/scrambled control T cells at 24 h post-transfection. (F) Cell viability of CD19-28z.CAR/TCR KO, CD19-28z.CAR/scrambled control, mock/TCR KO, and mock/scrambled control T cells at 24 h after production. Data are shown as means ± SEM (n = 3–6 biologically independent donors); Student's t test; n.s., not significant.

memory (Tem) (CD45RO+CD62L^{neg}CD95+), and terminally differentiated effector (CD45RA+CD62L^{neg}CD95+) subsets (Figure 2E, left). In both CD19-28z.CAR/TCR KO and CD19-28z.CAR/scrambled control T cells, expression of PD1 and CTLA4 was barely discernible, whereas TIM3 expression was moderate (Figure 2E, right). Cell viability declined to 32.3%–49.6% in the CD19-28z.CAR/TCR KO and CD19-28z.CAR/scrambled groups, consistent with DNA-induced toxicity (Figure 2F).

Transiently expressed CD19-28z.CAR/TCR KO T cells with antitumor functions *in vitro*

To characterize the functionality of CD19-28z.CAR/TCR KO and CD19-28z.CAR/scrambled T cells, we assessed their upregulation of the CD107a degranulation marker, oncolytic effect, and cytokine secretion pattern (Figure 3A). After a short incubation with CD19-expressing K562-CD19t, Raji, and NALM6 tumor cells (Figure S10), CD107a expression markedly increased in the CD19-28z.CAR/TCR

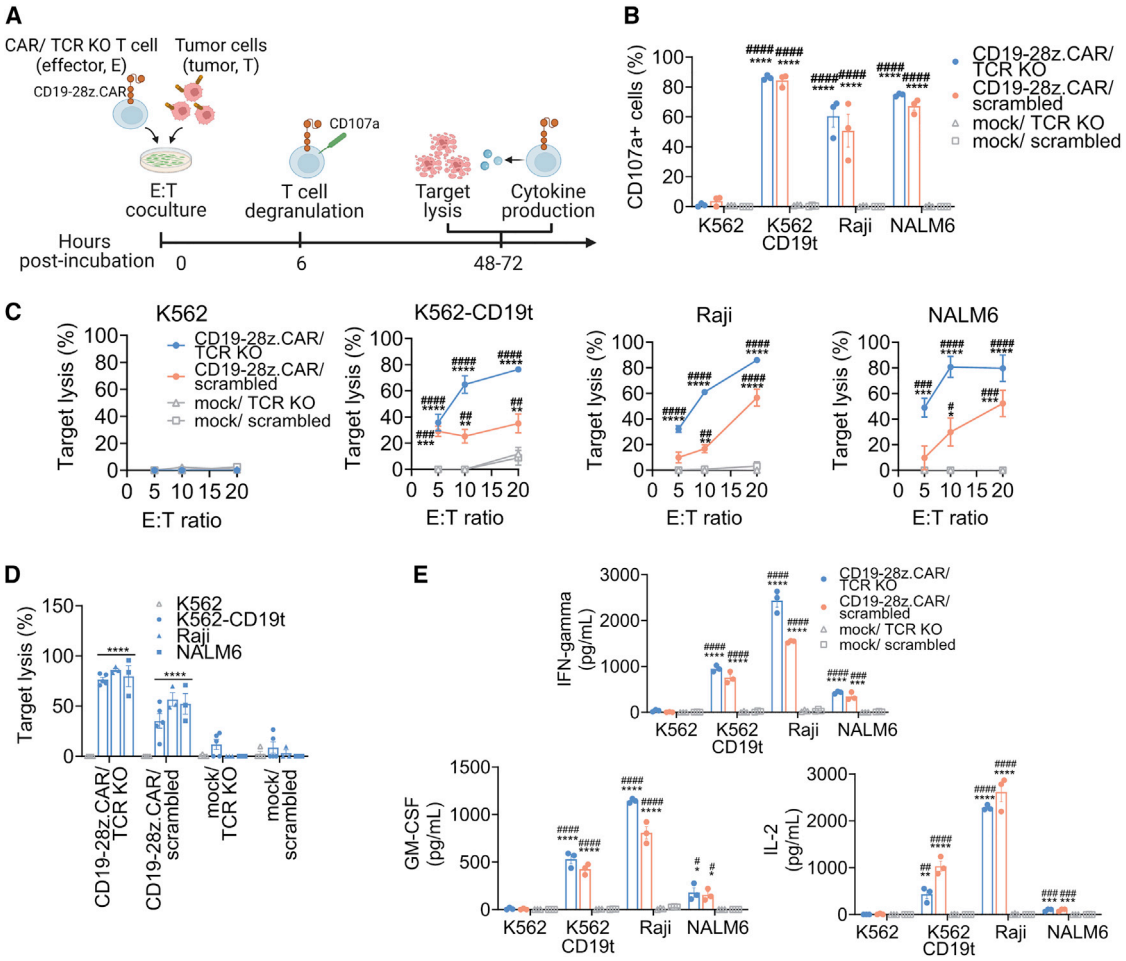

Figure 3. Transiently expressed CD19-redirected CAR/TCR KO T cells demonstrated a potent antitumor effect in response to CD19 antigen

(A) Schematic representation of experimental design. CD19-CAR/TCR KO, CD19-CAR/scrambled, mock/TCR KO, or mock/scrambled T cells were cocultured with CD19+ tumor cells (i.e., K562-CD19t, Raji, or NALM6) or CD19^{neg} tumor cells (i.e., K562) at specific effector:tumor cell ratios based on the assays for 6–72 h and were subjected for subsequent analyses. (B) Percentage of CD107a+ cells upon 6 h of incubation with CD19+ and control tumor cells (*compared with mock/TCR KO group; #compared with mock/scrambled control group). (C) Effector dose-response-specific lysis of effector cells (*compared with mock/TCR KO group; #compared with mock/scrambled control group). (D) Comparison of specific lysis of effector cells between incubation with CD19+ and K562 control tumor cells (*compared with K562 control cells). (E) Secretion of human IFN-γ, GM-CSF, and IL-2 cytokines from effector cells in response to target tumor cells (*compared with mock/TCR KO group; #compared with mock/scrambled control group) after 72 h post-coculture. Data are shown as means ± SEM (n = 3 biologically independent donors); one-way ANOVA with Dunnett's post hoc; n.s., not significant; */#p < 0.05, **/##p < 0.01, ***/###p < 0.001, ****/####p < 0.0001.

KO and CD19-28z.CAR/scrambled groups compared with K562 control tumor cells (Figures 3B, S11A, and S11B). In contrast, CD107a expression was similar among all mock/TCR KO and mock/scrambled groups (Figures 3B, S11A, and S11B). Both CD19-28z.CAR/TCR KO and CD19-28z.CAR/scrambled CAR T cells effectively eliminated CD19+ tumor cells in an effector cell dose-dependent fashion (Figure 3C). Prolonged incubation to 72 h led to a 30%–60% increase in tumor lysis (Figure S11C). CD19-negative K562 control cells were resistant to the cytolytic effects of the CD19-28z.CAR/TCR KO or CD19-28z.CAR/scrambled T cells, indicating that the tumor lysis was CD19 antigen specific (Figure 3D). Concordantly, co-incubation with CD19+ tumor cells increased cytokine production (interferon γ [IFN-γ], granulocyte-macrophage colony-stimulating factor [GM-CSF], and interleukin-2 [IL-2]) in CD19-28z.CAR/TCR KO and CD19-28z.CAR/scrambled CAR T (Figure 3E).

SB-mediated manufacture of CD19-specific CAR/TCR KO T cells for stable CAR expression

We next adapted our method to generate CD19-28z.CAR/TCR KO T cells stably expressing CAR using the SB transposon system. The mcDNA vectors mc-CD19-28z.CAR and mcSB100x harboring hyperactive SB100x transposase were co-transfected into CD8+ T cells initially transfected with TCR-1 or with scrambled RNPs as control (Figures 4A and 4B). The resulting transfected cells (designated as

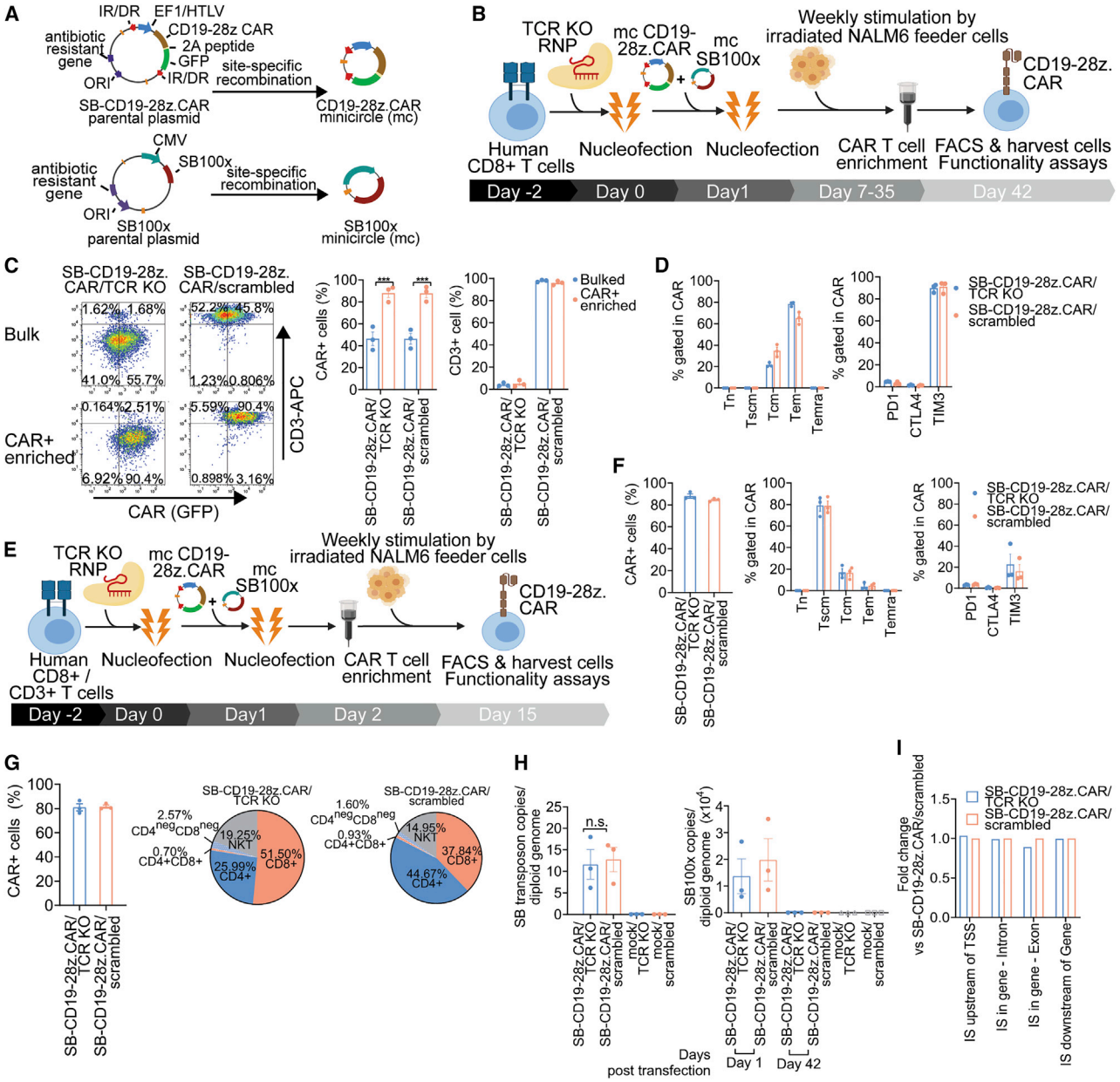

Figure 4. Production and characterization of CD19-specific CAR/TCR KO T cells using the non-viral CRISPR-Cas9 RNP-mcSB transposon platform for sustained CAR expression

(A) Schematic representation of the mcDNA vector generated from the parental plasmid via site-specific recombination, which further removed the bacterial backbone and minimized the overall vector size. The production of mcCD19-28z.CAR vector was described previously (Figure 2A).The mcSB100x vector harbors the gene encoding hyperactive SB100x transposase to modulate SB transposition driven by the cytomegalovirus (CMV) promotor. (B) Schematic representation of CAR T cell production approach without early CAR enrichment: 5×10^5 stimulated human CD8+ T cells were subjected to nucleofection of 70 pmol of TCR-1 RNP. Twenty-four hours later, the cells were transfected with 1 μg of mcCD19-28z.CAR and 0.5 μg of mcSB100x. Subsequently, the CD19-specific CAR T cells were selectively expanded by weekly addition of 100-Gy-irradiated NALM6 feeder cells. Recombinant IL-2, IL-7, and IL-15 cytokines were supplemented to the culture on a Monday/Wednesday/Friday schedule. On week 6 post-culture, the CAR+ T cells were enriched using the MACS method by incubating the cells with APC-conjugated recombinant human CD19 protein and magnetic bead-conjugated anti-APC antibody. The enriched CAR+ cells were rested in complete T cell medium and harvested for flow cytometry analysis and functionality tests. (C) (Left) Schematic flow cytometric plot, (middle) total CAR+ cell percentage, and (right) total CD3+ cell percentage of CAR T cells before and after CAR+ enrichment by MACS. (D) Immunophenotyping analysis of (left) T cell memory markers and (right) PD1, CTLA4, and TIM3 immune checkpoint markers of SB-CD19-28z.CAR/TCR KO and SB-CD19-28z.CAR/scrambled control T cells at 6 weeks post-culture. Data are shown as means ± SEM (n = 3 biologically independent donors); Student's t test; ***$p < 0.001$. (E) Schematic representation of CAR T cell production approach with early CAR enrichment: 5×10^5 stimulated human CD8+ or CD3+ T cells were subjected to nucleofection

(legend continued on next page)

SB-CD19-28z.CAR/TCR KO and SB-CD19-28z.CAR/scrambled) were then expanded using irradiated NALM6 feeder cells in the presence of human IL-2, IL-7, IL-15, and IL-21. After 6 weeks of expansion, CAR T cells were enriched by MACS (Figure 4B). This approach resulted in a ~10% weekly increase in the CAR+ T cell fraction (Figure S12B, left). An average 94- ± 28-fold expansion of CAR T cells in the bulk SB-CD19-28z.CAR/TCR KO and SB-CD19-28z.CAR/scrambled control T cell populations was observed at the end of expansion protocol (Figure S12B, right). Following selective expansion of CAR T cells and CAR enrichment with MACS, up to 89.7% and 90.6% of the SB-CD19-28z.CAR/TCR KO and SB-CD19-28z.CAR/scrambled groups expressed CAR (Figure 4C, left and middle). The SB-CD19-28z.CAR/TCR KO T cells exhibited only very low TCR expression levels compared with the SB-CD19-28z.CAR/scrambled T cells (Figure 4C, right), consistent with efficient TCR disruption in the CAR T cells. Similar results were obtained in the CAR-enriched and bulk CAR T cell populations (Figure 4C, right). Both the SB-CD19-28z.CAR/TCR KO and SB-CD19-28z.CAR/scrambled T cells predominately displayed the Tem phenotype (Figure 4D, left). PD1 and CTLA4 expression was barely detectable, whereas relatively high TIM 3 expression was observed in both effector cells (Figure 4D, right). Hence, the prolonged culture duration led to a more differentiated memory T cell phenotype and elevated TIM3 expression. To limit the cell expansion period, an early CAR+ T cell enrichment step was implemented at 24 h post-transfection. Subsequently, only the CAR+ T cell fraction was subjected to cell expansion for 14 days (Figure 4E). This was expected to delay terminal T cell differentiation and exhaustion caused by repeated NALM6 stimulation while attaining a high purity of CAR T cell production. Notably, using this method, an average of 88.1% ± 3.34% and 84.6% ± 1.42% of CAR expression was achieved after 14 days culture in SB-CD19-28z.CAR/TCR KO and SB-CD19-28z.CAR/scrambled cells, respectively (Figure 4F, left). The extent of the T cell expansion was comparable in both conditions (Figure S12C). In contrast to the previous approach based on the 6-week culture protocol, the phenotypes of these CAR T cells were mainly Tscm, and the percentage of the Tem subset was reduced (Figure 4F, middle). In addition to minimal PD1 and CTLA4 expression, the current method also decreased TIM3 expression by ~70% compared with the 6-week culture protocol (Figure 4F, right). Similar results were obtained from CD19 CAR T cells generated from human CD3+ T cells (Figures 4G and S12D–S12F). Notably, the expansion of CAR T cells obtained from CD3+ T cells was significantly higher compared with CAR T cells produced from purified CD8+ T cells (Figure S12F). SB-CD19-28z.CAR/TCR KO cells showed a slight difference with respect to CD8+ and CD4+ composition compared with SB-CD19-28z.CAR/scrambled cells, whereas the distribution of other T cell subsets was comparable among the groups (Figure 4G, right). Analysis of genomic DNA from SB-CD19-28z.CAR/TCR KO and SB-CD19-28z.CAR/scrambled cells (Table S4) indicated similar SB transposon copies (Figure 4H, left) and gradual loss of the transposase-encoding SB100x plasmid toward the end of the culture (Figure 4H, right). This disappearance of the transposase-encoding plasmid is a built-in self-limiting safety feature preventing continuous transposition in the transfected T cells.

The method of CAR T cell manufacturing described in our study is based on sequential electroporation of *TRAC*-targeted CRISPR RNP for TCR ablation and SB transposon/transposase DNA for CAR expression. Since the time interval between the CRISPR-mediated gene targeting and the SB transposon transfection is ~24 h, we agree with the reviewer that it cannot be excluded *a priori* that CRISPR-Cas9 activity may alter the overall SB transposon integration pattern. Moreover, CRISPR-Cas9-mediated double-stranded DNA breaks at *TRAC* loci (*TRAC* DSB) may potentially favor preferential SB transposon integration into these *TRAC* DSB regions since DSBs are known to "capture" exogenous DNA.[42,44] Hence, this could lead to differences in SB transposon integration profiles in the SB-CD19-28z.CAR/TCR KO T cells compared with the SB-CD19-28z.CAR/scrambled control T cells. To determine the effect of CRISPR-Cas9 activity on SB transposon insertion profiles in T cells, an unbiased genome-wide integration site analysis (ISA) of genomic DNA samples obtained from the SB-CD19-28z.CAR/TCR KO T cells and the SB-CD19-28z.CAR/scrambled control T cells was carried out. The ISA data showed that the relative frequencies of transgene insertion into different genomic features in the SB-CD19-28z.CAR/TCR KO T cells and the SB-CD19-28z.CAR/scrambled T cells control are highly similar (Figures 4I and S13A). The integration profile of the SB transposon vector in both samples displayed 51% of integration site (IS) in gene coding regions, of which 49% of ISs are located within intronic and 2% within exonic regions. The remaining 49% of ISs were found outside of the gene body with highly similar percentages of IS found either upstream of a transcriptional start site (TSS) (24%) or downstream of a gene (25%) (Figure S13A, upper). When compared with typical gammaretroviral and lentiviral profiles,[45–47] these SB transposon-modified CAR T cells have lower insertion site proportions in gene coding regions, indicating lower preference toward transcription active parts of the genome. Consistently, ISs were detected across all chromosomes and are found to be in line

of 70 pmol of TCR-1 RNP. Twenty-four hours later, the cells were transfected with 1 μg of mcCD19-28z.CAR and 0.5 μg of mcSB100x. Next day, only CAR+ T cells were enriched using the MACS method and subsequently expanded by weekly addition of 100-Gy-irradiated NALM6 feeder cells. Recombinant IL-2, IL-7, and IL-15 cytokines were supplemented to the culture on a Monday/Wednesday/Friday schedule. On week 2 post-culture, the CAR T cells were harvested for flow cytometry analysis and functionality tests. (F) (Left) Total CAR+ cell percentage, immunophenotyping analysis of (middle) T cell memory markers, and (right) PD1, CTLA4, and TIM3 immune checkpoint markers in SB-CD19-28z.CAR/TCR KO and SB-CD19-28z.CAR/scrambled control T cells generated from human CD8+ T cells at 2 weeks post-culture. Data are shown as means ± SEM (n = 3 biologically independent donors). (G) (Left) Total CAR+ cell percentage and (right) cellular composition of CD4+ and CD8+ CAR T cells generated from human CD3+ T cells at 2 weeks post-culture. (H) Quantitative analysis of (left) SB transposon copy number and (right) SB100x transposase after 6 weeks of CAR T cell expansion by qPCR assay (Table S4). Data are shown as means ± SEM (n = 3 biologically independent donors); Student's t test; n.s., not significant. (I) Fold difference of SB transposon integration site (IS) frequency in the different genomic features between SB-CD19-28z.CAR/TCR KO versus SB-CD19-28z.CAR/scrambled control T cells.

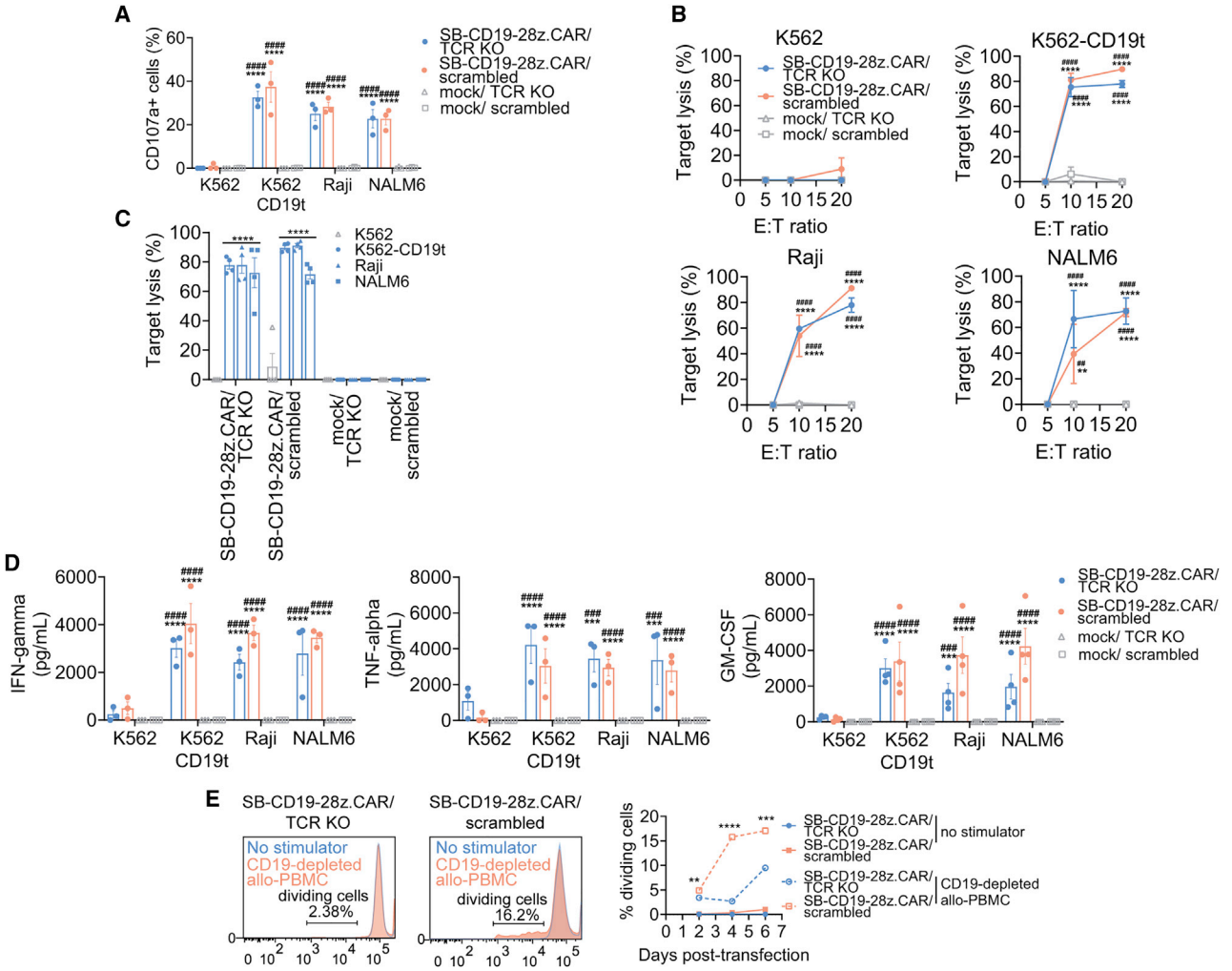

Figure 5. SB-CD19-28z.CAR/TCR KO were responsive to CD19-expressing tumor cells and displayed antigen-dependent effector functions

(A) Percentage of CD107a+ cells upon 6 h of incubation with CD19+ or K562 control tumor cells (*compared with mock/TCR KO group; #compared with mock/scrambled control group). (B) Effector dose-response-specific lysis of effector cells after 48 h of incubation with CD19+ or K562 control tumor cells. One-way ANOVA with Dunnett's post-hoc (*compared with mock/TCR KO group; #compared with mock/scrambled control group). (C) Comparison of specific lysis of effector cells between incubation with CD19+ and K562 control tumor cells. One-way ANOVA with Dunnett's post-hoc (*compared with K562 control group). (D) Secretion of human IFN-γ, GM-CSF, and TNF-α cytokines from effector cells in response to target tumor cells after 72 h post-coculture. One-way ANOVA with Dunnett's post-hoc (*compared with mock/TCR KO group; #compared with mock/scrambled control group). (E) (Left) Schematic flow cytometric plot on day 4 post-incubation and (right) percentages of proliferating effector cells after contact with CD19-depleted allogeneic PBMCs (allo-PBMCs) at different time points. Student's t test (*compared with SB-CD19-28z.CAR/TCR KO at each time point). Data are shown as means ± SEM (n = 3–4 biologically independent donors); **/##p < 0.01, ***/###p < 0.001, ****/####p < 0.0001.

with chromosome size, showing comparable frequencies in the SB-CD19-28z.CAR/TCR KO T cells and the SB-CD19-28z.CAR/scrambled T cells (Figure S13A, middle). The integration in both samples was distributed similarly throughout the gene relative to TSS, showing a reduced frequency upstream of the TSS (Figure S13A, lower). Both CAR T cells are highly polyclonal (Figure S13B) and absent of any integration site showing a relative contribution of >30% (of total retrieved integration sites) (Figure S13C), suggesting no biased insertion into any specific loci in the genome and clonal expansion. In particular, we did not observe an integration event within or nearby *TRAC* gene in the SB-CD19-28z.CAR/TCR KO T cells (Table S5), ruling out the possibility of preferential SB transposon insertion at *TRAC* DSBs.

The lack of SB transposon integration at *TRAC* DSBs was further confirmed using PCR amplification and DNA Sanger sequencing analysis. First, the plasmid library containing DNA variants derived from the *TRAC* DSBs was generated from genomic DNA of the SB-CD19-28z.CAR/TCR KO and the SB-CD19-28z.CAR/scrambled control T cells (Figure S14A). Next, we screened at least 100 plasmid clones

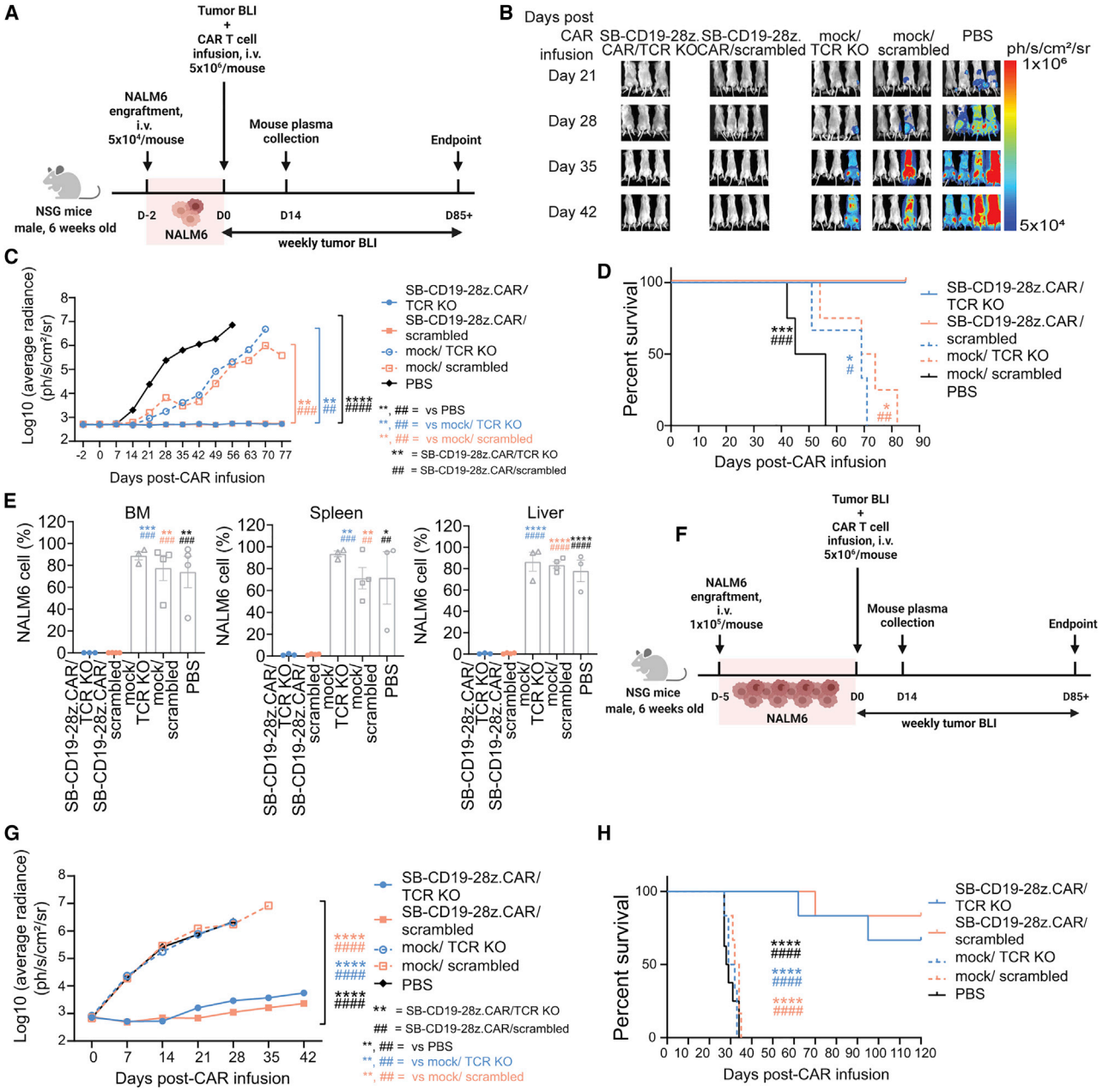

Figure 6. SB-CD19-28z.CAR/TCR KO T cells efficiently rejected CD19+ leukemic cells *in vivo*

(A) Schematic representation of experimental design with low tumor burden. Six-week-old male NSG mice received 5×10^4 NALM6 tumor cells expressing luciferase via intravenous tail vein injection. Two days post-tumor inoculation, 5×10^6 SB-CD19-28z.CAR/TCR KO or SB-CD19-28z.CAR/scrambled control T cells were intravenously infused into xenografted mice. For the control groups, the equivalent numbers of mock/TCR KO or mock/scrambled control T cells or equivalent volumes of PBS were administered to the mice. Non-invasive bioluminescence imaging (BLI) was performed weekly to monitor the tumor progression over time. (B) Representative BLI of tumor development from all groups at different time points. The BLI signals were expressed in average radiance (ph/s/cm^2/sr). (C) Quantitative tumor BLI signals from the whole mouse body at different time points. The BLI signals were expressed in log10(average radiance) (ph/s/cm^2/sr). (D) Kaplan-Meier survival curve analysis of mice from all groups. (E) Quantitative analysis showing the presence of NALM6 tumor cells in bone marrow, spleen, and liver tissues of all treated groups at endpoint. For the low tumor burden experiment, data are shown as means ± SEM (n = 3–4 mice); one-way ANOVA with Dunnett's post-hoc or log rank test for Kaplan-Meier survival analysis; */#p < 0.05, **/## p < 0.01, ***/###p < 0.001, ****/#### p< 0.0001. (F) Schematic representation of experimental design with high tumor burden. Six-week-old male NSG mice received 1×10^5 NALM6 tumor cells expressing luciferase via intravenous tail vein injection. Five days post-tumor inoculation, 5×10^6 SB-CD19-28z.CAR/TCR KO or SB-CD19-28z.CAR/scrambled control

(legend continued on next page)

to assess the presence of the SB transposon at the *TRAC* DSB library using PCR amplification specific to CAR DNA. The results showed that the SB transposon integration was undetectable at *TRAC* DSB regions in the SB-CD19-28z.CAR/TCR KO T cells (Figures S14B and S14C). Consistently, the DNA sequencing analysis indicated the absence of an SB transposon insertion in the *TRAC* DSBs (Figure S14D).

To evaluate the potential risks of insertional oncogenesis induced by SB transposon integration, the frequency of insertion sites harbored in 100 kb proximity to a TSS of the selected cancer-associated genes was determined. The results demonstrated that, in concordance with the polyclonal composition of SB-derived CAR T cells, the relative frequencies of these insertion sites that were found within or close to the proto-oncogenes, including CCND2 (AS1), HMGA2, LMO2, MECOM, or MN1, in previous gene therapy trials,[29,30,48–51] were very low (i.e., 0.0004%–0.0195%) (Table S6).

In vitro antitumor effects of SB-modified CD19-redirected CAR T cells devoid of TCR expression

We then explored whether SB-CD19-28z.CAR/TCR KO T cells were specifically responsive to CD19 antigen and exerted antitumor functions. CD19-expressing tumor cells induced ~20%–40% higher CD107a expression than K562 control cells in both SB-CD19-28z.CAR/TCR KO and SB-CD19-28z.CAR/scrambled groups (Figures 5A, S15A, and S15B). After 48 and 72 h of effector/CD19+ tumor cell coculture, an increase in target lysis was uniquely identified in the SB-CD19-28z.CAR/TCR KO and SB-CD19 28z.CAR/scrambled control T cells (Figures 5B and S15C) and positively correlated with a higher effector-to-target ratio (Figure 5B). Consistent with these findings, cytolytic functions of SB-CD19-28z.CAR/TCR KO and SB-CD19-28z.CAR/scrambled T cells were restricted to CD19+ tumor cells (Figure 5C). In the absence of CAR expression, minimal or no lysis of CD19+ target cells was apparent, confirming that the specificity of cell killing was determined by CAR expression (Figure 5C). This result corresponded with increased IFN-γ, GM-CSF, and tumor necrosis factor alpha (TNF-α) cytokine levels in the SB-CD19-28zCAR/TCR KO and SB-CD19-28z.CAR/scrambled groups upon exposure to CD19 antigen (Figure 5D). Following co-incubation with CD19-depleted allogeneic PBMCs (allo-PBMCs), the TCR ablation significantly decreased CAR T cell proliferation compared with the SB-CD19-28z.CAR/scrambled control T cells in a time-dependent manner (Figure 5E).

Potent *in vivo* antitumor functions of SB-engineered CD19-redirected CAR/TCR KO T cells

Next, we assessed the effect of SB-CD19-28z.CAR/TCR KO on CD19+ tumor progression in a xenograft model. For a low tumor burden setting, we administered 5×10^4 luciferase-expressing NALM6 cells by intravenous injection into NOD/SCID/IL2r−/− (NSG) male mice, followed by 5×10^6 SB-CD19-28z.CAR/TCR KO, SB-CD19-28z.CAR/scrambled, mock/TCR KO, or mock/scrambled T cell engraftment at 2 days post-NALM6 inoculation. As a negative control, NALM6-bearing mice were injected with phosphate-buffered saline (PBS) (Figure 6A). All PBS-injected tumor-bearing mice had a tumor burden from day 14, whereas most of the mock/TCR KO and mock/scrambled-treated groups developed tumors on day 42 (Figures 6B and 6C). In contrast, mice receiving the SB-CD19-28z.CAR/TCR KO CAR T cells or the SB-CD19-28z.CAR/scrambled control CAR T cells maintained complete tumor remission over an 11-week period (Figures 6B and 6C). The absence of tumor burden is consistent with a significantly prolonged median survival observed in SB-CD19-28z.CAR/TCR KO or SB-CD19-28z.CAR/scrambled control-injected groups compared with the control mice (Figure 6D). Moreover, endpoint examination of CAR T cell-treated mice showed that NALM6 cells were undetectable in the major lymphoid and non-lymphoid organs including bone marrow, spleen, and liver tissue (Figures 6E and S16A). In contrast, a marked accumulation of infiltrating NALM6 cells was identified in these organs obtained from all control groups (Figure S16A). In the next experiment, the same therapeutic dose of CD19 CAR T cells was tested in the NALM6-bearing mice with a higher tumor load (i.e., inoculation of 1×10^5 luciferase-expressing NALM6 cells per mouse; tumor was established for 5 days before CAR T cell infusion) (Figure 6F). Both SB-CD19-28z.CAR/TCR KO CAR T cells and SB-CD19-28z.CAR/scrambled control CAR T cells significantly reduced the leukemic burden in the mice with high tumor load and improved the survival rate compared with the control groups (Figures 6G, 6H, and S16B), consistent with the previous low tumor load experiment. Only few mice from these groups developed leukemia at later time points and had to be euthanized (i.e., two mice from SB-CD19-28z.CAR/TCR KO, euthanized on day 62 and 95 post-CAR infusion; one mouse from SB-CD19-28z.CAR/scrambled, euthanized on day 70 post-CAR infusion) (Figure 6H), indicating that CAR T cells exhibited antitumor effects in an effector cell dose-dependent manner. Collectively, both the SB-CD19-28z.CAR/TCR KO and the SB-CD19-28z.CAR/scrambled control T cells were equally efficient at suppressing NALM6 tumor progression and improving mouse survival compared with the non-CAR T cells (i.e., mock/TCR KO and mock/scrambled) and PBS control groups (Figure 6). Tumor growth of the mock/TCR KO and mock/scrambled groups was slightly reduced compared with the PBS control group, due to a CAR-independent T cell-mediated antitumor effect.

TCR disruption in SB-derived CAR T cell-alleviated xenogeneic GvHD development

We further evaluated whether the SB-CD19-28z.CAR/TCR KO cells with reduced TCR alloreactivity could lower the risk of GvHD development in mice. To induce GvHD, we administered 10×10^6

T cells were intravenously infused into xenografted mice. For the control groups, the equivalent numbers of mock/TCR KO or mock/scrambled control T cells or equivalent volumes of PBS were administered to the mice. (G) Quantitative tumor BLI signals from the whole mouse body at different time points. The BLI signals were expressed in log10(average radiance) (ph/s/cm^2/sr). (H) Kaplan-Meier survival curve analysis of mice from all groups. For high tumor burden experiment, data are shown as means ± SEM (n = 6–8 mice); one-way ANOVA with Dunnett's post-hoc or log rank test for Kaplan-Meier survival analysis; */#p < 0.05, **/##p < 0.01, ***/###p < 0.001, ****/####p < 0.0001.

SB-CD19-28z.CAR/TCR KO or SB-CD19-28z.CAR/scrambled control T cells into 2-Gy-irradiated NSG mice. Mice receiving only PBS served as a "healthy" control (Figure 7). Consistent with our results obtained from the alloreactivity experiment (Figure 5E) and previous studies,[20,22,60] most of the mice (4/6 mice) receiving the SB-CD19-28z.CAR/scrambled control T cells developed clinical signs of GvHD and died after 2 months, whereas all SB-CD19-28z.CAR/TCR KO-treated mice survived and remained disease-free over 3 months (Figure 7A–7C; Table S7). This corresponds with the presence of characteristic GvHD histopathology findings, including high infiltration of mononuclear cells in liver and lung, shortening and/or structural abnormality of intestinal villi, and bronchial luminal narrowing (Figure 7D) in the SB-CD19-28z.CAR/scrambled control mice, as opposed to the lack of any such pathologies in the SB-CD19-28z.CAR/TCR KO-treated mice.

Analysis of signaling pathways in T cells engineered with SB-CD19-28z.CAR in the presence and absence of endogenous TCR signaling

Generally, the antileukemic activities of CAR T cells mainly associate with CAR signaling upon specific tumor antigen recognition. However, this may not fully recapitulate the current allogeneic CAR treatment where endogenous TCR of donor-derived CAR T cells can be reactive to viral antigens and/or allo-antigens.[61,62] Hence, we believe that it is strongly necessary and relevant to explore the alteration of signaling profiles in the CAR/TCR KO cells compared with the CAR/scrambled control T cells under two different T cell signaling conditions: single CAR signaling (i.e., by stimulating the cells with NALM6) (Figure 8A) and dual CAR/endogenous TCR signaling (i.e., by stimulating the cells with NALM6 cell and anti CD3 antibody) (Figure 8D). This is aimed at providing a better molecular insight into allogeneic CAR T cell signaling in the absence and presence of endogenous TCR reactivity, respectively. As a negative control, the effector cells were cultured without stimulus to measure the background signals from the resting state.

First we assessed the phosphorylation states of essential protein kinases including tyrosine kinase ZAP70 (ZAP70),[63] phospholipase C-γ1 (PLCγ1),[63] and p38 mitogen-activated protein kinase (MAPK, p38),[64] which are responsible for the initiation of T cell signaling (Table S8). We found that a single CAR signaling induced by NALM6 stimulation (Figure 8A) enhanced the similar levels of ZAP70, PLCγ1, and p38 protein phosphorylation in the SB-CD19-28z.CAR/TCR KO and SB-CD19-28z.CAR/scrambled control T cells (Figures 8B and S17A). The engagement of CAR and/or TCR to antigens is known to trigger several signaling transduction pathways that are essential for T cell function. In particular, the phosphoinositide 3-kinase (PI3K) signaling pathway plays a crucial role by promoting effector T cell differentiation and regulating cell proliferation, apoptosis, and metabolic activity.[65,66] Therefore, the transcriptional profiles of genes associated with the PI3K pathway (total 29 genes) were compared in SB-CD19-28z.CAR/TCR KO and SB-CD19-28z.CAR/scrambled T cells in response to a signal CAR stimulation. As expected, the large majority of PI3K pathway genes (i.e., 24/29 = 82%) were not differentially expressed between SB-CD19-28z.CAR/TCR KO and SB-CD19-28z.CAR/scrambled control T cells, although some differences were apparent. In particular, only 5/29 differentially expressed genes (DEGs) belonging to the PI3K pathway were identified in the SB-CD19-28z.CAR/TCR KO compared with the SB-CD19-28z.CAR/scrambled control T cells following NALM6 stimulation (Figures 8C, S17B, and S17C). This suggests that, following single CAR signaling when exposed to CD19 antigen (on NALM6 cells), the SB-CD19-28z.CAR/TCR KO and the SB-CD19-28z.CAR/scrambled control T cells display comparable molecular signatures of T cell signaling (Figures 8A–8C), consistent with similar antitumor responses (Figure 5).

Nevertheless, dual CAR/endogenous TCR signaling (Figure 8D) led to a higher ZAP70 and PLCγ1 phosphorylation in SB-CD19-28z.CAR/scrambled T cells versus SB-CD19-28z.CAR/TCR KO T cells (Figures 8E and S17A), as opposed to a single CAR signaling. Consistently, comprehensive RNA analysis identified 14/29 DEGs (10 downregulated genes and 4 upregulated genes) belonging to the PI3K pathway in the SB-CD19-28z.CAR/TCR KO compared with the SB-CD19-28z.CAR/scrambled cells after simultaneous CAR/endogenous TCR signaling (Figures 8F, S17B, and S17D). This corresponded with the transcriptional alteration of the downstream processes that are associated with the PI3K pathway and influence apoptosis (10/19 DEGs), cell proliferation (12/19 DEGs), and metabolic activity (8/16 DEGs for glycolysis, 5/5 DEGs for fatty acid synthesis/oxidation, and 4/4 DEGs for amino acid metabolism) (Figures 8F, S17B, and S17D). Interestingly, the RNA expression fold changes of DEGs identified during single NALM6 stimulation were further augmented by additional anti-CD3 stimulation (Figures S17B and S17D). This suggests that TCR disruption in CAR T cells inhibits T cell signaling/protein phosphorylation and differential gene expression that is linked to the PI3K signaling pathway and some of its downstream processes compared with the control CAR T cells when endogenous TCR reactivation occurs (Figures 8D–8F and S18).

DISCUSSION

In this study, we validated a non-viral T cell engineering platform based on SB transposons and CRISPR-Cas9 as a potential universal off-the-shelf allogeneic CAR T cell therapy. For this purpose, we stably expressed CD19-CAR genes in purified human T cells using hyperactive SB transposons. The use of mc-harboring SB transposons allowed for superior transfection and transposition rates and reduced DNA-mediated toxicity compared with the plasmid-based SB transposon.[33,67] To minimize GvHD risk, endogenous TCR expression was inactivated using TCR gene-specific CRISPR-Cas9 RNPs. With optimized transfection and enrichment schemes, relatively robust CD19-CAR expression (90%) and TCR inactivation (99% TCR^{neg}) was achieved. Compared with the sequential transfection approach used in this study, a simultaneous co-transfection of CRISPR-Cas9 and SB transposon components would be more convenient by reducing the steps of CAR T cell manufacturing compared with a sequential transfection method. Simultaneous co-transfection of CRISPR-Cas9 RNP and linear dsDNA template in human T cells

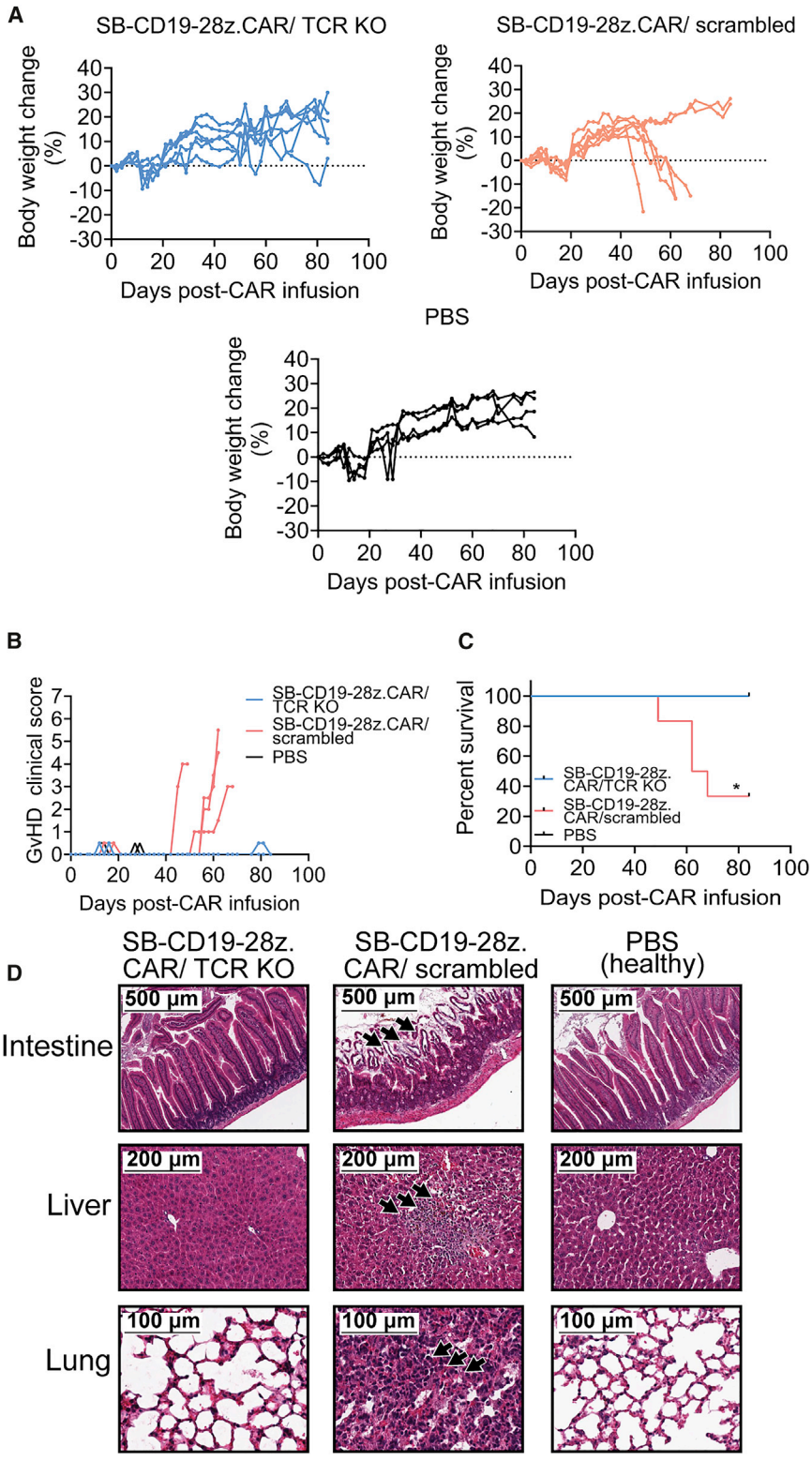

Figure 7. SB-CD19-28z.CAR/TCR KO T cells inhibited GvHD development *in vivo*

Six-week-old male NSG mice were irradiated at a dose of 2 Gy. After 6 h of irradiation, the mice received 10×10^6 SB-CD19-28z.CAR/TCR KO or SB-CD19-28z.CAR/ scrambled control T cell through intravenous administration. For the healthy control group, equivalent volumes of PBS were administered to the mice. (A and B) (A) Mouse body weight change and (B) GvHD clinical scoring were recorded over time. The GvHD clinical scoring criteria used in the experiment are described in Table S7.[52–54] (C) Kaplan-Meier survival analysis of mice from all groups (n = 4–6 mice); log rank test; *$p < 0.05$. (D) Histopathology of intestine, liver, and lung tissues obtained from all groups. Solid black arrows indicate GvHD pathology, including high infiltration of mononuclear cells in hepatic and lung tissues, shortening and/or structural abnormality of intestinal villi, and bronchial luminal narrowing.[55–59] The corresponding number at each scale bar indicates an image size (µm).

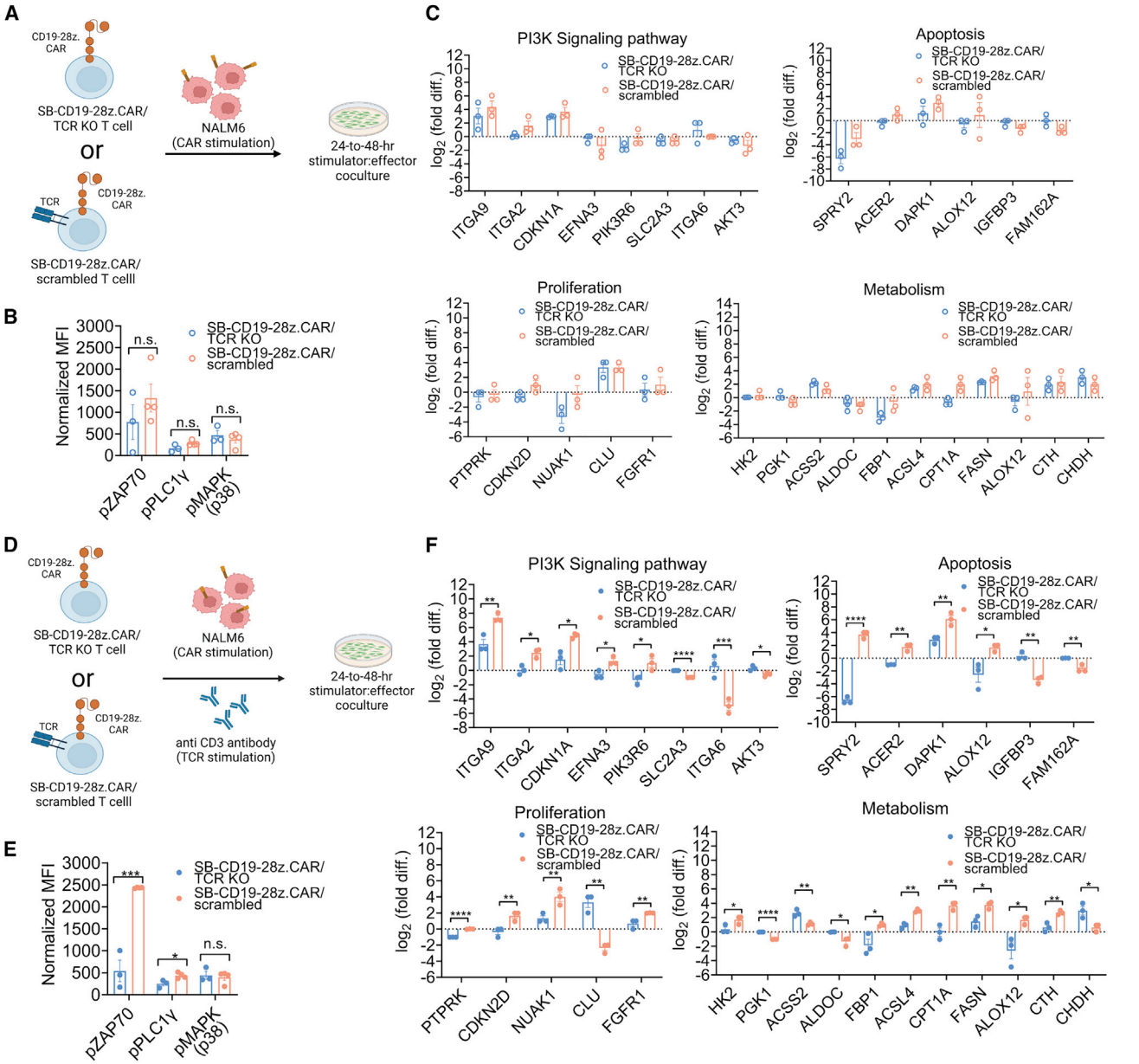

Figure 8. Effects of single CAR signaling and concomitant CAR/endogenous TCR co-signaling on molecular signature of SB-CD19-28z.CAR/TCR KO and SB-CD19-28zCAR/scrambled T cells

(A) Schematic representative of experimental design for analysis of single CAR-induced molecular signaling profile. A total of 3×10^6 SB-CD19-28z.CAR/TCR KO or SB-CD19-28z.CAR/scrambled T cells was stimulated with irradiated NALM6 cell (effector-to-target [E:T] = 1:1) for inducing CAR signaling for 24–48 h. As a negative control of resting state, CD19 CAR T cells were cultured in the absence of stimulus. (B) Quantitative analysis of ZAP70, PLCγ1, and p38 protein phosphorylation in CAR T cells after 24 h of stimulation. (C) Quantitative analysis of RNA expression profiling of selected genes associated with the PI3K signaling pathway, apoptosis, metabolism, and cell proliferation in SB-CD19-28z.CAR/TCR KO and SB-CD19-28z.CAR/scrambled T cells at 48 h post-stimulation. (D) Schematic representative of experimental design for analysis of simultaneous CAR/endogenous TCR-induced molecular signaling profile. A total of 3×10^6 SB-CD19-28z.CAR/TCR KO or SB-CD19-28z.CAR/scrambled T cells was stimulated with irradiated NALM6 cell (E:T = 1:1) and anti-CD3 antibody (bead:cell = 1:1) for inducing CAR and endogenous TCR co-signaling for 24–48 h. As a negative control of resting state, CD19 CAR T cells were cultured in the absence of stimulus. (E) Quantitative analysis of ZAP70, PLCγ1, and p38 protein phosphorylation in CAR T cells after 24 h of stimulation. (F) Quantitative analysis of RNA expression profiling of selected genes associated with the PI3K signaling pathway, apoptosis, metabolism, and cell proliferation in SB-CD19-28z.CAR/TCR KO and SB-CD19-28z.CAR/scrambled T cells at 48 h post-stimulation. Differentially expressed genes (DEGs) are defined as the genes showing $p < 0.05$ for differential expression. Data are shown as means ± SEM (n = 3 biologically independent donors); Student's t test; n.s., not significant; *$p < 0.05$, **$p < 0.01$, ***$p < 0.001$, ****$p < 0.0001$.

was demonstrated in a previous study,[68] suggesting the feasibility of this approach. Nevertheless, our study, which is based on a circular dsDNA (plasmid and mcDNA vector) transfection, clearly showed that simultaneous transfection of CRISPR-Cas9 RNP and transgene-encoding plasmid/mcDNA was relatively inefficient compared with a sequential transfection to produce the transgene-expressing TCR KO T cells (Figures S5B–S5D, left and S9A–S9C). In fact, co-electroporation of pmaxGFP plasmid and any CRISPR-Cas9 RNPs resulted in a significant reduction of the total GFP transfection efficiency compared with when the cells were transfected with only the pmaxGFP plasmid (Figure S5D, left). This suggests that the cellular uptake of the relatively large circular dsDNA during transfection could be hampered by the CRISPR-Cas9 RNP components, thereby compromising the overall efficiency of CAR/TCR KO T cell production. Most important, transplantation of CD19-specific CAR/TCR^{neg} T cells into a xenograft tumor model resulted in efficient CD19-specific oncolysis *in vitro* and complete tumor remission *in vivo*, consistent with increased IFN-γ, GM-CSF, and TNF-α production. Most of the SB-CD19-28z.CAR/TCR KO T cells exhibited a predominant memory phenotype. Clinical trials have shown that T cell memory phenotypes correlated with antileukemic response and CAR-T cell persistence in patients with B cell acute lymphoblastic leukemia.[69] Extended periods of CAR-T cell coculture with repeated antigen stimulation led to a relatively robust T cell expansion (100- to 1,000-fold expansion during a 6-week culture protocol and 10- to 30-fold expansion during a 2-week culture protocol with early CAR+ T cell enrichment. However, prolonged expansion may potentially contribute to T cell exhaustion.[70] Nevertheless, it is encouraging that these *in-vitro*-expanded CAR/TCR KO T cells remained fully functional, consistent with the absence or low expression of exhaustion markers such as PD1 and CTLA4. Although relatively high TIM3 expression was apparent in the CAR T cells based on the 6-week expansion protocol, this likely resulted from the supplement of IL-2, IL-7, IL-15, and IL-21 cytokines in the culture medium.[71] In accordance with our results, increased TIM3 expression without or only minimal PD1 expression in CAR T cells did not compromise CAR T cell functionality,[60,72] supporting the notion that TIM3 is dispensable for T cell exhaustion.[73] The prevailing memory phenotype and absence of a typical T cell exhaustion profile correlated with the antitumor effects and sustained and complete tumor remission in the xenograft model.[60,74,75] Reduction of TCR alloreactivity in CAR/TCR KO T cells observed in our study exhibited its therapeutic potentials to minimize the risk of GvHD in mice, which was demonstrated in previous studies.[22,60]

To our knowledge, this study is the first to demonstrate that the combination of SB transposons and CRISPR-Cas9 enables efficient manufacturing of allogeneic TCR-disrupted CD19-CAR T cells, underscoring its novelty. Previous studies using transposon-based engineering of T cells relied on zinc finger nucleases (ZFNs) to disrupt the TCR genes.[35] Here, we obtained significantly higher TCR targeting efficiencies (99%) with our optimized platform compared with the use of ZFNs, which usually yields ∼30% CD3/TCR^{neg} CAR T cells, requiring an additional CD3+ T cell depletion step.[35] The superior efficiency with the current approach may be due to more efficient delivery, expression, and/or stability of CRISPR-Cas9 RNPs compared with ZFN mRNA. However, we cannot exclude a contribution of differences in T cell activation status to these different targeting efficiencies. The relatively efficient nonviral platform described in this study supports its potential broad implications, not only for single *TRAC* gene disruption but also to achieve (simultaneous) multiple genetic ablations associated with HLA I/II expression including *β-2 microglobulin (B2M)* and *class II major histocompatibility complex transactivator (CIITA)* genes to generate universal off-the-shelf CAR T cells with minimal risks of GvHD and T cell graft rejection.[19,22] This could be achieved by a co-transfection of *TRAC*-, *B2M*-, and *CIITA*-targeting CRISPR-Cas9 RNPs into T cells followed by subsequent transfection of SB transposon vector for stable CAR expression (Figure S5A, middle and lower). Additional depletion of HLA I, HLA II, and TCR/CD3+ T cells could be carried out before SB transposon transfection to augment the overall efficiency of universal CAR T cell production (Figure S5A, lower).[19,22] The high and sustained CAR expression levels achieved with the SB transposon-CRISPR-Cas9 platform also compares favorably with previous findings typically attained with use of γ-retroviral or lentiviral vectors for CAR-T cell generation.[5,26,35–40] Moreover, the use of the 2-week expansion protocol with early CAR+ enrichment still yielded up to 70-fold expansion of the transposon-engineered CAR/TCR KO T cells with predominant memory phenotypes, consistent with the CAR/TCR KO T cell profiles generated from viral vector-based systems.[60] This improved protocol is also highly relevant for current clinical-grade CAR T cell manufacturing methods, which typically require 2 weeks of cell expansion before harvest.[34,76] However, it cannot be excluded that this platform allows for further shortening of CAR T cell production time by increasing higher numbers of input cells. For allogeneic treatment, ∼90×10^6 CAR T cells/patient (i.e., the dose ranges from $10^6/m^2$ to $10^8/m^2$ of recipient's calculated body surface area) is typically required.[34] By assuming (1) ∼40% of cell viability (Figure S12A) and (2) ∼50% of transfection efficiency (Figure S12B) upon gene transfer, we would need 56.3×10^6 allogenic CD3 T cells as a starting material to primarily obtain 11.25×10^6 CAR T cells, which would undergo ∼8-fold CAR expansion after 7 days of culture (Figure S12F) and result in 90×10^6 CAR T cells. Given a high abundance of T cells (∼60%) in PBMCs,[77] this cell number is achievable from a single donor using lymphocyte apheresis. Interestingly, a recent study demonstrated that the SB transposon-mediated CAR T cells can be generated as early as 8 days and display cytotoxicity against CD19+ tumors,[72] thus supporting the feasibility of our approach. Although non-viral DNA transfection can trigger some acute cytotoxicity, using mcDNA vector rather than conventional plasmids to deliver transposons reduced this effect.[60]

Interaction of the CAR-CD3 zeta domain with the endogenous TCR/CD3 complex may be required to optimize CAR T cell reactivity toward target antigens.[78] Consequently, endogenous TCR disruption may perturb CAR signaling upon antigen engagement and compromise the oncolytic potential of CAR T cells. This scenario is supported by recent data showing that TCR ablation impairs CAR T cell function, accounting for incomplete tumor suppression *in vivo*.[60]

Nevertheless, it is particularly encouraging that we observed no significant impact of TCR disruption on the antileukemic function of CD19 CAR T cells in response to CD19+ tumor cells and in NALM6-bearing mice, consistent with similar protein kinase phosphorylation and transcriptional profiles in both T cells following CD19-mediated single CAR signaling. The comparative RNA expression analysis revealed only few DEGs involved with the PI3K signaling pathway. To our knowledge, studies reporting the roles of these DEGs (i.e., *RXRA*, *IL3*, *COL6A5*, *PPP2R2B*, and *EFNA4*) in CAR T cell antitumor functions are currently limited, warranting further investigation. Among these DEGs, *retinoid X receptor alpha* (*RXRA*) gene disruption limits T cell proliferation and promotes apoptosis following antigen stimulation. Moreover, deficiency of RXRA activity drives T cell differentiation to secrete more Th1 cytokines, including IFN-γ and TNF-α.[79,80] Interestingly, we found that *RXRA* downregulation in the SB-CD19-28z.CAR/TCR KO cells compared with the SB-CD19-28z.CAR/scrambled control T cells does not significantly enhance IFN-γ and TNFα secretion upon CAR signaling in response to CD19+ tumor cells (Figure 5D).

It has been shown that dual CAR and TCR signaling contributes to differential expression of genes responsible for apoptosis, effector functions, and cellular metabolism compared with CAR activation in the mouse system.[81] Our current findings complement these murine studies and provide further insights into the molecular interplay between CAR and endogenous TCR/CD3 signaling in human T cells, which alters the protein phosphorylation and RNA expression of genes associated with the PI3K pathway and its downstream processes (Figures S17 and S18). ZAP70 and PLC1γ proteins play key roles in signal transduction in T cells by inducing protein phosphorylation cascades and stabilizing the linker for activation of T cell protein complex during T cell signaling.[82] In addition, a loss of ZAP70 activity impairs T cell activation, proliferation, and effector and memory T cell responses to target antigens.[83] Suboptimal ZAP70 phosphorylation triggered by CAR-low-density antigen engagement leads to poor proximal receptor signaling and attenuation of T cell functions.[84] Hence, an increase of ZAP70 and/or PLC1γ phosphorylation mediated by reactive endogenous TCR during CAR signaling may promote the overall sensitivity of CAR T cells to antigens and enhance antitumor response. Activation of PI3K pathway signaling is crucial to activate T cells and enhances CAR T cell function *in vivo*.[85] However, the constitutive signaling of the PI3K pathway drives the terminal differentiation of T cells into short-lived effector T cells, which is less favorable toward achieving CAR T cell persistence.[65] Furthermore, inhibition of the PI3K pathway reduces GvHD development by promoting tolerance of alloreactive T cells.[86] Hence, the temporal regulation of the PI3K signaling pathway in response to CD19-specific T cell activation may not only improve CAR T cell persistence but also minimize GvHD risk. Our study is the first to confirm that TCR-disrupted CD19 CAR T cells are relatively resistant to endogenous TCR/CD3 signaling. Moreover, they maintain a stable molecular signaling profile. This may potentially minimize undesirable T cell signaling and/or adverse events caused by TCR reactivation.[81,87]

Based on the previous studies, it is possible that most DEGs identified in T cells following dual CAR/endogenous TCR signaling may enhance CAR T cell cytolytic functions. For example, upregulation of *integrin subunit alpha 2* in activated endogenous TCR/CAR T cells could improve T cell growth and increase cytokine production.[88] *Cyclin-dependent kinase inhibitor 1A* serves as an essential mediator to regulate an optimal proliferation and a homeostasis of activated/memory T cells.[89,90] *Death-associated protein kinase 1* (*DAPK1*) plays a crucial role in CD8+ T cell activation, trafficking, and potent antitumor effects.[91] In addition, *DAPK1*-mediated mTORC1 pathway signaling enhances CD8+ T cell response and memory differentiation in a PI3K/AKT-independent manner.[92] An increased *fibroblast growth factor receptor 1* expression induced by CAR/endogenous TCR activation in T cells could augment IL-2 production and cell proliferation through NFAT and AP-1 activity.[93] Upregulation of *carnitine palmitoyltransferase 1A* may facilitate mitochondrial fatty acid oxidation to support CD8+ memory T cell phenotype.[94] *Cystathionine gamma-lyase* overexpression in the dual CAR/endogenous TCR-activated T cells may improve antitumor effects by controlling amino acid abundance in tumor microenvironment.[95] *Protein tyrosine phosphatase receptor type K* regulates the ERK phosphorylation pathway, which is required for CD4+ T cell development.[96] Nevertheless, for some DEGs observed upon CAR/endogenous TCR activation, it remains unclear whether their expression alteration provides biological advantages to CAR T cells. *Hexokinase 2* (*HK2*) expression is essential for glycolysis and oxidative phosphorylation in activated T cells and supports antitumor effects through IFN-γ secretion,[97] consistent with HK2 upregulation in CAR/TCR-activated T cells observed in our study. However, inhibition of *HK2*-directed glycolysis may enhance memory T cell formation and long-term persistence.[98] *Acyl-CoA synthetase long-chain family member 4* expression in T cell is indispensable for effective antitumor response in mice but may compromise T cell survival through iron-dependent programmed cell death pathway activation.[99]

This study takes advantage of the versatility of the SB and CRISPR-Cas9 technology and further expands their potential in an allogeneic TCR KO setting to minimize the risk of GvHD and open the way to a universal, off-the-shelf immunotherapy for lymphoid cancers. Autologous transposon-modified CAR T cells have been explored in clinical trials (NCT03389035, NCT04289220, and NCT04284254), demonstrating therapeutic efficacy toward leukemia and solid tumors.[34,69,100,101] SB transposon-based vectors typically integrate close to random into the target cell genome, which sets them apart from γ-retroviral and lentiviral vectors that exhibit a biased integration into (active) genes, as also demonstrated in our current result (Figures 4I and S13A). We also found that CRISPR-Cas9 activity does not alter the SB transposon insertion patterns and does not skew the transposon insertions toward on-target DSBs in T cells (Figure S14), consistent with the previous study showing the absence of transposon insertion into CRISPR-Cas9-mediated DSBs.[102] The current SB transposon-CRISPR-Cas9 RNP technology enables generation of universal allogenic CAR T cells with a relatively safe

integration profile consistent with (1) lower integration bias toward transcriptionally active regions of the genome compared with integrating viral vectors,[45–47] (2) polyclonal integration pattern and no dominant insertion preference, and (3) extremely low occurrence of insertion sites in the vicinity of proto-oncogenes. Although insertional oncogenesis cannot be excluded, the current available data support the safety advantages and feasibility of this approach for clinical translation. Nevertheless, caution is warranted in the face of recent reports that showed two out of ten patients developed T cell lymphomas derived from CD19-CAR T cells that were generated with the *piggyBac* transposon system.[103–106] Although no transposon insertions into typical oncogenes were apparent in both patients, lymphoma cells harbored structural variants (SVs) and copy number variations (CNVs), including gains and losses. In contrast to SB, the *piggyBac* transposase is known to interact with the bromodomain-containing protein 4, a keeper of genome stability. Whether this could have contributed to the observed high incidence of SVs and CNVs warrants further investigation. Of interest, both lymphomas shared ISs in the *BACH2* locus, which encodes a transcription factor that regulates T cell plasticity, but it is unclear whether this is a contributing factor in lymphomagenesis. Although long-term follow-up of SB-based CAR T cell therapy revealed no evidence of malignant transformation,[107] future studies are aimed at further reducing the risk of insertional oncogenesis either by reducing the number of integrations per cell by SB transposase mRNA delivery[33,108] or ultimately by achieving targeted transposition.

MATERIALS AND METHODS

The design of CAR-expressing vector and guided RNA, detection of CRISPR-Cas9 on-target effects, primary human T cell isolation and culture, cell lines, flow cytometry, cytotoxicity assays, selective CAR T cell expansion, and other relevant information are described in the supplemental information.

Delivery of CRISPR-Cas9 RNP into human CD8+ T cells by nucleofection

The P3 Primary Cell 4D-Nucleofector X Kit was used in all nucleofection experiments. 5×10^5 cells were washed with 1× Dulbecco's PBS and resuspended in 20 μL of kit P3 Primary Cell 4D-Nucleofector X (Lonza). The prepared 70 pmol of CRISPR-Cas9 RNP particles was added to the cell-buffer mixture and mixed well. Nucleofection was carried out in a 16-well strip using the EH-115 program. Immediately after nucleofection, 80 μL of pre-warmed complete T cell medium containing 50 U/mL of human rIL-2 was immediately added to cells, and the cells were rested for 30 min in 5% CO_2 at 37°C. The transfected cells were transferred to 1 mL of complete T cell medium and culture for 48 h at 5% CO_2 and 37°C.

Generation of CD19-28z.CAR/TCR KO T cells and SB-CD19-28z.CAR/TCR KO T cells

Sequential nucleofection of *TRAC*-targeting CRISPR-Cas9 RNP and mcDNA vector encoding CD19-28z.CAR was used to engineer CAR/TCR^{neg} T cells for transient and sustained CAR expression. To generate CD19-28z.CAR/TCR KO T cells for transient CAR expression, 700 pmol of TCR-1 RNP particles was transfected into 5×10^6 CD8+ T cells using the EH-115 program to obtain TCR^{neg} T cells. TCR-1 RNP was substituted with scrambled gRNA RNP to generate the scrambled control T cells. Twenty-four hours later, 10 μg of mcCD19-28z.CAR was transfected into 5×10^6 TCR^{neg} or scrambled control T cells using the EO-115 program. Alternatively, 10 μg of mcCD19-28z.CAR and 5 μg of mcSB100x were transfected into 5×10^6 TCR^{neg} or scrambled control T cells using the EO-115 program to produce SB-CD19-28z.CAR/TCR KO and SB-CD19-28z.CAR/scrambled T cells for stable CAR expression, respectively. As a control devoid of CAR expression, mock transfection of TCR^{neg} and scrambled control T cells was carried out to generate mock/TCR KO and mock/scrambled control T cells, respectively. After 24 h of transfection, the surface CAR and TCR expression was examined by flow cytometry analysis, and the cells were harvested for functionality assays or CAR T cell culture.

Animal experiments

All animal experiments were carried out under the procedures approved by the Institutional Animal Ethics Committee of the Vrije Universiteit Brussel (Brussels, Belgium). The experimental details are described in the corresponding figure legends and supplemental information. The development of tumor burden was assessed weekly using non-invasive *in vivo* bioluminescence imaging. At several weeks post-NALM6 tumor engraftment, some mice developed the clinical signs of significant weight loss, severely hunched back, poor grooming, hindlimb paralysis, and/or limited mobility. These mice were euthanized as an endpoint by CO_2 inhalation or cervical dislocation.

Statistical analysis and software

Data analysis was performed using GraphPad Prism 8 software. Schematic representatives were generated using BioRender software. Comparison of two mean values from two experimental groups was performed using two-tailed independent Student's t tests. Alternatively, a one-way analysis of variance (ANOVA) test was used, with Dunnett's post-hoc applied for multiple comparison of mean values from more than two experimental cohorts. Results are reported as the mean ± standard error of mean (SEM), and $p < 0.05$ was taken to indicate significance.

Data availability statement

The data that support the findings of this study are available from the corresponding author on reasonable request.

SUPPLEMENTAL INFORMATION

Supplemental information can be found online at https://doi.org/10.1016/j.ymthe.2022.06.006.

ACKNOWLEDGMENTS

We thank Red Cross Flanders (Rode Kruis-Vlaanderen, Belgium) for supplying buffy coat samples for the study. This work was supported by the Fonds Wetenschappelijk Onderzoek (FWO, project nos. G041616N, G019114N), Stichting Tegen Kanker (STK, project no. C/2014/239), and the UPGRADE (Unlocking Precision Gene

Therapy) project, that has received funding from the European Union's Horizon 2020 research and innovation program under grant agreement no. 825825, to M.K.C. and T.V., and J.T. was supported by an FWO Aspirant and Research Grant (project no. 1531116N), the Award Cancer Research – Oncology Center Vrije Universiteit Brussel, funded by the bequests of the late Ms. Esther Desmedt and the late Ms. Irma Noë, and Wetenschappelijk Fonds Willy Gepts (WFWG) foundation – VUB.

AUTHOR CONTRIBUTIONS

J.T. designed and performed all experiments, analyzed data, and wrote the paper. E.S.-K. provided essential assistance in animal experiments. T.G. provided essential assistance in irradiation experiments. T.V. and M.K.C. designed the experiments, analyzed data, wrote and approved the paper, and led the study. T.V. and M.K.C. applied for and obtained financial support for this study. All authors approved the final manuscript.

DECLARATION OF INTERESTS

The authors declare no competing interests.

REFERENCES

1. Brown, C.E., and Mackall, C.L. (2019). CAR T cell therapy: inroads to response and resistance. Nat. Rev. Immunol. *19*, 73–74. https://doi.org/10.1038/s41577-018-0119-y.

2. Majzner, R.G., and Mackall, C.L. (2019). Clinical lessons learned from the first leg of the CAR T cell journey. Nat. Med. *25*, 1341–1355. https://doi.org/10.1038/s41591-019-0564-6.

3. Zheng, P.P., Kros, J.M., and Li, J. (2018). Approved CAR T cell therapies: ice bucket challenges on glaring safety risks and long-term impacts. Drug Discov. Today *23*, 1175–1182. https://doi.org/10.1016/j.drudis.2018.02.012.

4. Townsend, M.H., Bennion, K., Robison, R.A., and O'Neill, K.L. (2020). Paving the way towards universal treatment with allogenic T cells. Immunol. Res. *68*, 63–70. https://doi.org/10.1007/s12026-020-09119-7.

5. Graham, C.E., Jozwik, A., Quartey-Papafio, R., Ioannou, N., Metelo, A.M., Scala, C., Dickson, G., Stewart, O., Almena-Carrasco, M., Peranzoni, E., et al. (2021). Gene-edited healthy donor CAR T cells show superior anti-tumour activity compared to CAR T cells derived from patients with lymphoma in an in vivo model of high-grade lymphoma. Leukemia *35*, 3581–3584. https://doi.org/10.1038/s41375-021-01324-z.

6. Maude, S.L., Laetsch, T.W., Buechner, J., Rives, S., Boyer, M., Bittencourt, H., Bader, P., Verneris, M.R., Stefanski, H.E., Myers, G.D., et al. (2018). Tisagenlecleucel in children and young adults with B-cell lymphoblastic leukemia. N. Engl. J. Med. *378*, 439–448. https://doi.org/10.1056/nejmoa1709866.

7. Schuster, S.J., Svoboda, J., Chong, E.A., Nasta, S.D., Mato, A.R., Anak, Ö., Brogdon, J.L., Pruteanu-Malinici, I., Bhoj, V., Landsburg, D., et al. (2017). Chimeric antigen receptor T cells in refractory B-cell lymphomas. N. Engl. J. Med. *377*, 2545–2554. https://doi.org/10.1056/nejmoa1708566.

8. Neelapu, S.S., Locke, F.L., Bartlett, N.L., Lekakis, L.J., Miklos, D.B., Jacobson, C.A., Braunschweig, I., Oluwole, O.O., Siddiqi, T., Lin, Y., et al. (2017). Axicabtagene ciloleucel CAR T-cell therapy in refractory large B-cell lymphoma. N. Engl. J. Med. *377*, 2531–2544. https://doi.org/10.1056/NEJMoa1707447.

9. Benjamin, R., Graham, C., Yallop, D., Jozwik, A., Mirci-Danicar, O.C., Lucchini, G., Pinner, D., Jain, N., Kantarjian, H., Boissel, N., et al.; UCART19 Group (2020). Genome-edited, donor-derived allogeneic anti-CD19 chimeric antigen receptor T cells in paediatric and adult B-cell acute lymphoblastic leukaemia: results of two phase 1 studies. Lancet *396*, 1885–1894. https://doi.org/10.1016/S0140-6736(20)32334-5.

10. Depil, S., Duchateau, P., Grupp, S.A., Mufti, G., and Poirot, L. (2020). 'Off-the-shelf' allogeneic CAR T cells: development and challenges. Nat. Rev. Drug Discov. *19*, 185–199. https://doi.org/10.1038/s41573-019-0051-2.

11. Anwer, F., Shaukat, A.A., Zahid, U., Husnain, M., McBride, A., Persky, D., Lim, M., Hasan, N., and Riaz, I.B. (2017). Donor origin CAR T cells: graft versus malignancy effect without GVHD, a systematic review. Immunotherapy *9*, 123–130. https://doi.org/10.2217/imt-2016-0127.

12. Cai, B., Guo, M., Wang, Y., Zhang, Y., Yang, J., Guo, Y., Dai, H., Yu, C., Sun, Q., Qiao, J., et al. (2016). Co-infusion of haplo-identical CD19-chimeric antigen receptor T cells and stem cells achieved full donor engraftment in refractory acute lymphoblastic leukemia. J. Hematol. Oncol. *9*, 131. https://doi.org/10.1186/s13045-016-0357-z.

13. Gallardo, D., García-López, J., SuredA, A., SuredA, A., Ferra, C., Cancelas, J., Berlanga, J., Brunet, S., Boqué, C., Picón, M., et al. (1997). Low-dose donor CD8+ cells in the CD4-depleted graft prevent allogeneic marrow graft rejection and severe graft-versus-host disease for chronic myeloid leukemia patients in first chronic phase. Bone Marrow Transplant. *20*, 945–952. https://doi.org/10.1038/sj.bmt.1701008.

14. Champlin, R., Ho, W., Gajewski, J., Feig, S., Burnison, M., Holley, G., Greenberg, P., Lee, K., SchmId, I., and Giorgi, J. (1990). Selective depletion of CD8+ T lymphocytes for prevention of graft-versus-host disease after allogeneic bone marrow transplantation. Blood *76*, 418–423. https://doi.org/10.1182/blood.v76.2.418.bloodjournal762418.

15. Shlomchik, W.D. (2007). Graft-versus-host disease. Nat. Rev. Immunol. *7*, 340–352. https://doi.org/10.1038/nri2000.

16. Bertaina, A., Merli, P., Rutella, S., Pagliara, D., Bernardo, M.E., Masetti, R., Pende, D., Falco, M., Handgretinger, R., Moretta, F., et al. (2014). HLA-haploidentical stem cell transplantation after removal of αβ+ T and B cells in children with nonmalignant disorders. Blood *124*, 822–826. https://doi.org/10.1182/blood-2014-03-563817.

17. Balashov, D., Shcherbina, A., Maschan, M., Trakhtman, P., Skvortsova, Y., Shelikhova, L., Laberko, A., Livshits, A., Novichkova, G., and Maschan, A. (2015). Single-center experience of unrelated and haploidentical stem cell transplantation with TCRαβ and CD19 depletion in children with primary immunodeficiency syndromes. Biol. Blood Marrow Transpl. *21*, 1955–1962. https://doi.org/10.1016/j.bbmt.2015.07.008.

18. Morris, G.P., and Allen, P.M. (2009). Cutting edge: highly alloreactive dual TCR T cells play a dominant role in graft-versus-host disease. J. Immunol. *182*, 6639–6643. https://doi.org/10.4049/jimmunol.0900638.

19. Ren, J., Liu, X., Fang, C., Jiang, S., June, C.H., and Zhao, Y. (2017). Multiplex genome editing to generate universal CAR T cells resistant to PD1 inhibition. Clin. Cancer Res. *23*, 2255–2266. https://doi.org/10.1158/1078-0432.ccr-16-1300.

20. Poirot, L., Philip, B., Schiffer-Mannioui, C., Le Clerre, D., Chion-Sotinel, I., Derniame, S., Potrel, P., Bas, C., Lemaire, L., Galetto, R., et al. (2015). Multiplex genome-edited T-cell manufacturing platform for "Off-the-Shelf" adoptive T-cell immunotherapies. Cancer Res. *75*, 3853–3864. https://doi.org/10.1158/0008-5472.can-14-3321.

21. Eyquem, J., Mansilla-Soto, J., Giavridis, T., van der Stegen, S.J.C., Hamieh, M., Cunanan, K.M., Odak, A., Gönen, M., and Sadelain, M. (2017). Targeting a CAR to the TRAC locus with CRISPR/Cas9 enhances tumour rejection. Nature *543*, 113–117. https://doi.org/10.1038/nature21405.

22. Kagoya, Y., Guo, T., Yeung, B., Saso, K., Anczurowski, M., Wang, C.H., Murata, K., Sugata, K., Saijo, H., Matsunaga, Y., et al. (2020). Genetic ablation of HLA class I, class II, and the T-cell receptor enables allogeneic T cells to be used for adoptive T-cell therapy. Cancer Immunol. Res. *8*, 926–936. https://doi.org/10.1158/2326-6066.cir-18-0508.

23. Levine, B.L., Miskin, J., Wonnacott, K., and Keir, C. (2017). Global manufacturing of CAR T cell therapy. Mol. Ther. Methods Clin. Dev. *4*, 92–101. https://doi.org/10.1016/j.omtm.2016.12.006.

24. Tang, J., Hubbard-Lucey, V.M., Pearce, L., O'Donnell-Tormey, J., and Shalabi, A. (2018). The global landscape of cancer cell therapy. Nat. Rev. Drug Discov. *17*, 465–466. https://doi.org/10.1038/nrd.2018.74.

25. Gu, Q., and Cynader, M.S. (1993). Immunocytochemical localization of enkephalin in the cat visual cortex. Brain Res. *620*, 155–158. https://doi.org/10.1016/0006-8993(93)90284-t.

26. Wang, X., and Rivière, I. (2016). Clinical manufacturing of CAR T cells: foundation of a promising therapy. Mol. Ther. Oncolytics *3*, 16015. https://doi.org/10.1038/mto.2016.15.

27. Tipanee, J., Chai, Y.C., VandenDriessche, T., and Chuah, M.K. (2017). Preclinical and clinical advances in transposon-based gene therapy. Biosci. Rep. *37*. BSR20160614. https://doi.org/10.1042/bsr20160614.

28. Tipanee, J., VandenDriessche, T., and Chuah, M.K. (2017). Transposons: moving forward from preclinical studies to clinical trials. Hum. Gene Ther. *28*, 1087–1104. https://doi.org/10.1089/hum.2017.128.

29. Deichmann, A., Hacein-Bey-Abina, S., Schmidt, M., Garrigue, A., Brugman, M.H., Hu, J., Glimm, H., Gyapay, G., Prum, B., Fraser, C.C., et al. (2007). Vector integration is nonrandom and clustered and influences the fate of lymphopoiesis in SCID-X1 gene therapy. J. Clin. Invest. *117*, 2225–2232. https://doi.org/10.1172/jci31659.

30. Hacein-Bey-Abina, S., Garrigue, A., Wang, G.P., Soulier, J., Lim, A., Morillon, E., Clappier, E., Caccavelli, L., Delabesse, E., Beldjord, K., et al. (2008). Insertional oncogenesis in 4 patients after retrovirus-mediated gene therapy of SCID-X1. J. Clin. Invest. *118*, 3132–3142. https://doi.org/10.1172/jci35700.

31. Walisko, O., Schorn, A., Rolfs, F., Devaraj, A., Miskey, C., Izsvák, Z., and Ivics, Z. (2008). Transcriptional activities of the Sleeping Beauty transposon and shielding its genetic cargo with insulators. Mol. Ther. *16*, 359–369. https://doi.org/10.1038/sj.mt.6300366.

32. Mátés, L., Chuah, M.K.L., Belay, E., Jerchow, B., Manoj, N., Acosta-Sanchez, A., Grzela, D.P., Schmitt, A., Becker, K., Matrai, J., et al. (2009). Molecular evolution of a novel hyperactive Sleeping Beauty transposase enables robust stable gene transfer in vertebrates. Nat. Genet. *41*, 753–761. https://doi.org/10.1038/ng.343.

33. Monjezi, R., Miskey, C., Gogishvili, T., Schleef, M., SchMeer, M., Einsele, H., Ivics, Z., and Hudecek, M. (2017). Enhanced CAR T-cell engineering using non-viral Sleeping Beauty transposition from minicircle vectors. Leukemia *31*, 186–194. https://doi.org/10.1038/leu.2016.180.

34. Kebriaei, P., Singh, H., Huls, M.H., Figliola, M.J., Bassett, R., Olivares, S., Jena, B., Dawson, M.J., Kumaresan, P.R., Su, S., et al. (2016). Phase I trials using Sleeping Beauty to generate CD19-specific CAR T cells. J. Clin. Invest. *126*, 3363–3376. https://doi.org/10.1172/jci86721.

35. Torikai, H., Reik, A., Liu, P.Q., Zhou, Y., Zhang, L., Maiti, S., Huls, H., Miller, J.C., Kebriaei, P., Rabinovitch, B., et al. (2012). A foundation for universal T-cell based immunotherapy: T cells engineered to express a CD19-specific chimeric-antigen-receptor and eliminate expression of endogenous TCR. Blood *119*, 5697–5705. https://doi.org/10.1182/blood-2012-01-405365.

36. Ivics, Z., Hackett, P.B., Plasterk, R.H., and Izsvák, Z. (1997). Molecular reconstruction of Sleeping Beauty, a Tc1-like transposon from fish, and its transposition in human cells. Cell *91*, 501–510. https://doi.org/10.1016/s0092-8674(00)80436-5.

37. Berdien, B., Mock, U., Atanackovic, D., Fehse, B., and Mock, U. (2014). TALEN-mediated editing of endogenous T-cell receptors facilitates efficient reprogramming of T lymphocytes by lentiviral gene transfer. Gene Ther. *21*, 539–548. https://doi.org/10.1038/gt.2014.26.

38. Zhang, Z., Qiu, S., Zhang, X., and Chen, W. (2018). Optimized DNA electroporation for primary human T cell engineering. BMC Biotechnol. *18*, 4. https://doi.org/10.1186/s12896-018-0419-0.

39. Ingegnere, T., Mariotti, F.R., Pelosi, A., Quintarelli, C., De Angelis, B., Tumino, N., Besi, F., Cantoni, C., Locatelli, F., Vacca, P., and Moretta, L. (2019). Human CAR NK cells: a new non-viral method allowing high efficient transfection and strong tumor cell killing. Front. Immunol. *10*, 957. https://doi.org/10.3389/fimmu.2019.00957.

40. Huang, R.S., Lai, M.C., Shih, H.A., and Lin, S. (2021). A robust platform for expansion and genome editing of primary human natural killer cells. J. Exp. Med. *218*. e20201529. https://doi.org/10.1084/jem.20201529.

41. Hutson, T.H., Buchser, W.J., Bixby, J.L., Lemmon, V.P., and Moon, L.D.F. (2011). Optimization of a 96-well electroporation assay for postnatal rat CNS neurons suitable for cost-effective medium-throughput screening of genes that promote neurite outgrowth. Front. Mol. Neurosci. *4*, 55. https://doi.org/10.3389/fnmol.2011.00055.

42. Riepe, C., Zelin, E., Frankino, P.A., Meacham, Z.A., Fernandez, S.G., Ingolia, N.T., and Corn, J.E. (2022). Double stranded DNA breaks and genome editing trigger loss of ribosomal protein RPS27A. FEBS J. *289*, 3101–3114. https://doi.org/10.1111/febs.16321.

43. Kay, M.A., He, C.Y., and Chen, Z.Y. (2010). A robust system for production of minicircle DNA vectors. Nat. Biotechnol. *28*, 1287–1289. https://doi.org/10.1038/nbt.1708.

44. Mátrai, J., Cantore, A., Bartholomae, C.C., Annoni, A., Wang, W., Acosta-Sanchez, A., Samara-Kuko, E., De Waele, L., Ma, L., Genovese, P., et al. (2011). Hepatocyte-targeted expression by integrase-defective lentiviral vectors induces antigen-specific tolerance in mice with low genotoxic risk. Hepatology *53*, 1696–1707. https://doi.org/10.1002/hep.24230.

45. Wu, X., and Burgess, S.M. (2004). Integration target site selection for retroviruses and transposable elements. Cell Mol. Life Sci. *61*, 2588–2596. https://doi.org/10.1007/s00018-004-4206-9.

46. Demeulemeester, J., De Rijck, J., Gijsbers, R., and Debyser, Z. (2015). Retroviral integration: site matters: mechanisms and consequences of retroviral integration site selection. Bioessays *37*, 1202–1214. https://doi.org/10.1002/bies.201500051.

47. Bougnères, P., Hacein-Bey-Abina, S., Labik, I., Adamsbaum, C., Castaignède, C., Bellesme, C., and Schmidt, M. (2021). Long-term follow-up of hematopoietic stem-cell gene therapy for cerebral adrenoleukodystrophy. Hum. Gene Ther. *32*, 1260–1269. https://doi.org/10.1089/hum.2021.053.

48. Hacein-Bey-Abina, S., Von Kalle, C., Schmidt, M., McCormack, M.P., Wulffraat, N., Leboulch, P., Lim, A., Osborne, C.S., Pawliuk, R., Morillon, E., et al. (2003). LMO2-associated clonal T cell proliferation in two patients after gene therapy for SCID-X1. Science *302*, 415–419. https://doi.org/10.1126/science.1088547.

49. Ott, M.G., Schmidt, M., Schwarzwaelder, K., Stein, S., Siler, U., Koehl, U., Glimm, H., Kühlcke, K., Schilz, A., Kunkel, H., et al. (2006). Correction of X-linked chronic granulomatous disease by gene therapy, augmented by insertional activation of MDS1-EVI1, PRDM16 or SETBP1. Nat. Med. *12*, 401–409. https://doi.org/10.1038/nm1393.

50. Howe, S.J., Mansour, M.R., Schwarzwaelder, K., Bartholomae, C., Hubank, M., Kempski, H., Brugman, M.H., Pike-Overzet, K., Chatters, S.J., de Ridder, D., et al. (2008). Insertional mutagenesis combined with acquired somatic mutations causes leukemogenesis following gene therapy of SCID-X1 patients. J. Clin. Invest. *118*, 3143–3150. https://doi.org/10.1172/jci35798.

51. Braun, C.J., Boztug, K., Paruzynski, A., Witzel, M., Schwarzer, A., Rothe, M., Modlich, U., Beier, R., Göhring, G., Steinemann, D., et al. (2014). Gene therapy for Wiskott-Aldrich syndrome–long-term efficacy and genotoxicity. Sci. Transl. Med. *6*, 227ra33. https://doi.org/10.1126/scitranslmed.3007280.

52. Naserian, S., Leclerc, M., Thiolat, A., Pilon, C., Le Bret, C., Belkacemi, Y., Maury, S., Charlotte, F., and Cohen, J.L. (2018). Simple, reproducible, and efficient clinical grading system for murine models of acute graft-versus-host disease. Front. Immunol. *9*, 10. https://doi.org/10.3389/fimmu.2018.00010.

53. Lai, H.Y., Chou, T.Y., Tzeng, C.H., and Lee, O.K.S. (2012). Cytokine profiles in various graft-versus-host disease target organs following hematopoietic stem cell transplantation. Cell Transplant. *21*, 2033–2045. https://doi.org/10.3727/096368912x653110.

54. Westphal, S., McGeary, A., Rudloff, S., Wilke, A., and Penack, O. (2017). The green tea catechin epigallocatechin gallate ameliorates graft-versus-host disease. PLoS One *12*, e0169630. https://doi.org/10.1371/journal.pone.0169630.

55. Morin, F., Kavian, N., Nicco, C., Cerles, O., Chéreau, C., and Batteux, F. (2016). Improvement of sclerodermatous graft-versus-host disease in mice by niclosamide. J. Invest. Dermatol. *136*, 2158–2167. https://doi.org/10.1016/j.jid.2016.06.624.

56. Pai, C.C.S., Hsiao, H.H., Sun, K., Chen, M., Hagino, T., Tellez, J., Mall, C., Blazar, B.R., Monjazeb, A., Abedi, M., and Murphy, W.J. (2014). Therapeutic benefit of bortezomib on acute graft-versus-host disease is tissue specific and is associated with interleukin-6 levels. Biol. Blood Marrow Transplant. *20*, 1899–1904. https://doi.org/10.1016/j.bbmt.2014.07.022.

57. Matsukuma, K.E., Wei, D., Sun, K., Ramsamooj, R., and Chen, M. (2016). Diagnosis and differential diagnosis of hepatic graft versus host disease (GVHD). J. Gastrointest. Oncol. *7*, S21–S31. https://doi.org/10.3978/j.issn.2078-6891.2015.036.

58. Lu, Y., Sakamaki, S., Kuroda, H., Kusakabe, T., Konuma, Y., Akiyama, T., Fujimi, A., Takemoto, N., Nishiie, K., Matsunaga, T., et al. (2001). Prevention of lethal acute graft-versus-host disease in mice by oral administration of T helper 1 inhibitor, TAK-603. Blood *97*, 1123–1130. https://doi.org/10.1182/blood.v97.4.1123.

59. Tago, Y., Kobayashi, C., Ogura, M., Wada, J., Yamaguchi, S., Yamaguchi, T., Hayashi, M., Nakaishi, T., Kubo, H., and Ueda, Y. (2021). Human amnion-derived mesenchymal stem cells attenuate xenogeneic graft-versus-host disease by preventing T cell activation and proliferation. Sci. Rep. *11*, 2406. https://doi.org/10.1038/s41598-021-81916-y.

60. Stenger, D., Stief, T.A., Kaeuferle, T., Willier, S., Rataj, F., Schober, K., Vick, B., Lotfi, R., Wagner, B., Grünewald, T.G.P., et al. (2020). Endogenous TCR promotes in vivo persistence of CD19-CAR-T cells compared to a CRISPR/Cas9-mediated TCR knockout CAR. Blood *136*, 1407–1418. https://doi.org/10.1182/blood.2020005185.

61. Cruz, C.R.Y., Micklethwaite, K.P., Savoldo, B., Ramos, C.A., Lam, S., Ku, S., Diouf, O., Liu, E., Barrett, A.J., Ito, S., et al. (2013). Infusion of donor-derived CD19-redirected virus-specific T cells for B-cell malignancies relapsed after allogeneic stem cell transplant: a phase 1 study. Blood *122*, 2965–2973. https://doi.org/10.1182/blood-2013-06-506741.

62. Yang, K.S., Im, H., Hong, S., Pergolini, I., del Castillo, A.F., Wang, R., Clardy, S., Huang, C.H., Pille, C., Ferrone, S., et al. (2017). Multiparametric plasma EV profiling facilitates diagnosis of pancreatic malignancy. Sci. Transl. Med. *9*, eaal3226. https://doi.org/10.1126/scitranslmed.aal3226.

63. Malissen, B., Grégoire, C., Malissen, M., and Roncagalli, R. (2014). Integrative biology of T cell activation. Nat. Immunol. *15*, 790–797. https://doi.org/10.1038/ni.2959.

64. Ashwell, J.D. (2006). The many paths to p38 mitogen-activated protein kinase activation in the immune system. Nat. Rev. Immunol. *6*, 532–540. https://doi.org/10.1038/nri1865.

65. Zheng, W., O'Hear, C.E., Alli, R., Basham, J.H., Abdelsamed, H.A., Palmer, L.E., Jones, L.L., Youngblood, B., and Geiger, T.L. (2018). PI3K orchestration of the in vivo persistence of chimeric antigen receptor-modified T cells. Leukemia *32*, 1157–1167. https://doi.org/10.1038/s41375-017-0008-6.

66. Lucas, C.L., Chandra, A., Nejentsev, S., Condliffe, A.M., and Okkenhaug, K. (2016). PI3Kδ and primary immunodeficiencies. Nat. Rev. Immunol. *16*, 702–714. https://doi.org/10.1038/nri.2016.93.

67. Cheng, C., Tang, N., Li, J., Cao, S., Zhang, T., Wei, X., and Wang, H. (2019). Bacteria-free minicircle DNA system to generate integration-free CAR-T cells. J. Med. Genet. *56*, 10–17. https://doi.org/10.1136/jmedgenet-2018-105405.

68. Roth, T.L., Puig-Saus, C., Yu, R., Shifrut, E., Carnevale, J., Li, P.J., Hiatt, J., Saco, J., Krystofinski, P., Li, H., et al. (2018). Reprogramming human T cell function and specificity with non-viral genome targeting. Nature *559*, 405–409. https://doi.org/10.1038/s41586-018-0326-5.

69. Magnani, C.F., Gaipa, G., Lussana, F., Belotti, D., Gritti, G., Napolitano, S., Matera, G., Cabiati, B., Buracchi, C., Borleri, G., et al. (2020). Sleeping Beauty-engineered CAR T cells achieve antileukemic activity without severe toxicities. J. Clin. Invest. *130*, 6021–6033. https://doi.org/10.1172/jci138473.

70. Neal, L.R., Bailey, S.R., Wyatt, M.M., Bowers, J.S., Majchrzak, K., Nelson, M.H., Haupt, C., Paulos, C.M., and Varela, J.C. (2017). The basics of artificial antigen presenting cells in T cell-based cancer immunotherapies. J. Immunol. Res. Ther. *2*, 68–79.

71. Mujib, S., Jones, R.B., Lo, C., Aidarus, N., Clayton, K., Sakhdari, A., Benko, E., Kovacs, C., and Ostrowski, M.A. (2012). Antigen-independent induction of Tim-3 expression on human T cells by the common gamma-chain cytokines IL-2, IL-7, IL-15, and IL-21 is associated with proliferation and is dependent on the phosphoinositide 3-kinase pathway. J. Immunol. *188*, 3745–3756. https://doi.org/10.4049/jimmunol.1102609.

72. Chicaybam, L., Abdo, L., Viegas, M., Marques, L.V.C., de Sousa, P., Batista-Silva, L.R., Alves-Monteiro, V., Bonecker, S., Monte-Mór, B., and Bonamino, M.H. (2020). Transposon-mediated generation of CAR-T cells shows efficient anti B-cell leukemia response after ex vivo expansion. Gene Ther. *27*, 85–95. https://doi.org/10.1038/s41434-020-0121-4.

73. Avery, L., Filderman, J., Szymczak-Workman, A.L., and Kane, L.P. (2018). Tim-3 co-stimulation promotes short-lived effector T cells, restricts memory precursors, and is dispensable for T cell exhaustion. Proc. Natl. Acad. Sci. USA *115*, 2455–2460. https://doi.org/10.1073/pnas.1712107115.

74. Konduri, V., Joseph, S.K., Byrd, T.T., Nawas, Z., Vazquez-Perez, J., Hofferek, C.J., Halpert, M.M., Liu, D., Liang, Z., Baig, Y., et al. (2021). A subset of cytotoxic effector memory T cells enhances CAR T cell efficacy in a model of pancreatic ductal adenocarcinoma. Sci. Transl. Med. *13*, eabc3196. https://doi.org/10.1126/scitranslmed.abc3196.

75. Maiti, S.N., Huls, H., Singh, H., Dawson, M., Figliola, M., Olivares, S., Rao, P., Zhao, Y.J., Multani, A., Yang, G., et al. (2013). Sleeping beauty system to redirect T-cell specificity for human applications. J. Immunother. *36*, 112–123. https://doi.org/10.1097/cji.0b013e3182811ce9.

76. Kebriaei, P., Huls, H., Neel, R.N.S., Olivares, S., Orozco, A., Su, S., Maiti, S., Smith, A., Groot, E.D., Kantarjian, H., et al. (2017). Shortening the time to manufacture CAR+T cells with sleeping beauty system supports T-cell engraftment and anti-tumor effects in patients with refractory CD19+Tumors. Blood *130*, 2060.

77. Stroncek, D.F., Lee, D.W., Ren, J., Sabatino, M., Highfill, S., Khuu, H., Shah, N.N., Kaplan, R.N., Fry, T.J., and Mackall, C.L. (2017). Elutriated lymphocytes for manufacturing chimeric antigen receptor T cells. J. Transl. Med. *15*, 59. https://doi.org/10.1186/s12967-017-1160-5.

78. Bridgeman, J.S., Hawkins, R.E., Bagley, S., Blaylock, M., Holland, M., and Gilham, D.E. (2010). The optimal antigen response of chimeric antigen receptors harboring the CD3ζ transmembrane domain is dependent upon incorporation of the receptor into the endogenous TCR/CD3 complex. J. Immunol. *184*, 6938–6949. https://doi.org/10.4049/jimmunol.0901766.

79. Stephensen, C.B., Borowsky, A.D., and Lloyd, K.C.K. (2007). Disruption of Rxra gene in thymocytes and T lymphocytes modestly alters lymphocyte frequencies, proliferation, survival and T helper type 1/type 2 balance. Immunology *121*, 484–498. https://doi.org/10.1111/j.1365-2567.2007.02595.x.

80. Dawson, H.D., Collins, G., Pyle, R., Key, M., and Taub, D.D. (2008). The Retinoic Acid Receptor-alpha mediates human T-cell activation and Th2 cytokine and chemokine production. BMC Immunol. *9*, 16. https://doi.org/10.1186/1471-2172-9-16.

81. Yang, Y., Kohler, M.E., Chien, C.D., Sauter, C.T., Jacoby, E., Yan, C., Hu, Y., Wanhainen, K., Qin, H., and Fry, T.J. (2017). TCR engagement negatively affects CD8 but not CD4 CAR T cell expansion and leukemic clearance. Sci. Transl. Med. *9*, eaag1209. https://doi.org/10.1126/scitranslmed.aag1209.

82. Zeng, L., Palaia, I., Šarić, A., and Su, X. (2021). PLCγ1 promotes phase separation of T cell signaling components. J. Cell Biol. *220*. e202009154. https://doi.org/10.1083/jcb.202009154.

83. Lo, W.L., Shah, N.H., Rubin, S.A., Zhang, W., Horkova, V., Fallahee, I.R., Stepanek, O., Zon, L.I., Kuriyan, J., and Weiss, A. (2019). Slow phosphorylation of a tyrosine residue in LAT optimizes T cell ligand discrimination. Nat. Immunol. *20*, 1481–1493. https://doi.org/10.1038/s41590-019-0502-2.

84. Gudipati, V., Rydzek, J., Doel-Perez, I., Gonçalves, V.D.R., Scharf, L., Königsberger, S., Lobner, E., Kunert, R., Einsele, H., Stockinger, H., et al. (2020). Inefficient CAR-proximal signaling blunts antigen sensitivity. Nat. Immunol. *21*, 848–856. https://doi.org/10.1038/s41590-020-0719-0.

85. Zhong, X.S., Matsushita, M., Plotkin, J., Riviere, I., and Sadelain, M. (2010). Chimeric antigen receptors combining 4-1BB and CD28 signaling domains augment PI3kinase/AKT/Bcl-XL activation and CD8+ T cell-mediated tumor eradication. Mol. Ther. *18*, 413–420. https://doi.org/10.1038/mt.2009.210.

86. Herrero-Sánchez, M.C., Rodríguez-Serrano, C., Almeida, J., San Segundo, L., Inogés, S., Santos-Briz, Á., García-Briñón, J., Corchete, L.A., San Miguel, J.F., del Cañizo, C., and Blanco, B. (2016). Targeting of PI3K/AKT/mTOR pathway to inhibit T cell activation and prevent graft-versus-host disease development. J. Hematol. Oncol. *9*, 113. https://doi.org/10.1186/s13045-016-0343-5.

87. Lapteva, N., Gilbert, M., Diaconu, I., Rollins, L.A., Al-Sabbagh, M., Naik, S., Krance, R.A., Tripic, T., Hiregange, M., Raghavan, D., et al. (2019). T-cell receptor stimulation enhances the expansion and function of CD19 chimeric antigen receptor-expressing T cells. Clin. Cancer Res. *25*, 7340–7350. https://doi.org/10.1158/1078-0432.ccr-18-3199.

88. He, P., Wang, B.H., Cao, R.R., Zhu, D.C., Ge, B., Zhou, X., Wu, L.F., Lei, S.F., and Deng, F.Y. (2021). ITGA2 protein is associated with rheumatoid arthritis in

Chinese and affects cellular function of T cells. Clin. Chim. Acta *523*, 208–215. https://doi.org/10.1016/j.cca.2021.09.024.

89. Arias, C.F., Ballesteros-Tato, A., García, M.I., Martín-Caballero, J., Flores, J.M., Martínez-A, C., and Balomenos, D. (2007). p21CIP1/WAF1 controls proliferation of activated/memory T cells and affects homeostasis and memory T cell responses. J. Immunol. *178*, 2296–2306. https://doi.org/10.4049/jimmunol.178.4.2296.

90. Daszkiewicz, L., Vázquez-Mateo, C., Rackov, G., Ballesteros-Tato, A., Weber, K., Madrigal-Avilés, A., Di Pilato, M., Fotedar, A., Fotedar, R., Flores, J.M., et al. (2015). Distinct p21 requirements for regulating normal and self-reactive T cells through IFN-gamma production. Sci. Rep. *5*, 7691. https://doi.org/10.1038/srep07691.

91. Wei, Z., Du, Q., Li, P., Liu, H., Xia, M., Chen, Y., Bi, G., Tang, Z.H., Cheng, X., Lu, Y., et al. (2021). Death-associated protein kinase 1 (DAPK1) controls CD8(+) T cell activation, trafficking, and antitumor activity. FASEB J. *35*, e21138. https://doi.org/10.1096/fj.201903067rr.

92. Wei, Z., Li, P., He, R., Liu, H., Liu, N., Xia, Y., Bi, G., Du, Q., Xia, M., Pei, L., et al. (2021). DAPK1 (death associated protein kinase 1) mediates mTORC1 activation and antiviral activities in CD8(+) T cells. Cell Mol. Immunol. *18*, 138–149. https://doi.org/10.1038/s41423-019-0293-2.

93. Byrd, V.M., Kilkenny, D.M., Dikov, M.M., Reich, M.B., Rocheleau, J.V., Armistead, W.J., Thomas, J.W., and Miller, G.G. (2003). Fibroblast growth factor receptor-1 interacts with the T-cell receptor signalling pathway. Immunol. Cell Biol. *81*, 440–450. https://doi.org/10.1046/j.1440-1711.2003.01199.x.

94. van der Windt, G.J., Everts, B., Chang, C.H., Curtis, J., Freitas, T., Amiel, E., Pearce, E., and Pearce, E. (2012). Mitochondrial respiratory capacity is a critical regulator of CD8+ T cell memory development. Immunity *36*, 68–78. https://doi.org/10.1016/j.immuni.2011.12.007.

95. Lancien, M., Gueno, L., Salle, S., Merieau, G., Beriou, K., Nguyen, T.H., Abidi, A., Solomon, P., and Poschmann, J. (2021). Cystathionine-gamma-lyase overexpression in T cells enhances antitumor effect independently of cysteine autonomy. Cancer Sci. *112*, 1723–1743. https://doi.org/10.1111/cas.14862.

96. Erdenebayar, N., Maekawa, Y., Nishida, J., Kitamura, A., and Yasutomo, K. (2009). Protein-tyrosine phosphatase-kappa regulates CD4+ T cell development through ERK1/2-mediated signaling. Biochem. Biophys. Res. Commun. *390*, 489–493. https://doi.org/10.1016/j.bbrc.2009.09.117.

97. Gu, M., Zhou, X., Sohn, J.H., Zhu, L., Jie, Z., Yang, J.Y., Zheng, X., Xie, X., Yang, J., Shi, Y., et al. (2021). NF-κB-inducing kinase maintains T cell metabolic fitness in antitumor immunity. Nat. Immunol. *22*, 193–204. https://doi.org/10.1038/s41590-020-00829-6.

98. Sukumar, M., Liu, J., Ji, Y., Subramanian, M., Crompton, J.G., Yu, Z., Roychoudhuri, R., Palmer, D.C., Muranski, P., Karoly, E.D., et al. (2013). Inhibiting glycolytic metabolism enhances CD8+ T cell memory and antitumor function. J. Clin. Invest. *123*, 4479–4488. https://doi.org/10.1172/jci69589.

99. Drijvers, J.M., Gillis, J.E., Muijlwijk, T., Nguyen, T.H., Gaudiano, E.F., Harris, I.S., LaFleur, M.W., Ringel, A.E., Yao, C.H., Kurmi, K., et al. (2021). Pharmacologic screening identifies metabolic vulnerabilities of CD8(+) T cells. Cancer Immunol. Res. *9*, 184–199. https://doi.org/10.1158/2326-6066.cir-20-0384.

100. Zhang, Y., Zhang, Z., Ding, Y., Fang, Y., Wang, P., Chu, W., Jin, Z., Yang, X., Wang, J., Lou, J., and Qian, Q. (2021). Phase I clinical trial of EGFR-specific CAR-T cells generated by the piggyBac transposon system in advanced relapsed/refractory non-small cell lung cancer patients. J. Cancer Res. Clin. Oncol. *147*, 3725–3734. https://doi.org/10.1007/s00432-021-03613-7.

101. Prommersberger, S., Reiser, M., Beckmann, J., Danhof, S., Amberger, M., Quade-Lyssy, P., Einsele, H., Hudecek, M., Bonig, H., and Ivics, Z. (2021). CARAMBA: a first-in-human clinical trial with SLAMF7 CAR-T cells prepared by virus-free Sleeping Beauty gene transfer to treat multiple myeloma. Gene Ther. *28*, 560–571. https://doi.org/10.1038/s41434-021-00254-w.

102. Hu, B., Zou, Y., Zhang, L., Tang, J., Niedermann, G., Firat, E., Huang, X., and Zhu, X. (2019). Nucleofection with plasmid DNA for CRISPR/Cas9-Mediated inactivation of programmed cell death protein 1 in CD133-specific CAR T cells. Hum. Gene Ther. *30*, 446–458. https://doi.org/10.1089/hum.2017.234.

103. Schambach, A., Morgan, M., and Fehse, B. (2021). Two cases of T cell lymphoma following Piggybac-mediated CAR T cell therapy. Mol. Ther. *29*, 2631–2633. https://doi.org/10.1016/j.ymthe.2021.08.013.

104. Bishop, D.C., Clancy, L.E., Simms, R., Burgess, J., Mathew, G., Moezzi, L., Street, J.A., Sutrave, G., Atkins, E., McGuire, H.M., et al. (2021). Development of CAR T-cell lymphoma in 2 of 10 patients effectively treated with piggyBac-modified CD19 CAR T cells. Blood *138*, 1504–1509. https://doi.org/10.1182/blood.2021010813.

105. Micklethwaite, K.P., Gowrishankar, K., Gloss, B.S., Li, Z., Street, J.A., Moezzi, L., Mach, M.A., Sutrave, G., Clancy, L.E., Bishop, D.C., et al. (2021). Investigation of product-derived lymphoma following infusion of piggyBac-modified CD19 chimeric antigen receptor T cells. Blood *138*, 1391–1405. https://doi.org/10.1182/blood.2021010858.

106. Wilson, M.H., and Gottschalk, S. (2021). Expect the unexpected: piggyBac and lymphoma. Blood *138*, 1379–1380. https://doi.org/10.1182/blood.2021012349.

107. Srour, S.A., Singh, H., McCarty, J., de Groot, E., Huls, H., Rondon, G., Qazilbash, M., Ciurea, S., Bardelli, G., Buck, J., et al. (2020). Long-term outcomes of Sleeping Beauty-generated CD19-specific CAR T-cell therapy for relapsed-refractory B-cell lymphomas. Blood *135*, 862–865. https://doi.org/10.1182/blood.2019002920.

108. Querques, I., Mades, A., Zuliani, C., Miskey, C., Alb, M., Grueso, E., Machwirth, M., Rausch, T., Einsele, H., Ivics, Z., et al. (2019). A highly soluble Sleeping Beauty transposase improves control of gene insertion. Nat. Biotechnol. *37*, 1502–1512. https://doi.org/10.1038/s41587-019-0291-z.

YMTHE, Volume *30*

Supplemental Information

Universal allogeneic CAR T cells engineered with *Sleeping Beauty* transposons and CRISPR-CAS9 for cancer immunotherapy

Jaitip Tipanee, Ermira Samara-Kuko, Thierry Gevaert, Marinee K. Chuah, and Thierry VandenDriessche

Supplemental method

Construction of DNA transposon/transposase vector and minicircle production

A multicistronic vector was generated to co-express the CD19-targeting chimeric receptor (CD19-28z.CAR) consisting of i) the variable sequence of the FMC63,[1] ii) the human CD28 signaling domain, and iii) the CD3-zeta domain (GenBank: HM852952.1), and a GFP reporter via the self-cleavable 2A peptide. The DNA sequence was codon-optimized for high mammalian gene expression and synthesized by GeneArt (Life Technologies, Belgium). The resulting gene fragment was subcloned into a parental SB transposon plasmid for gene expression under the control of the hybrid EF1/HTLV promoter (Invivogen, Belgium). The pCMV-SB100x was generated as described to express hyperactive SB transposase for SB transposition.[2] The production of mcDNA vectors encoding CD19-28z.CAR (mcCD19-28z.CAR) and SB100x (mcSB100x) was achieved by PlasmidFactory (Bielefeld, Germany) through site-specific DNA recombination, followed by affinity chromatography purification.

Primary human T cell isolation and culture

Human peripheral blood–derived buffy coats from anonymous blood donors were obtained from Biobank Rode Kruis-Vlaanderen (Mechelen, Belgium). All procedures were approved by Commissie Medische Ethiek of Universitair Ziekenhuis Brussel (Belgium). Buffy coat samples were diluted two times using 1× Dulbecco's PBS without calcium and magnesium, and diluted samples were subjected to density gradient centrifugation using Ficoll (GE Healthcare) at 800 ×*g* for 40 minutes without brake to isolate peripheral blood mononuclear cells. Next, human CD8+ T cells or CD3+ T cells were enriched from peripheral blood mononuclear cells using the CD8+ T Cell Isolation Kit or Pan T Cell Isolation Kit (Miltenyi Biotec), respectively. Prior to nucleofection, human T cells were stimulated with Dynabeads Human T-Activator CD3/CD28 (ThermoFisher Scientific) with a 1:1 bead-to-cell ratio. The cells were cultured in complete T cell medium (RPMI-1640 medium supplemented with Glutamax + 10% of heat-inactivated fetal bovine serum + 100 U/mL penicillin-streptomycin; Life Technologies, Belgium) in the presence of 30 U/mL of recombinant human IL-2 (Miltenyi Biotec) at a cell density of 1×10^6 cells/mL for 48 to 72 hours under 5% CO_2 at 37°C.

Cell lines

Human chronic myeloid leukemia in blast crisis K562, human Burkitt lymphoma Raji, and B cell precursor leukemia NALM6 cell lines were purchased from Deutsche Sammlung von Mikroorganismen und Zellkulturen. K562 expressing truncated CD19 antigen (K562-CD19t), which harbors the extracellular and transmembrane domains (amino acid positions 1 to 312) and lacks the intracellular domain, was generated by lentiviral vector transduction of LV-CMV-CD19t. Subsequently, K562, K562-CD19t, Raji, and NALM6 cell lines were lentivirally transduced by LV-CMV-Luc-2A-GFP to co-express GFP and firefly *Photinus pyralis* luciferase reporter proteins. All cell lines are cultured in complete T cell medium at cell density $3–5\times10^5$ cells/mL.

Design of sgRNAs targeting *TRAC* and *TRBC2*

The first exon regions of the *TRAC* and *TRBC2* genes were used as the target sequences for gene disruption, and targeted sgRNAs were designed with the ZiFiT Targeter Version 4.2 online software[3] and/or Sigma Aldrich custom design. All sgRNA sequences targeting *TRAC* and *TRBC2* genes in this study are given in the supplemental information (Table S1).

CRISPR/Cas9 system for gene disruption

All *TRAC* and *TRBC2*-targeting gRNA were pre-screened in HEK 293 cell lines to select the most efficient gRNAs for TCR disruption. Different gRNAs were cloned into the pLV-U6g-EPCG all-in-one vector CRISPR/Cas9 vector plasmid (Sigma Aldrich, Belgium), and each pLV-U6g-EPCG harboring specific gRNA was transfected into HEK293 cells using Lipofectamine 3000 (Life Technologies, Belgium) and cultured for 7 days under puromycin selection. Next, genomic DNA was further extracted from transfected cells for subsequent analysis by the T7E1 assay to determine the specific gRNAs that displayed the highest gene knockout efficiency. These *TRAC* and *TRBC2*-targeting gRNAs were selected for subsequent validation in human CD8+ T cells.

For targeted disruption of *TRAC* and *TRBC2* genes in human CD8+ T cells, CRISPR/Cas9 RNP particles were prepared using chemically modified 2'-O-methyl 3'phosphorothioate synthesized sgRNA (Synthego, USA) and Alt-R® S.p. Cas9 Nuclease V3 (Integrated DNA Technologies, Belgium). For a single reaction, 70 pmol of chemically

modified sgRNA was slowly mixed with 70 pmol of Cas9 nuclease and left to stand at room temperature for 15 minutes to obtain 70 pmol of CRISPR/Cas9 RNP particles.

Generation of GFP+/TCR^{neg} human CD8+ T cells

The pmaxGFP control plasmid supplied with the P3 Primary Cell 4D-Nucleofector™ X Kit was employed for GFP reporter expression in human CD8+ T cells. For generation of GFP+/TCR^{neg} T cells using the single nucleofection approach, 0.5 µg of pmaxGFP plasmid and 70 pmol of *TRAC*-targeting TCR-1 RNP particles were transfected into 5×10^5 CD8+ T cells using the EH-115 program. Alternatively, sequential nucleofection of TCR-1 and pmaxGFP was used to produce GFP+/TCR^{neg} T cells. First, 70 pmol of TCR-1 RNP particles was transfected into 5×10^5 CD8+ T cells using the EH-115 program. Twenty-four hours post-transfection, 0.5 µg of pmaxGFP was subsequently delivered into 5×10^5 transfected cells using the EO-115 program. For a sequential nucleofection with CD3+ depletion, the TCR/CD3^{neg} T cell population was magnetically enriched using human CD3 MicroBeads (Miltenyi Biotec, Belgium) after 24 hours of TCR-1 nucleofection. Only purified TCR/CD3^{neg} T cells after MACS were used for subsequent pmaxGFP nucleofection.

Selective expansion of SB-CD19-28z.CAR/TCR KO T cells

For the conventional selective expansion of SB-CD19-28z.CAR/TCR KO and SB-CD19-28.CAR/scrambled control T cells, the transfected cells were cocultured with 100 Gy-irradiated NALM6 feeder cells (TrueBeam STX radiotherapy system, Varian) at an effector-to-target ratio of 1:2 in the complete T cell medium in the presence of 50 U/mL human rIL-2 (Miltenyi Biotec), 30 ng/mL human IL-21 (Miltenyi Biotec), 10 ng/mL human IL-15 (Miltenyi Biotec), and 10 ng/mL human IL-7 (Miltenyi Biotec). The CAR T cells were counted by flow cytometry for weekly addition of feeder cells, and media change with cytokine supplement was carried out on a Monday/Wednesday/Friday schedule. At the end of the 6-week CAR T cell expansion, the fraction of CAR+ T cells was enriched by MACS using allophycocyanin (APC)-conjugated recombinant human CD19 protein (Creative Biolabs, USA) and anti-APC microbeads (Miltenyi Biotec). The enriched CAR+ T cells were rested in the complete T cell medium and harvested for subsequent assays. Alternatively, for the short expansion protocol, CAR+ T cells were enriched by MACS system after 24 hours post-transfection, and only CAR+ cell fraction was expanded for 14 days by weekly NALM6 stimulation in completed T cell medium supplemented with cytokines.

CD107a degranulation assay

A total of 2×10^5 CAR or control T cells was cocultured with the different target tumor cells at an effector:target ratio of 1:2 in 100 µL of phenol-free RPMI-1640 containing 0.1% BD GolgiStop Protein Transport Inhibitor-Monensin + PE Mouse Anti-Human CD107a, Clone H4A3 (BD Bioscience, Belgium). The effector–target cell mixture was plated in a U-bottom 96-well plate and incubated at 37°C under 5% CO_2 for at least 6 hours. The cells were stained for CAR expression and subjected to flow cytometry analysis.

Luciferase-based cytotoxicity assay

A total of 3×10^3 target tumor cells was cocultured with CAR or control T cells at the different effector-to-target ratios in 200 µL of the phenol-free RPMI-1640 for 48 and 72 hours based on the experimental setting, and the target/effector cocultures were subjected to luciferase activity measurement to determine the residual target tumor cells at the endpoint. The 20 µL of ONE-Glo EX Luciferase Assay System (Promega, Belgium) luciferin substrate was added to the coculture, and the mixture was incubated for 1 minute at room temperature. The luciferase signal generated by the remaining tumor cells was acquired by GloMax® Discover Microplate Reader (Promega, Belgium). The percentage of target lysis was determined using the formula [1-(RLUsample+target cells/RLUtarget cell only)]× 100 in relation to untreated cells.[4]

Cytokine secretion assay

A total of 3×10^3 different target tumor cells was cocultured with CAR or control T cells at the effector:target ratios of 10:1 in 200 µL of the phenol-free RPMI-1640 for 48–72 hours. Next, the cell supernatant containing secreted cytokines was harvested, and the cytokine levels were measured using the human MACSPlex Cytokine 12 Kit (Miltenyi Biotec, The Netherlands) and the human ELISA MAX™ Deluxe Set (Biolegend, The Netherlands).

Alloreactivity assay

To mitigate the CAR-mediated effector cell proliferation due to CD19 antigen stimulation, 30 Gy-irradiated bulk allogeneic PBMCs (allo-PBMCs) were subjected to CD19 depletion by MACS sorting using anti human CD19 conjugated with microbead (Miltenyi Biotec, The Netherlands). Irradiation CD19-depleted allo-PBMCs were later used as a stimulator of CAR effector cells to determine the alloreactivity effects. A total of 1×10^6 CAR effector cells were labelled with CellTrace™ Far Red Cell Proliferation Kit (Life Technologies) and were subsequently cocultured with 5×10^6 CD19-depleted allo-PBMCs (E:T = 1:5) in the complete medium for 2, 4, and 6 days. Next, effector cell proliferation at different time points was analyzed by flow cytometry, and the percentages of proliferating cells with CD19-depleted allo-PBMC treatment were determined based on their counterparts without stimulator.

Animal experiments

All animal experiments were carried out under the procedures approved by the Institutional Animal Ethics Committee of the Vrije Universiteit Brussel (Brussels, Belgium). Six-week-old NSG male mice were purchased from Jackson Laboratory and housed in individually ventilated Thoren cages containing hygienic animal bedding from Lignocel at 21°C and 50%–60% humidity. Animals were fed *ad libitum* using SsniFF laboratory animal food (ABEDD Vertriebs, Vienna, Austria). For the NALM6-bearing tumor model with low tumor burden, the mice were inoculated via intravenous injection with 5×10^4 NALM6 cells expressing luciferase. Two days after NALM6 engraftment, 5×10^6 CAR or control T cells were intravenously infused into NALM6-bearing mice through the tail vein. Alternatively, to evaluate CAR T cell therapeutic efficacy in mice exhibiting high tumor burden, the mice received 1×10^5 NALM6 cells expressing luciferase, and intravenous administration of 5×10^6 effector T cells was carried out in NALM6-infused mice after 5 days of NALM6 engraftment. The development of tumor burden was assessed weekly using non-invasive *in vivo* bioluminescence imaging (BLI). In brief, 150 mg/kg body weight of D-Luciferin (Promega, Belgium) was administered intraperitoneally to each mouse, and the BLI signal was acquired for 7 minutes using an *in vivo* optical imaging system (PhotonImager, Biospace Lab, Paris, France). The data were processed and analyzed using M3 Vision software (Biospace) and expressed in average radiance (photons/s/cm^2/sr).

At several weeks post-NALM6 tumor engraftment, some mice developed the clinical signs of significant weight loss, severely hunched back, poor grooming, hind-limb paralysis, and/or limited mobility. These mice were euthanized as an endpoint by CO_2 inhalation or cervical dislocation. To determine the NALM6 tumor loads in the major lymphoid and non-lymphoid organs, single cell suspension was isolated from liver, spleen, and femur-derived bone marrow using mechanical tissue disruption, filtered through a 40-µm cell strainer and resuspended in Dulbecco's modified Eagle's medium + 10% heat-inactivated fetal bovine serum. Bulked cell pellets were treated with ACK Lysing Buffer (Life Technologies, Belgium) to eliminate red blood cells and resuspended in the PEB buffer (Miltenyi Biotec, The Netherlands). The isolated cells were subsequently used for CD19 staining using anti-human CD19 antibody (Miltenyi Biotec, The Netherlands).

For GvHD experiment, the mice were irradiated at the dose of 2 Gy on day 0. Six hours post-irradiation, 10×10^6 CAR T cells were intravenously infused into irradiated mice through the tail vein. The development of GvHD was assessed every Monday-Wednesday-Friday by observing the clinical GvHD signs (Table S7), and the clinical GvHD scores were assigned for each measurement. When the total score reached 6 or higher, or the score of any specific criteria reaches 2 (the highest severity), the mice were considered at humane endpoint and euthanized for subsequent analysis. Liver, small intestine and lung tissues were formalin fixed and subjected to histological analysis using HE staning to confirm GvHD histopathology.

Flow cytometry

In all flow cytometry experiments, cells were stained with 7-AAD Viability Staining Solution (Biolegend) to measure cell viability. Antibodies used in this study are listed in the Supplemental Information (Table S8). Surface staining of samples was performed in cold PEB buffer prepared from MACS BSA Stock Solution and autoMACS Running Buffer as per the manufacturer's instructions (Miltenyi Biotec). Flow-cytometric data acquisition was achieved using the BD FACSCanto™ II flow cytometry system (BD Biosciences). Data analysis was performed with BD FACSDiva™ software (BD Biosciences) and FlowJo version 7.6.1 software (BD Biosciences).

T7E1 mismatch detection assay

Total genomic DNA was extracted from T cells using DNeasy Blood & Tissue kits (Qiagen) following the manufacturer's protocols. Subsequently, 100 ng of genomic DNA was used as a DNA template for nested PCR amplification of gRNA-targeting DNA regions in the genome using DreamTaq Green PCR Master Mix (2×) (Life

Technologies). The primer sets used in nested PCR amplification are listed in the Supplemental Information (Table S2). For the first round of PCR amplification, 50 µL of PCR reaction was carried out at 95°C for 5 minutes, followed by 1 cycle of 95°C for 1 minute, 30 cycles of 57°C for 30 seconds, 72°C for 30 seconds, and 1 cycle of 72°C for 5 minutes. Next, 1 µL of the first-round PCR reaction was used as a template in 50 µL total volume during the second round PCR amplification under the following conditions: 95°C for 5 minutes, 1 cycle of 95°C for 1 minute, 35 cycles of 60°C for 30 seconds, 72°C for 30 seconds, and 1 cycle of 72°C for 5 minutes. The PCR product was cleaned up to remove excess PCR primers using the QIAquick PCR Purification Kit (Qiagen). For the T7E1 mismatch detection assay, 500 ng of purified nested PCR products in 20 µL of 1× NEBuffer 2 buffer (New England Biolabs) was reannealed at 1 cycle of 95°C for 5 minutes, followed by 95–85°C at a ramp-down rate of -2°C/second, 1 cycle of 85°C for 2 minutes, and 85–25°C at a ramp-down rate of -0.1°C/second. To cleave the mismatched DNA duplexes after reannealing, 10 U of T7 endonuclease I (New England Biolabs) was added to reannealed PCR product, and the reaction was incubated at 37°C for 30 minutes. The cleaved DNA fragments were subsequently separated using 1.5% agarose gel electrophoresis at 125 V for 80 minutes. Mean intensity values of both cleaved and uncleaved DNA bands were quantified using ImageJ software (NIH).[5] The indel percentage was calculated as follows: (total mean intensity value of cleaved DNA bands ×100)/ (total mean intensity value of cleaved DNA bands + total mean intensity value of uncleaved DNA bands).

Detection of CRISPR/Cas9-mediated indel mutation by DNA sequencing

The uncleaved nested PCR samples obtained by the T7E1 assay were ligated to the NEBNext® Ultra II Ligation modules (New England Biolabs) for sample preparation. A-tailing and ligation of sequencing adapters of the resulting product were performed according to the procedure described in the NEBNext Ultra End Repair module and NEBNext Ultra II Ligation module instruction manual. The processed samples were sequenced and analyzed using the NovaSeq6000 platform according to manufacturer's protocols (GenomeScan). Prior to sequence alignment, the reads were trimmed for adapter sequences and filtered for sequence quality. Presumed adapter sequences were removed from the read using Trimmomatic v0.30 when the bases matched a sequence in the adapter sequence set (TruSeq adapters) with two or fewer mismatches and an alignment score of at least 12. To remove noise introduced by sequencing errors, the first base of each read was removed, then the reads were filtered and clipped based on the base quality scores. Quality filtering was performed with Sickle v1.3.3. The filtered reads were mapped to the reference sequences of *TRAC* (NCBI accession number NC_000014.9) and *TRBC2* (NCBI accession number NC_000007.14) genes obtained from Homo sapiens GRCh38.p13 Primary Assembly. The mapping was performed with BWA v0.7.4, a short-read aligner based on Burrows–Wheeler Transform, with default settings. The resulting mapping was used for indel calling and mutation analysis. Indel frequencies and deletions were detected based on the mapped reads (BAM file). Each mapped read was analyzed for the presence of small deletions using the CIGAR string, and a custom shell script was used. The frequency of each deletion was calculated based on position and length as a fraction of the total number of mapped reads.

Integration site analysis by S-EPTS/LM-PCR and deep sequencing

Standard S-EPTS/LM-PCR and deep sequencing were performed to identify SB transposon flanking genomic sequences in Human T cell samples transduced with the mcCD19-28z.CAR vector. Briefly, 1500 ng genomic DNA per sample were sheared to a median length of 500 bp using the Covaris M220 instrument. Sheared DNA was purified, and each sample was split equally into triplicates. Primer extension was performed using an inverted terminal repeat (ITR)-specific biotinylated primer. The extension product was again purified, followed by magnetic capture of the biotinylated DNA for at least 60 minutes and two washing steps with 100 µl H_2O. The captured DNA was ligated to linker cassettes including a molecular barcode. The ligation product was amplified in a first exponential PCR using biotinylated vector- and linker cassette-specific primers. Biotinylated PCR-products were magnetically captured, washed and half of this eluate served as template for amplification in a second exponential PCR step, allowing deep sequencing by MiSeq technology (Illumina) after purification. Preparation for deep sequencing was previously described[6, 7]. DNA double barcoding was applied to allow parallel sequencing of multiple samples in a single sequencing run while minimizing sample cross-contamination.

IS were identified using the S-EPTS/LM-PCR protocol, an advanced version of EPTS/LM-PCR[8], and thereafter analyzed using the GENE-IS tool suite[9]. Briefly, raw data was initially filtered according to sequence quality score (Phred ≥30: probability of incorrect base call being 1 in 1000 bases and base accuracy ≥99.9 %)[10, 11]. In addition, only sequences showing complete identity in both molecular barcodes, linker cassette barcode and sequencing barcode, were further processed. These S EPTS/LM-PCR barcode combinations are unique to each replicate and are

used for de-multiplexing. Those sequences were trimmed (defined vector- and linker cassette-specific parts were removed) and aligned to the human genome (UCSC assembly hg38), while nearby genes and other integrating features were annotated as previously described[7, 12].

The integration profile of gamma-retroviruses and lentiviruses and derived vectors has been described previously[13-18]. Using unique IS found through S-EPTS/LM-PCR, IS distribution across the genome and within gene coding regions was determined. IS position data was plotted for both samples separately to display chromosomal distribution, integration within gene coding regions and vicinity (10 kb upstream and downstream), integration relative to transcription start sites (TSS) and relative positions within gene coding regions.

Based on the properties of Rényi entropies[19], a clonality plane was constructed taking into account two extreme components of the diversity: richness and evenness. Richness represents the number of IS present in a particular sample, while evenness is a measure for equal frequency distribution of these IS within a sample and its theoretical maximum polyclonality/monoclonality. The ratio of distance from theoretical maximal polyclonality and monoclonality defines the polyclonal-monoclonal distance (PMD)[20].

For applications involving integrating viral vectors, it is relevant to determine whether IS accumulate near cancer-related genes. Cancer-related genes are obtained from the Catalogue of Somatic Mutations in Cancer (COSMIC) Cancer Gene Census[21]. This list includes the top 2 categories (tier 1 and tier 2) of cancer-related genes and contains 714 well-defined cancer genes (http://cancer.sanger.ac.uk/census; v95).

Severe adverse events due to insertional mutagenesis in clinical trials were described in a distance of around 40 kb to transcription start sites (TSS). However, some studies described deregulations of neighboring genes up to 300 kb from the genes[22-24]. Thus, we have chosen to investigate integration events within an arbitrary 100 kb window of the TSS of cancer genes. Cancer gene annotations (Chromosome, Gene Start, Gene End, Strand, Gene Name, Transcript Count, TSS and Transcript Support Level (TSL)) were obtained from Ensembl human genes (http://www.ensembl.org/biomart/martview/; version GRCh38.p13).

Molecular profiling of CAR and CAR/endogenous TCR-activated effector T cells

A total of 3×10^6 SB-CD19-28z.CAR/TCR KO or SB-CD19-28z.CAR/scrambled T cells were stimulated with irradiated NALM6 cell (E:T = 1:1) for CAR activation, or irradiated NALM6 cell (E:T = 1:1) and anti CD3-coated superparamagnetic beads (75µL/ reaction, bead:cell = 1:1) for CAR and endogenous TCR activation for 24-48 hours, in the complete T cell medium. CD19 CAR T cells were left unstimulated for the same duration to assess the background signals from cell resting state. To measure the protein phosphorylation of ZAP70, PLCγ1, and p38, the cells were harvested after 24 hours of coculture, washed with PEB buffer and fixed using Fixation Buffer (Cat. 420801, BioLegend), and permeabilized using True-Phos™ Perm Buffer (Cat. 425401, BioLegend) based on the manufacturer's protocol. Next, the treated cells were stained with anti-human ZAP70, PLCγ1, and p38 antibodies (Table S8) for flow cytometric analysis. To explore the differential expressions of genes associated with PI3K signaling pathway and its downstream functions, total RNA of effector cells was extracted using AllPrep DNA/RNA/Protein Mini Kit (Qiagen) at 48 hours post-stimulation and used for cDNA synthesis using SuperScript™ III First-Strand Synthesis System (Life Technologies). Next, quantitative reverse transcription PCR (qRT-PCR) was carried out using SYBR™ Green PCR Master Mix (Life Technologies) and selected primers mentioned in the supplemental information (Table S9)[25]. Differential RNA expression was calculated using $2^{-\Delta\Delta Ct}$ formula by normalizing Ct values of these genes with human GAPDH mRNA and their counterparts from unstimulated groups. The genes were designated as differentially expressed genes (DEGs) when *P* value is lower than 0.05.

Table S1: single guide RNA (sgRNA) targeting human *TRAC* or *TRBC2* genes used in this study

Name	**Target genes**	**guide RNA sequence (5'->3')**	**Source**	**Predicted cleavage site of target gene**
TCR-1	*TRAC*	GAGAATCAAAATCGGTGAAT	ZiFiT Software	73 bp of 1st exon in *TRAC* gene
TCR-2	*TRAC*	GCTGGTACACGGCAGGGTCA	ZiFiT Software	16 bp of 1st exon in *TRAC* gene
TCR-3	*TRAC*	AAGTCAGATTTGTTGCTCC	Sigma Aldrich	195 bp of 1st exon in *TRAC* gene
TCR-4	*TRAC*	GGAATAATGCTGTTGTTGA	Sigma Aldrich	231 bp of 1st exon in *TRAC* gene
TCR-5	*TRAC*	ACACCTTCTTCCCCAGCCC	Sigma Aldrich	268 bp of 1st exon in TRAC gene
TCR-6	*TRBC2*	GAGCAGCCGCCTGAGGGTCT	ZiFiT Software	243 bp of 1st exon in *TRBC2* gene
TCR-7	*TRBC2*	GCAGTATCTGGAGTCATTGA	ZiFiT Software	207 bp of 1st exon in *TRBC2* gene
TCR-8	*TRBC2*	GGCTGCTCCTTGAGGGGCTG	ZiFiT Software	182 bp of 1st exon in *TRBC2* gene
TCR-9	*TRBC2*	CGGGGGTTCTGCCAGAAGG	Sigma Aldrich	255 bp of 1st exon in *TRBC2* gene
TCR-10	*TRBC2*	CTGGACTTGACAGCGGAAG	Sigma Aldrich	280 bp of 1st exon in *TRBC2* gene
TCR-11	*TRBC2*	GACGAGTGGACCCAGGATA	Sigma Aldrich	333 bp of 1st exon in *TRBC2* gene
Scrambled sgRNA	Non-targeting sgRNA	CGCGATAGCGCGAATATATT	Sigma Aldrich	

Table S2: Nested PCR primers used in T7 Endonuclease 1 (T7E1) assay

Target gene	Nested PCR amplification	Primer name	Primer sequence (5'->3')
TRAC	1st round amplification	TRAC-outer-F	GAGTCCCAGTCCATCACGAG
		TRAC-outer-R	GGGGCTTAGAATGAGGCCTAG
	2nd round amplification	TRAC-inner-F	CTGGCATCTGGACTCCAGCC
		TRAC-inner-R	GAGAGACTGAGGCTGGGCC
TRBC2	1st round amplification	TRBC2-outer-F	CAGGCAAGGAAGGGGTAGAAC
		TRBC2-outer-R	GGTGCTCCATTCAGCCTCTA
	2nd round amplification	TRBC2-inner-F	GGTGACCCCAAAGCAAGGAGG
		TRBC2-inner-R	CCCACCTTGTCCACTCTGGC

Table S3: Selected nucleotide positions of targeted TCR genes showing highest gene editing efficiency following CRISPR/Cas9-mediated TCR knockout
(Separated MS Excel sheet due to large file size)

Table S4: PCR primers for mcCD19-28z.CAR transposon and mcSB100x transposase detection

Target gene	Primer name	Primer sequence	Assay type	Product size (bp)
mcCD19-28z.CAR transposon	mcCD19CAR-PCR-F	GCCGCTATCGAAGTGATGTACCC	Traditional PCR amplification	767 bp
	mcCD19CAR-PCR R	ATGCGGCACTCGATCTCCATG		
mcCD19-28z.CAR transposon	mcCD19CAR-qPCR-F	GCAAGAGTCTGGCCCTG	qPCR amplification	141 bp
	mcCD19CAR-qPCR-R	ATCACGCCCAGCCATTCC		
mcSB100x transposase	SB100X-qPCR-F	TGCAAGCCGAAGAACACC	qPCR amplification	96 bp
	SB100X-qPCR-1-R	GTGAAGTGCACCAGTCCC		

Table S5: Total identified insertion sites in SB-CD19-28z.CAR/TCR KO and SB-CD19-28z.CAR/scrambled control T cell samples from the unbiased genome-wide integration site analysis (ISA)

(Separated MS Excel sheet due to large file size)

Table S6: List of all insertion sites within or close to proto-oncogenes associated with severe adverse events in SB-CD19-28z.CAR/TCR KO sample

Proto-oncogene	Distance to TSS (nt)	Chr	Sense	Integration Locus	Relative contribution (%)
CCND2	-93220	12	+	4176551	0.0011
CCND2	-84901	12	-	4184870	0.0004
CCND2	31079	12	-	4309879	0.007
CCND2	55303	12	+	4334103	0.0011
CCND2	99115	12	+	4377915	0.0007
HMGA2	-98738	12	-	65725722	0.004
HMGA2	-22917	12	+	65801543	0.0086
HMGA2	26111	12	-	65854112	0.0015
LMO2	-52392	11	+	33812759	0.0007
LMO2	-7852	11	-	33884224	0.0004
LMO2	82752	11	-	33974828	0.0195
MECOM	-94803	3	+	169027869	0.0007
MECOM	-93710	3	-	169175528	0.004
MECOM	61200	3	+	169330438	0.0037
MECOM	-85800	3	+	169577738	0.0034
MECOM	-68173	3	+	169595445	0.0015
MECOM	-5880	3	+	169657738	0.0004
MECOM	1366	3	+	169665141	0.0004
MECOM	8005	3	-	169671780	0.0019
MECOM	66125	3	+	169729900	0.0015
MN1	-1194	22	+	27795702	0.0004

Table S7: GvHD clinical scoring system used in the study.[26-28]

Score	Weight loss	Posture	Fur	Activity	Skin	Diarrhea
0	<5%	Normal	No ruffling	Normal	Normal	No
0.5	>5%	Mild hunching, only at rest	Mild ruffling (<20%)	Mild decreased	Reddish, irritated areas	
1	>10%	Moderate hunching	Moderate ruffling (>20%), mild loss of fur	Moderate decreased, isolation	Scaling and/or dry skin areas (<20%)	Yes
1.5	>15%	Severe hunching with slight defect in movement	Severe ruffling (>40%), mild loss of fur	Stationary until stimulated	Scaling and/or dry skin areas (>20%)	
2 (humane endpoint)	>20%	Severe hunching with severe defect in movement	Severe ruffling (>60%), moderate to severe loss of fur	Severely decreased, paralysis, lethargy	Scaling and/or dry skin areas (>40%),	

Table S8: Antibodies used in the study

No.	Name	Cat. no.	Manufacture
1	Human CD279(PD1)-APC	130-117-694	Miltenyi Biotec
2	Human CD19-APC	130-114-168	Miltenyi Biotec
3	Human CD3-APC	130-113-135	Miltenyi Biotec
4	Human CD8-APC	130-110-817	Miltenyi Biotec
5	Human CD62L-PE	130-114-151	Miltenyi Biotec
6	Human CD45RA-PerCP-Vio700	130-113-930	Miltenyi Biotec
7	Human CD45RO-APC-Vio770	130-114-083	Miltenyi Biotec
8	Human CD95 (FAS)-APC	130-113-070	Miltenyi Biotec
9	Human TCRa/b-FITC	130-109-919	Miltenyi Biotec
10	REA Control Antibody-Human IgG1-FITC	130-113-437	Miltenyi Biotec
11	REA Control Antibody-Human IgG1-APC	130-113-434	Miltenyi Biotec
12	REA Control Antibody, human IgG1, APC-Vio770	130-113-447	Miltenyi Biotec
13	REA Control Antibody, human IgG1, PerCP-Vio700	130-113-453	Miltenyi Biotec
14	REA Control Antibody, human IgG1, PE, REAfinity	130-113-450	Miltenyi Biotec
15	APC anti-human CD19	302212	Biolegend
16	APC anti-human CD152 (CTLA-4) Antibody	349907	Biolegend
17	APC Mouse IgG1, κ Isotype Ctrl (FC) Antibody	400121	Biolegend
18	PE/Cyanine7 anti-human ZAP70 Phospho (Tyr493)	396007	Biolegend
19	PE anti-PLCDžPhospho (Tyr783)	612403	Biolegend
20	PE anti-p38 MAPK Phospho (Thr180/Tyr182)	690203	Biolegend
21	PE Mouse Anti-Human CD107a, Clone H4A3	555801	BD Bioscience

Table S9: qPCR primers for detection of RNA expression in CD19 CAR T cells

(Separated MS Excel sheet due to large file size)

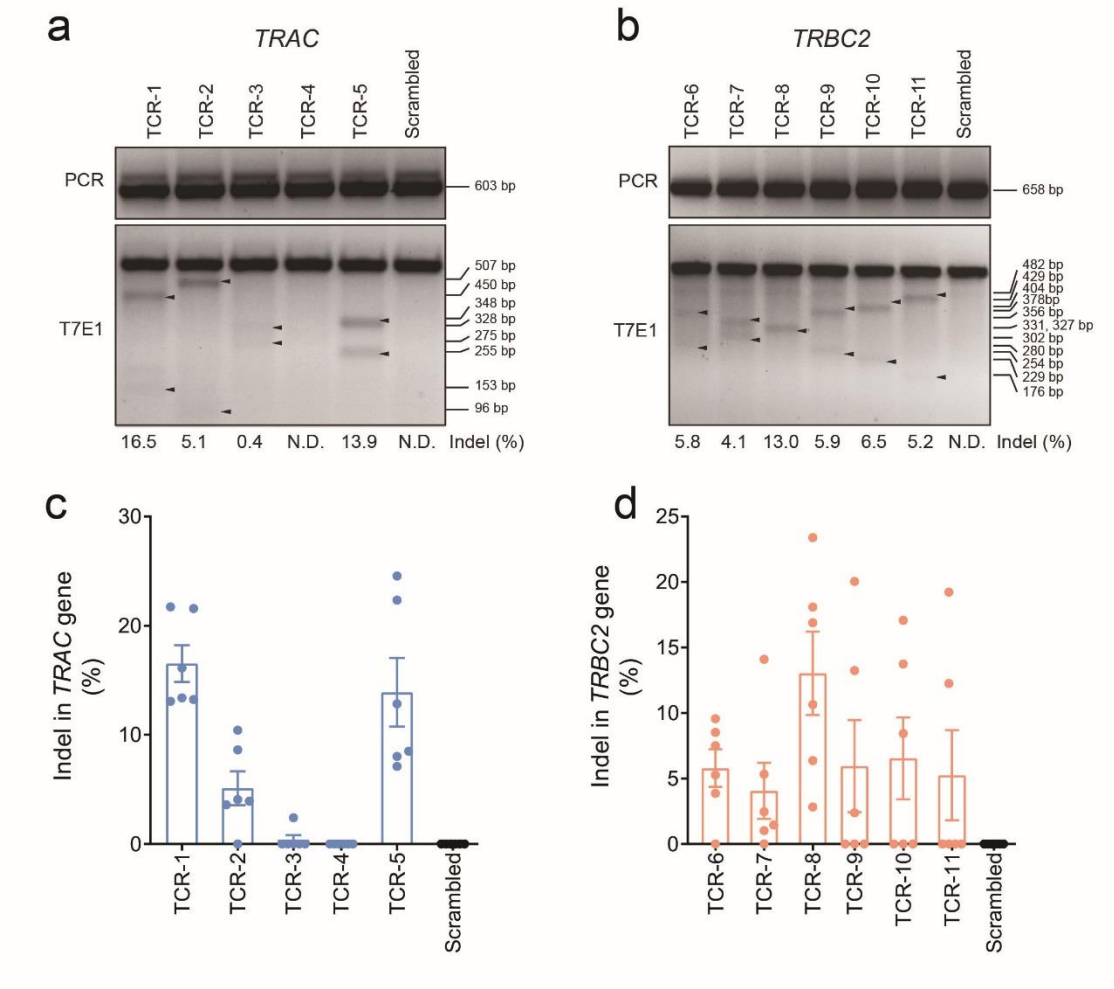

Figure S1: Assessment of TCR gene disruption activity mediated by the CRISPR/Cas9 system in HEK cells. On day 0, HEK cells were transfected with 2.5 µg of plasmid pLV-U6g-EPCG encoding TCR-targeting sgRNAs or scramble control sgRNA, and Cas9 protein using Lipofectamine 3000. The transfected cells were then subjected to 2 µg/mL of puromycin selection for 7 days, and the cells were subsequently harvested for T7E1 analysis. (**a**-**b)**, Schematic representation of **a**, *TRAC* and **b**, *TRBC*-targeting CRISPR/Cas9 system on day 7 post-transfection measured by T7E1 assay. The average of indel percentage mediated by each sgRNA was designated as % indel. (**c**-**d)**, Quantitative analysis of indel percentage mediated by **c**, *TRAC* and **d**, *TRBC*-targeting CRISPR/Cas9 system on day 7 post-transfection measured by T7E1 assay. Data are shown as means ± s.e.m. (n=3 independent experiments).

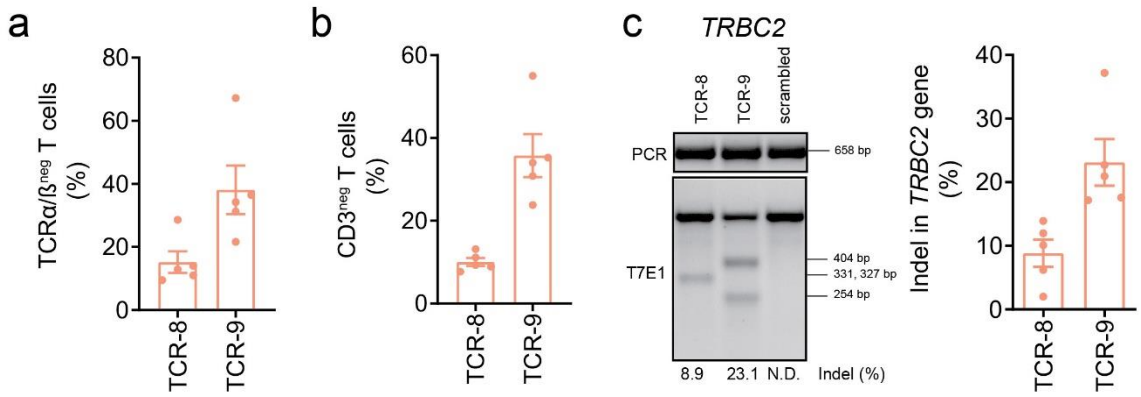

Figure S2: CRISPR/Cas9-mediated TCR KO in human CD8+ T cells using ribonucleoprotein (RNP) particles. After 48 hours post-CD3/CD28 stimulation, 5×10^5 human CD8+ T cells were subjected to nucleofection of 70 pmol *TRBC2*-targeting TCR-8 and TCR-9 RNP particles (Cas9:sgRNA ratio of 1:1. **a**, Percentages of TCRα/β^{neg} and, **b**, CD3^{neg} T cell population by flow cytometry after 48 hours post-*TRBC2*-targeting RNP nucleofection. **c**, (**left**) Schematic representatives and, (**right**) Quantitative analysis of indel mutation detected by T7E1 assay after 48 hours of *TRBC2* -targeting RNP nucleofection. Data are shown as means ± s.e.m. (n=5 biologically independent donors); Student's t-test: ****P<0.0001.

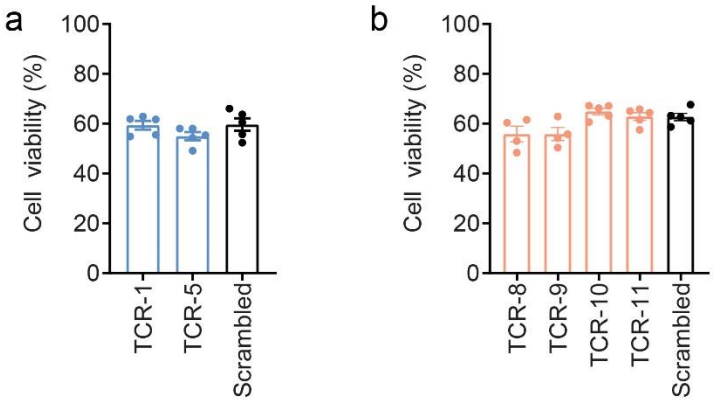

Figure S3: Cell viability of transfected cells following CRISPR/Cas9-mediated TCR gene knockout in human CD8+ T cells using RNP. After 48 hours of prestimulation, 5×10^5 human CD8+ T cells were subjected to nucleofection of 70 pmol *TRAC* or *TRBC2* CRISPR/Cas9 RNP particles (Cas9:sgRNA ratio of 1:1). Cell viability percentages of cells transfected with **a**, *TRAC* or **b**, *TRBC2* at 48 hours post-transfection. Data are shown as means ± s.e.m. (n=5 biologically independent donors).

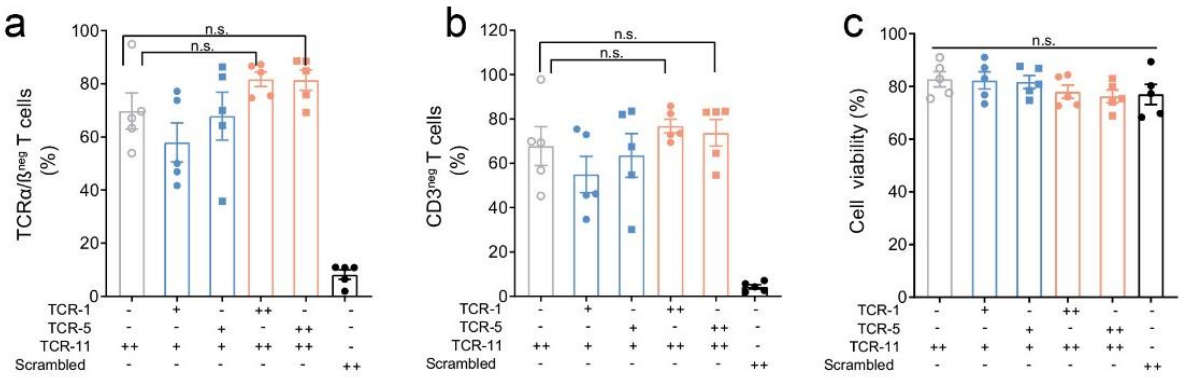

Figure S4: CRISPR/Cas9-mediated dual gene KO in human CD8+ T cells using ribonucleoprotein (RNP) particles. After 48 hours of prestimulation, 5×10^5 human CD8+ T cells were subjected to nucleofection of 70 pmol CRISPR/Cas9 RNP particles with Cas9:sgRNA ratio 1:1 or 1:2. The symbols "+" and "++" indicate 70 and 140 pmol of target sgRNA being used in the corresponding group. 70 pmol of Cas9 protein was used in all experimental groups. **a**, Percentages of TCRα/β^{neg}; **b**, $CD3^{neg}$ T cell population; and **c**, cell viability measured by 7-AAD staining measured by flow cytometric analysis after 48 hours following RNP nucleofection. Data are shown as means ± s.e.m. (n=5 biologically independent donors). One-way ANOVA with Dunnett's'post-hoc.

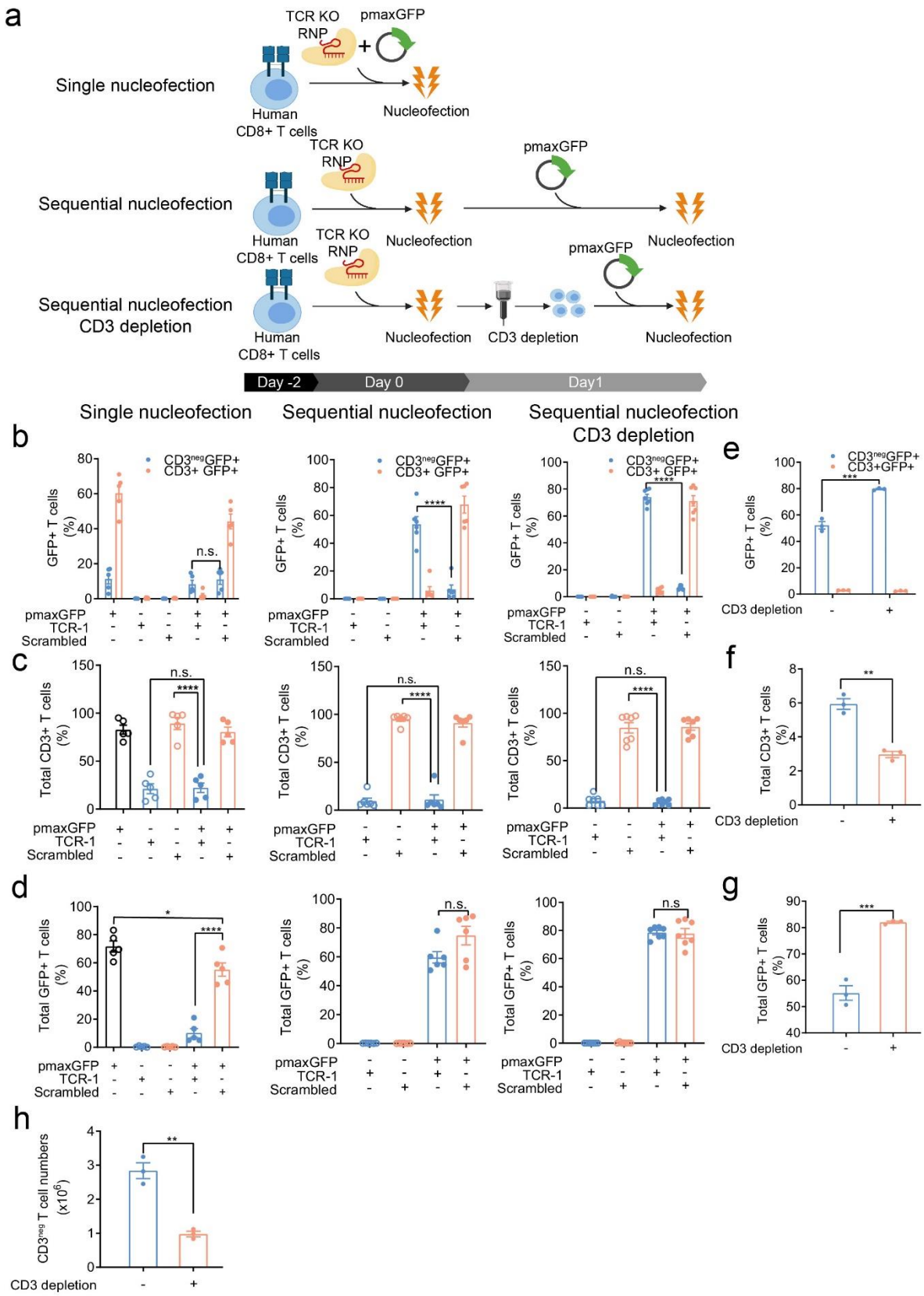
a
Single nucleofection
TCR KO RNP
pmaxGFP
Human CD8+ T cells
Nucleofection
Sequential nucleofection
Nucleofection
Nucleofection
Sequential nucleofection CD3 depletion
CD3 depletion
Day -2
Day 0
Day1
Single nucleofection
Sequential nucleofection
Sequential nucleofection CD3 depletion
b
GFP+ T cells (%)
CD3negGFP+
CD3+ GFP+
n.s.
pmaxGFP
TCR-1
Scrambled
c
Total CD3+ T cells (%)
d
Total GFP+ T cells (%)
e
CD3negGFP+
CD3+GFP+
CD3 depletion
f
g
h
CD3neg T cell numbers (x10^6)

Figure S5: Optimization of an efficient method to generate GFP+/TCR^{neg} T cells using CRISPR/Cas9 RNP nucleofection. a, Schematic representation of a different non-viral strategy to generate GFP+/TCR^{neg} cells including single nucleofection (**upper**) and sequential nucleofection of *TRAC*-targeting TCR-1 RNP and pmaxGFP without (**middle**) or with CD3 depletion (**lower**). After 48 hours of CD3/CD28 stimulation, 5×10^5 human CD8+ T cells were subjected to single electroporation of 70 pmol of TCR-1 RNP and 500 ng of pmaxGFP (**b-d**, **left**). Alternatively, sequential delivery of 70 pmol of TCR-1 RNP and 500 ng of pmaxGFP (after 24 hours) was performed on bulk CD3+/CD3^{neg} cells (**b**–**d**, **middle**) or enriched CD3^{neg} cells (**b-d, right**). **b**, Percentage of fractioned GFP+/CD3+ and GFP+/CD3^{neg} T cells; **c**, percentage of total CD3+ T cells; and **d**, percentage of total GFP+ T cells analyzed by flow cytometry at 48 hours post-nucleofection. **e**, Percentage of fractioned GFP+/CD3+ and GFP+/CD3^{neg}; **f**, total CD3+; **g**, total GFP+ T cells analyzed by flow cytometry; and **h**, total cell numbers of CD3^{neg} population at 48 hours post-nucleofection to compare the effect of CD3+ depletion. Data are shown as means ± s.e.m. (n=3-7 biologically independent donors); Student's t-test: ***P<0.001.

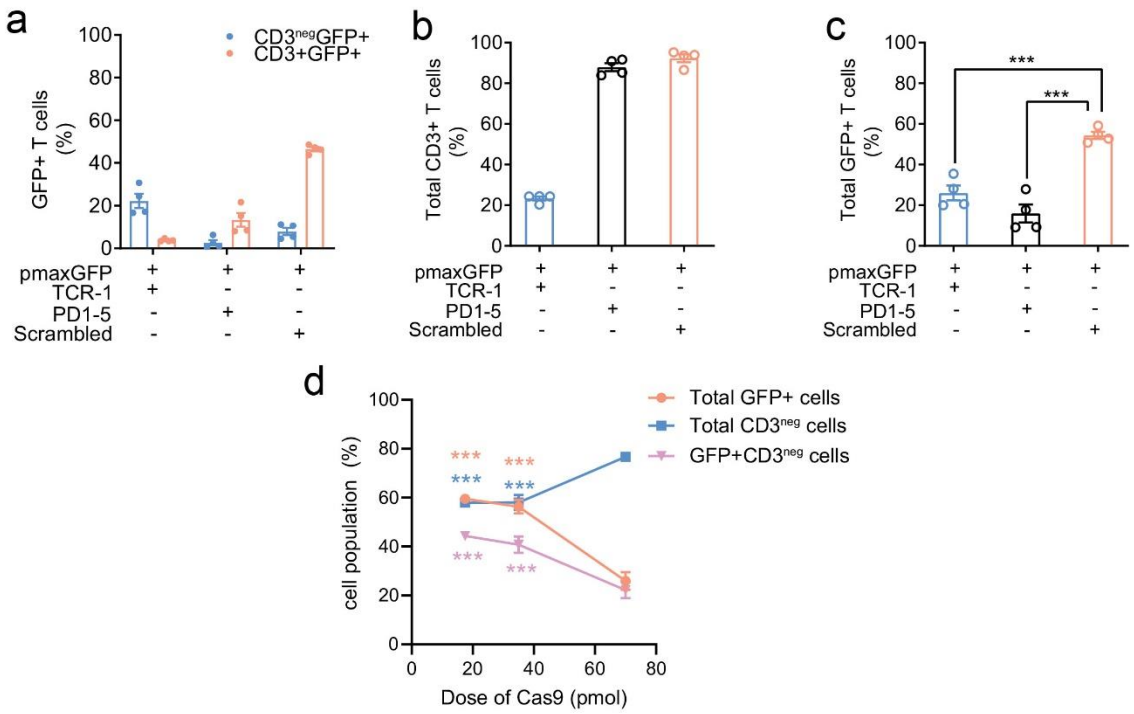

Figure S6: Enhanced efficiency of single nucleofection of pmaxGFP/ CRISPR/Cas9 RNP for GFP+/TCR^{neg} T cell production After 48 hours of CD3/CD28 stimulation, 5×10^5 human CD8+ T cells were subjected to single electroporation of 70 pmol of TCR-1, *Programmed cell death protein 1 (PD-1)*-targeting PD1-5, or scrambled RNP and 500 ng of pmaxGFP. After 48 hours of transfection, the percentage of **a**, GFP+/CD3+ and GFP+/CD3^{neg}; **b**, total CD3+ and **c**, total GFP+ T cells were analyzed by flow cytometry. Data are shown as means ± s.e.m. (n=4 biologically independent donors); Student's t-test: ***P<0.001. **d,** Cas9 dose-dependent study to assess its effect on GFP expression in T cells. After 48 hours of CD3/CD28 stimulation, 5×10^5 human CD8+ T cells. were subjected to single nucleofection of i) 70 pmol TCR-1 sgRNA, ii) indicated dose of Cas9 protein (17.5, 35, and 70 pmol), and iii) 500 ng of pmaxGFP plasmid. At 48 hours post-transfection, the percentages of GFP+/CD3^{neg} (triangular purple line), total GFP+ (circular orange line), total CD3^{neg} cells (squared blue line) were determined by flow cytometry. Data are shown as means ± s.e.m. (n=4 biologically independent donors); Student's t-test: *** P<0.001 (*** = total GFP% of the indicated group compared to 70 pmol group)

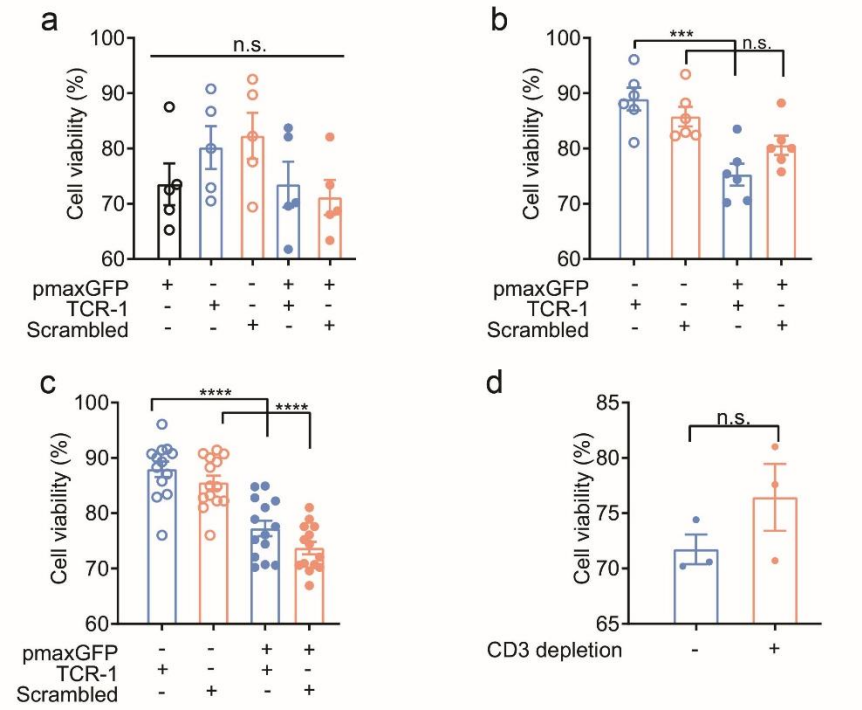

Figure S7 Cell viability of GFP+/TCR^{neg} T cells generated by CRISPR/Cas9 RNP-mediated nucleofection. After 48 hours of CD3/CD28 stimulation, 5×10^5 human CD8+ T cells were subjected to single electroporation of 70 pmol of TCR-1 RNP and 500 ng of pmaxGFP. Alternatively, sequential delivery of 70 pmol of TCR-1 RNP and 500 ng of pmaxGFP (after 24 hours) was performed on bulk CD3+/CD3^{neg} cells or enriched CD3^{neg} cells. Cell viability of **a**, single nucleofection; **b**, sequential nucleofection; **c**, sequential nucleofection with CD3+ depletion; and **d**, comparative analysis of CD3+ depletion effects analyzed by flow cytometry at 48 hours post-nucleofection. Data are shown as means ± s.e.m. (left, single nucleofection, n=5 biologically independent donors; middle, sequential nucleofection, n=6 biologically independent donors; right, sequential nucleofection with CD3+ depletion, n=7 biologically independent donors); Student's t-test: *** P<0.001, **** P<0.0001; n.s. not significant.

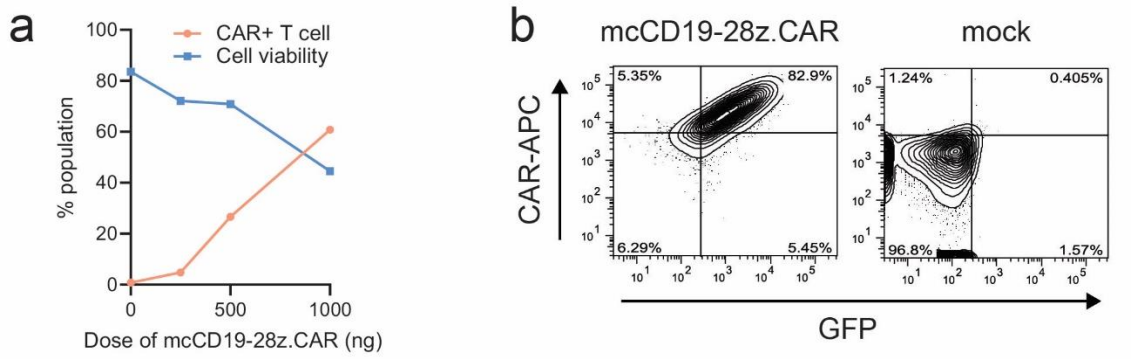

Figure S8 Assessment of optimal dose of mcCD19-28z.CAR minicircle DNA for efficient transfection in T cells. 5×10^5 human CD8+ T cells stimulated for 48 hours were transfected with indicated amounts of CD19-28z.CAR mcDNA. The next day, the cells were subjected to flow cytometry analysis to measure CAR+ and/or GFP+ (surrogate reporter) cells. **a,** Percentages of CAR+ T cells (through measuring GFP surrogate reporter expression, orange circular line) and cell viability (blue square line) with respect to the transfected dosages of CD19-28z.CAR mcDNA vector. **b,** Schematic representation of CD19-specific CAR and GFP surrogate reporter coexpression in human CD8+ T cells at 1 μg of mcCD19-28z.CAR minicircle DNA transfection.

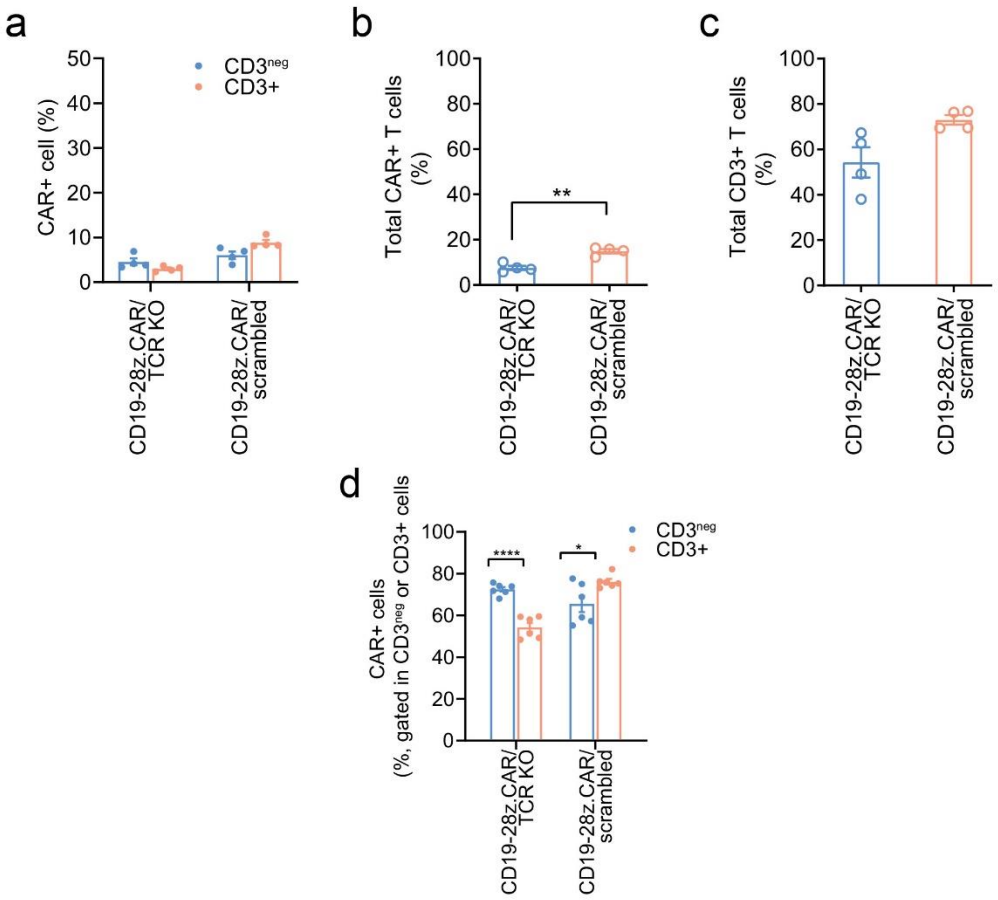

Figure S9: CD19-28z.CAR/ TCR KO T cell production using single nucleofection or sequential nucleofection of mcCD19-28z.CAR DNA and TCR-1 RNPs. (a-c), After 48 hours of CD3/CD28 stimulation, 5×10^5 human CD8+ T cells were subjected to single electroporation of 70 pmol of TCR-1, or scrambled RNP and 1 µg of mcCD19-28z.CAR DNA (i.e. single nucleofection method). **(d),** Alternatively, the cells were nucleofected with 70 pmol of TCR-1, or scrambled RNP on day 0, followed by transfection of 1 µg of mcCD19-28z.CAR DNA into these nucleofected cells on day 1 (i.e. sequential nucleofection method). The percentage of **a**, CAR+/CD3+ and CAR+/CD3^{neg}; **b**, total CAR+ and **c**, total CD3+ T cells from CD19-specific CAR T cells obtained from single nucleofection of TCR RNP/mcCD19-28z.CAR vector were analyzed by flow cytometry. Data are shown as means ± s.e.m. (n=4 biologically independent donors); Student's t-test: $^{**}P<0.01$. **d,** Percentage of CAR+ population gated in CD3+ or CD3^{neg} cell fraction analyzed by flow cytometry after 48 hours of transfection to determine the biased CAR transfection towards highly abundant population. Data are shown as means ± s.e.m. (n=6 biologically independent donors); Student's t-test: $^{*}P<0.05$; $^{***}P<0.001$.

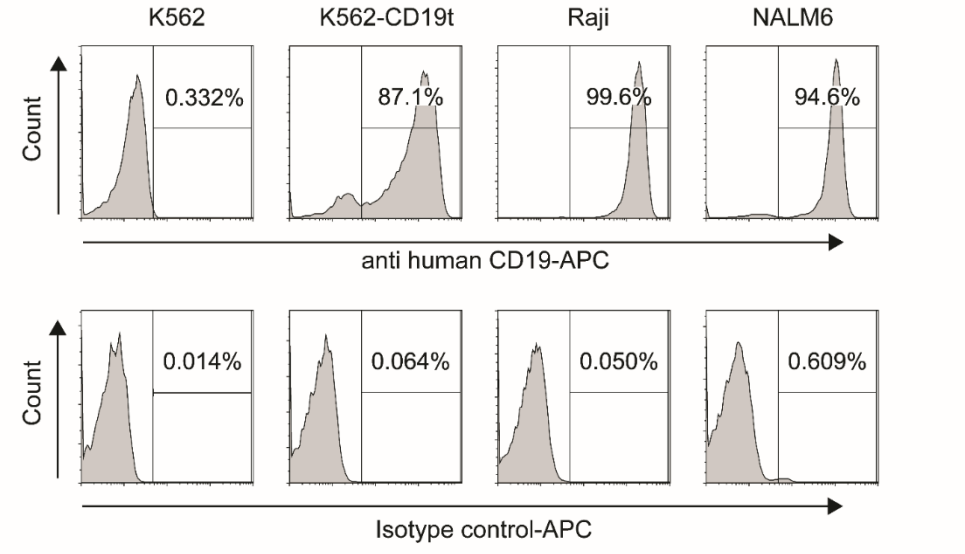

Figure S10: Schematic representation of surface CD19 expression in different tumor cell lines. Following the indicated specific genetic modifications, all tumor cell lines used in this study were stained with APC-conjugated anti-human CD19 antibody and subjected to flow cytometry analysis

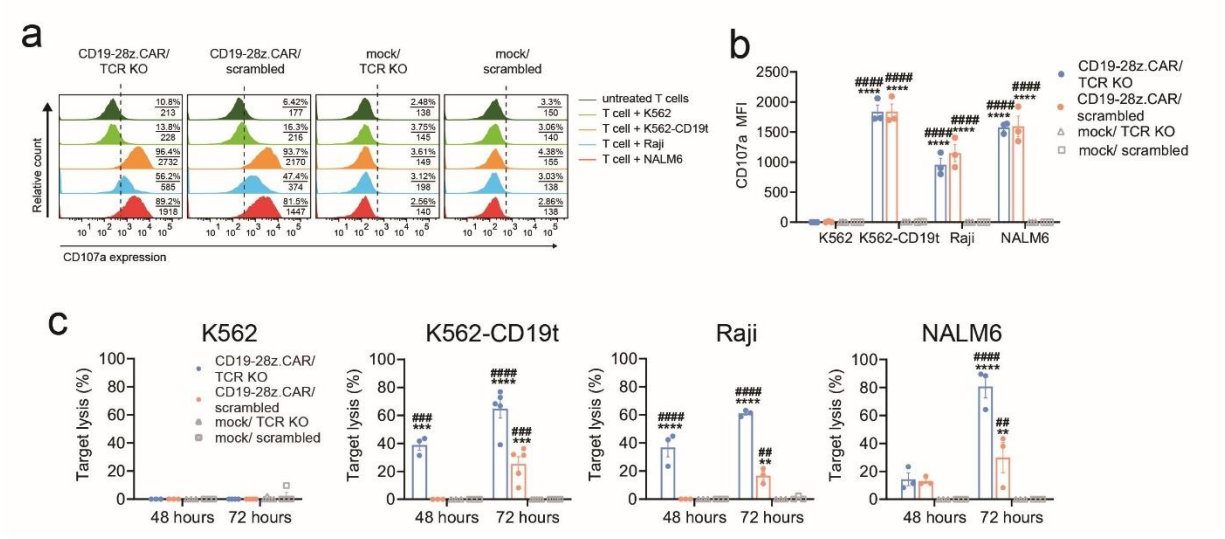

Figure S11: Assessment of *in vitro* antitumor activity of transiently transfected CD19-28z.CAR/TCR KO T cells in response to CD19 antigen. a. Representative flow cytometric profile of CD107a expression and **b,** CD107a median fluorescence intensity (MFI) in CD19-28z.CAR/TCR KO, CD19-28z.CAR/scrambled, mock/TCR KO, mock/scrambled T cells following 6-hour incubation with or without target tumor cells. Each numerator and denominator pair indicates the percentage of CD107a+ cells and total CD107a median fluorescent intensity (MFI), respectively, obtained from a specified condition. **c**, Time-response specific lysis of effector cells after 48- and 72-hour incubations with CD19+ and control tumor cells. Data are shown as means ± s.e.m. (n=3 biologically independent donors); one-way ANOVA with Dunnett's post-hoc; n.s., not significant; */#*P*<0.05; **/##*P*<0.01; ***/###*P*<0.001 (*, compared to mock/TCR KO group; #, compared to mock/scrambled control group).

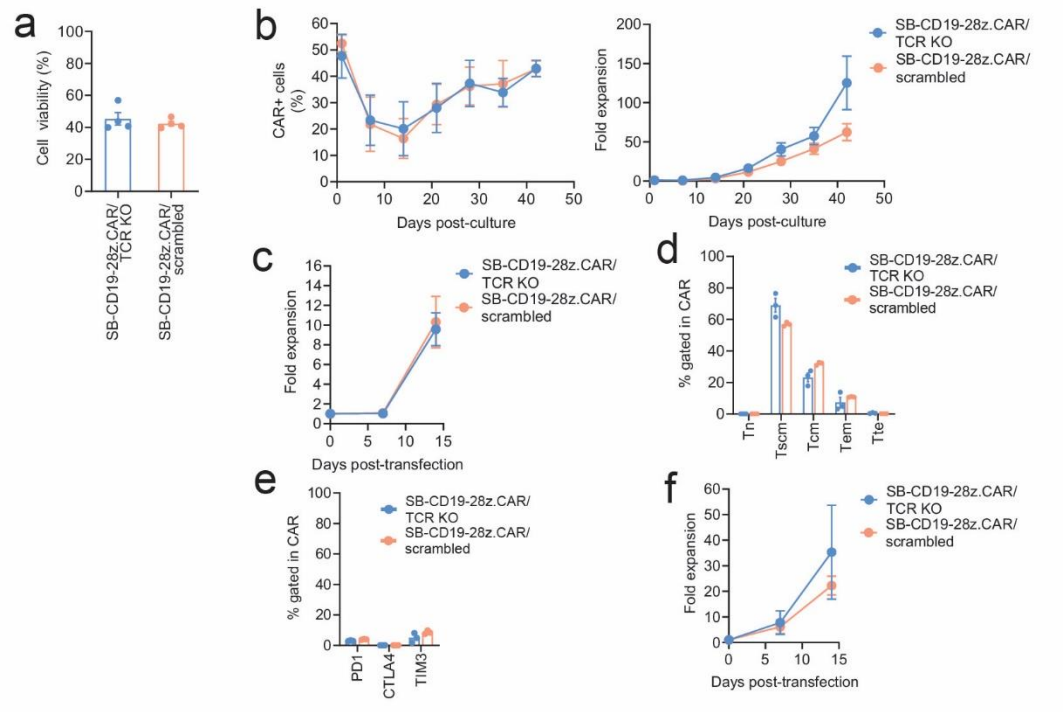

Figure S12: Production and characterization of CD19-specific CAR/TCR KO T cells using the non-viral CRISPR/Cas9 RNP-mcSB transposon platform for sustained CAR expression. (a-b), a, Cell viability after 24 of transfection. **b**, (left) total CAR+ cell percentage, and (right) fold expansion of CAR T cells generated from human CD8+ T cell over 6 weeks of culture using the conventional CAR T cell production method without early CAR+ enrichment. Data are shown as means ± s.e.m. (n=3 biologically independent donors). **c**, fold expansion of CAR T cells generated from human CD8+ T cell over 14 days of culture using the improved CAR T cell production method with early CAR+ enrichment. Data are shown as means ± s.e.m. (n=3 biologically independent donors). **(d-f)**, Immunophenotyping analysis of, **d**, T cell memory markers, and **e**, PD1, CTLA4, and TIM3 immune checkpoint markers and **f**, fold expansion of CAR T cells of SB-CD19-28z.CAR/TCR KO and SB-CD19-28z.CAR/scrambled control T cells generated from human CD3+ T cells at 2 weeks post-culture using the improved CAR manufacturing approach with early CAR+ enrichment. Data are shown as means ± s.e.m. (n=3 biologically independent donors).

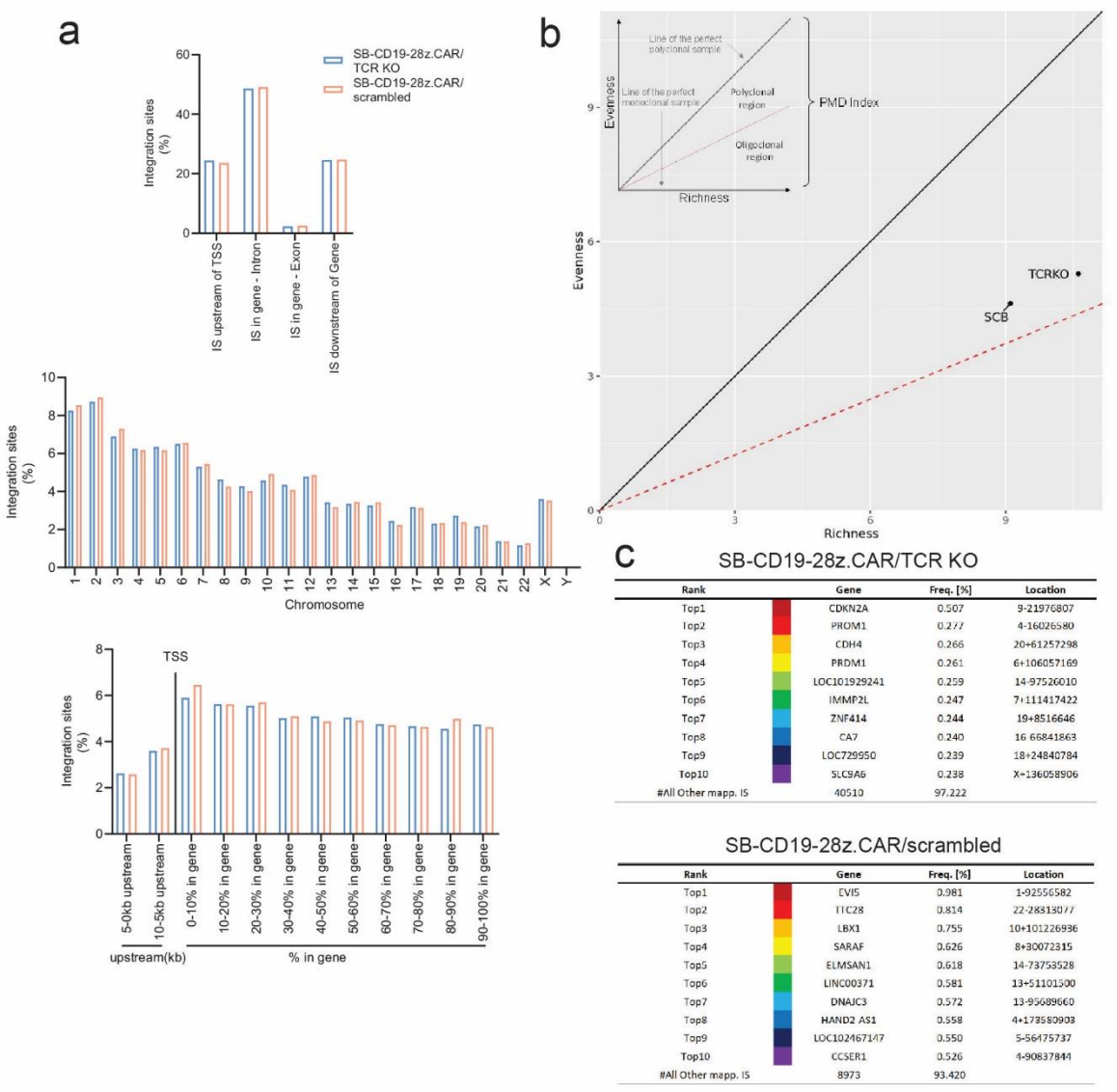

Figure S13: SB-CD19-28z.CAR/TCR KO and SB-CD19-28z.CAR/scrambled control T cells display similar SB transposon insertion patters with safety profiles. a, (**upper**) Integration site (IS) frequency in the various genomic features (i.e. upstream of TSS, within the gene coding regions (exon or intron) and downstream of a gene), (**middle**) IS frequency distribution across all chromosomes, and (**lower**) IS frequency relative to transcriptional start site (TSS) in kb. **b,** Polyclonal-monoclonal distance (PMD) clonal framework per sample (TCRKO = SB-CD19-28z.CAR/TCR KO; SCB = SB-CD19-28z.CAR/scrambled). **c**, Cumulative retrieval frequencies of the ten most prominent insertion sites detected in the SB-CD19-28z.CAR/TCR KO (**upper**) and SB-CD19-28z.CAR/scrambled control (**lower**) T cells.

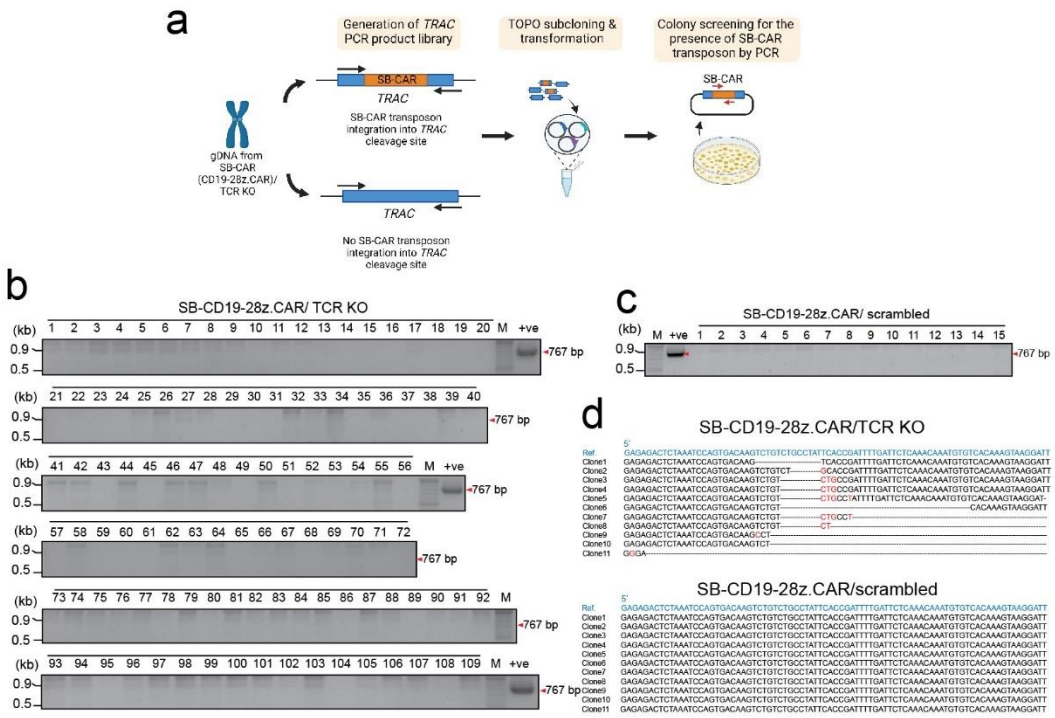

Figure S14: Confirmation of the absence of SB transposon integration into *TRAC* double-stranded breaks sites in SB-CD19-28z.CAR/TCR KO T cells using PCR amplification and Sanger DNA sequencing analysis. a, Schematic representation to analyze SB-CD19-28z.CAR transposon integration into *TRAC* double-stranded breaks (DSBs) sites. *TRAC* DSB regions from gDNA of SB-CD19-28z.CAR/TCR KO cells was enriched using nested PCR amplification and subsequently subcloned into TOPO cloning plasmid to establish *TRAC* DSB DNA library. Each plasmid containing single *TRAC* DSB clone was used as template for detection of SB-CD19-28z.CAR transposon. **b,** PCR amplification assay of 109 *TRAC* DSB DNA library clones derived from SB-CD19-28z.CAR/TCR KO samples and, **c**, 15 *TRAC* DSB DNA library clones derived from SB-CD19-28z.CAR/scrambled samples (negative control) by using CAR-specific primers (Table S4). The red arrow indicates the expected DNA band (767 bp) when there is a presence of SB-CD19-28z.CAR transposon in gDNA samples. **d**, DNA sequence alignment of *TRAC* DSB clones obtained from Sanger DNA sequencing analysis. The uppermost DNA sequence in blue indicates the wildtype *TRAC* DNA sequence, and the red letter indicates base mutations.

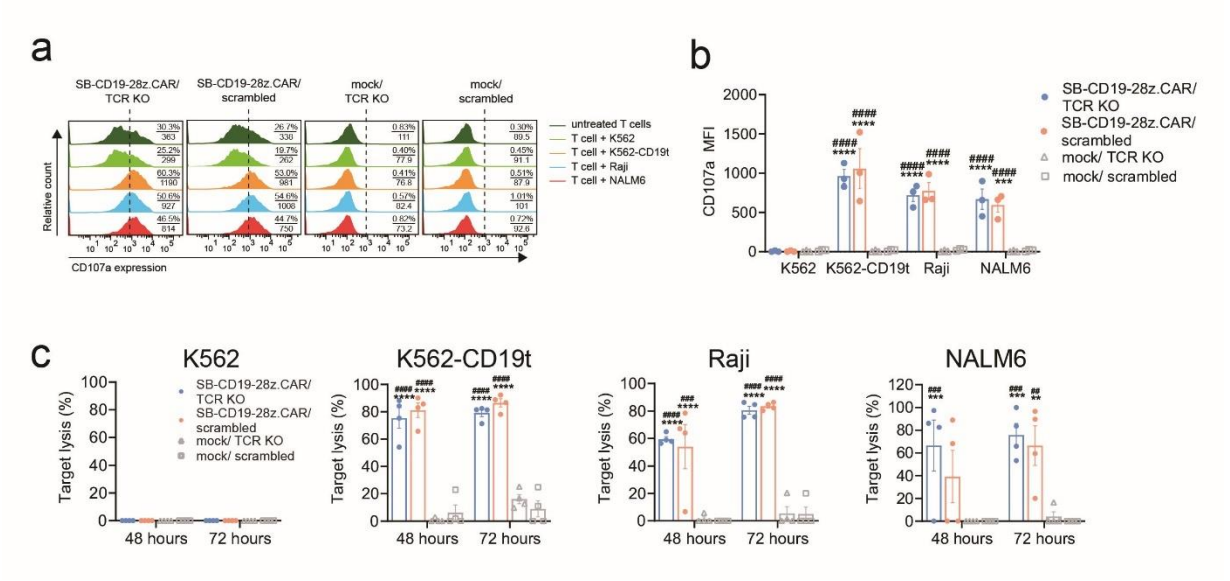

Figure S15: Assessment of *in vitro* antitumor activity of stably transfected SB-CD19-28z.CAR/TCR KO T cells in response to CD19 antigen. a, Representative flow cytometric profile of CD107a expression and **b,** CD107a median fluorescence intensity (MFI) in SB-CD19-28z.CAR/TCR KO, SB-CD19-28z.CAR/scrambled, mock/TCR KO, mock/scrambled T cells following 6-hour incubation with or without target tumor cells. Each numerator and denominator pair indicates the percentage of CD107a+ cells and total CD107a median fluorescent intensity (MFI), respectively, obtained from a specified condition. **c**, Time-response specific lysis of effector cells after 48- and 72-hour incubations with CD19+ and control tumor cells. Data are shown as means ± s.e.m. (n=3 biologically independent donors); one-way ANOVA with Dunnett's post-hoc; n.s., not significant; */#*P*<0.05; **/##*P*<0.01; ***/###*P*<0.001 (*, compared to mock/TCR KO group; #, compared to mock/scrambled control group).

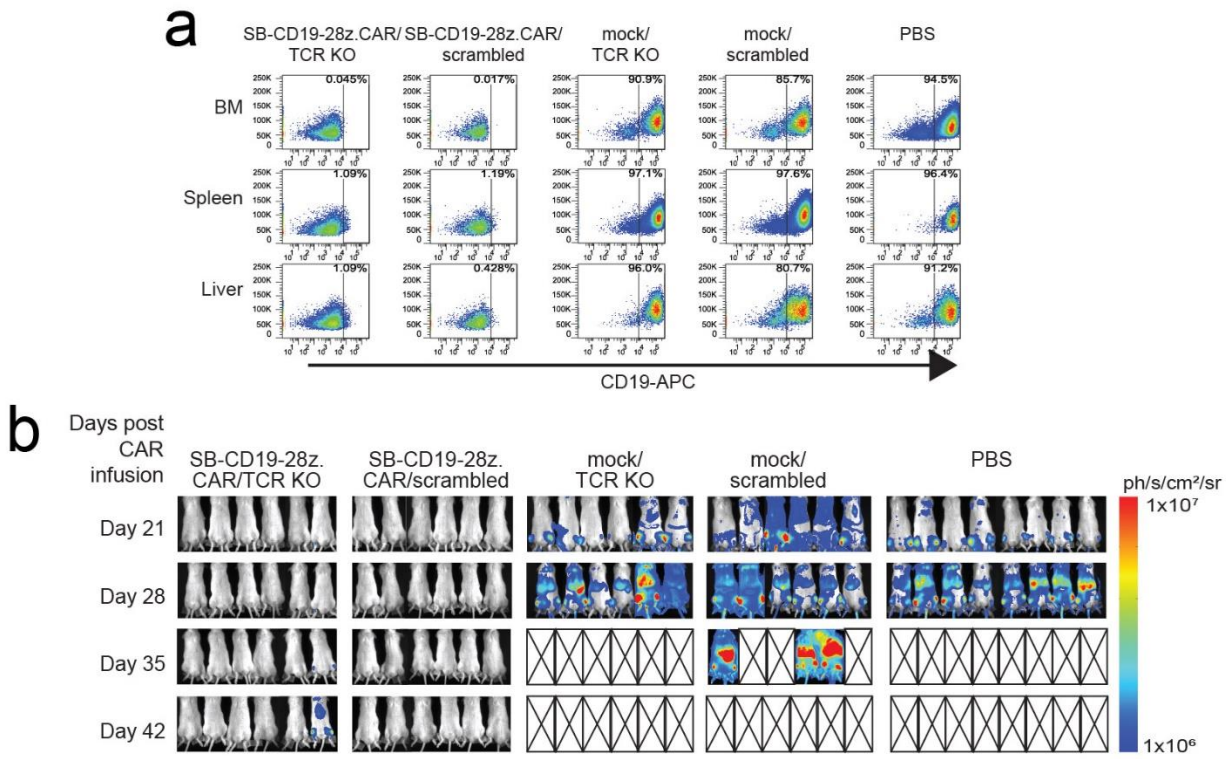

Figure S16: SB-CD19-28z.CAR/TCR KO T cells suppressed CD19+ leukemic progression *in vivo*. a, Representative flow cytometric plot showing the presence of NALM6 tumor cells (indicated in black box) in bone marrow, spleen, and liver tissues of all treated groups at endpoint. **b**, Representative BLI of tumor development and from all groups at different timepoints from high-tumor burden experiment. The BLI signals were expressed in average radiance (ph/s/cm^2/sr).

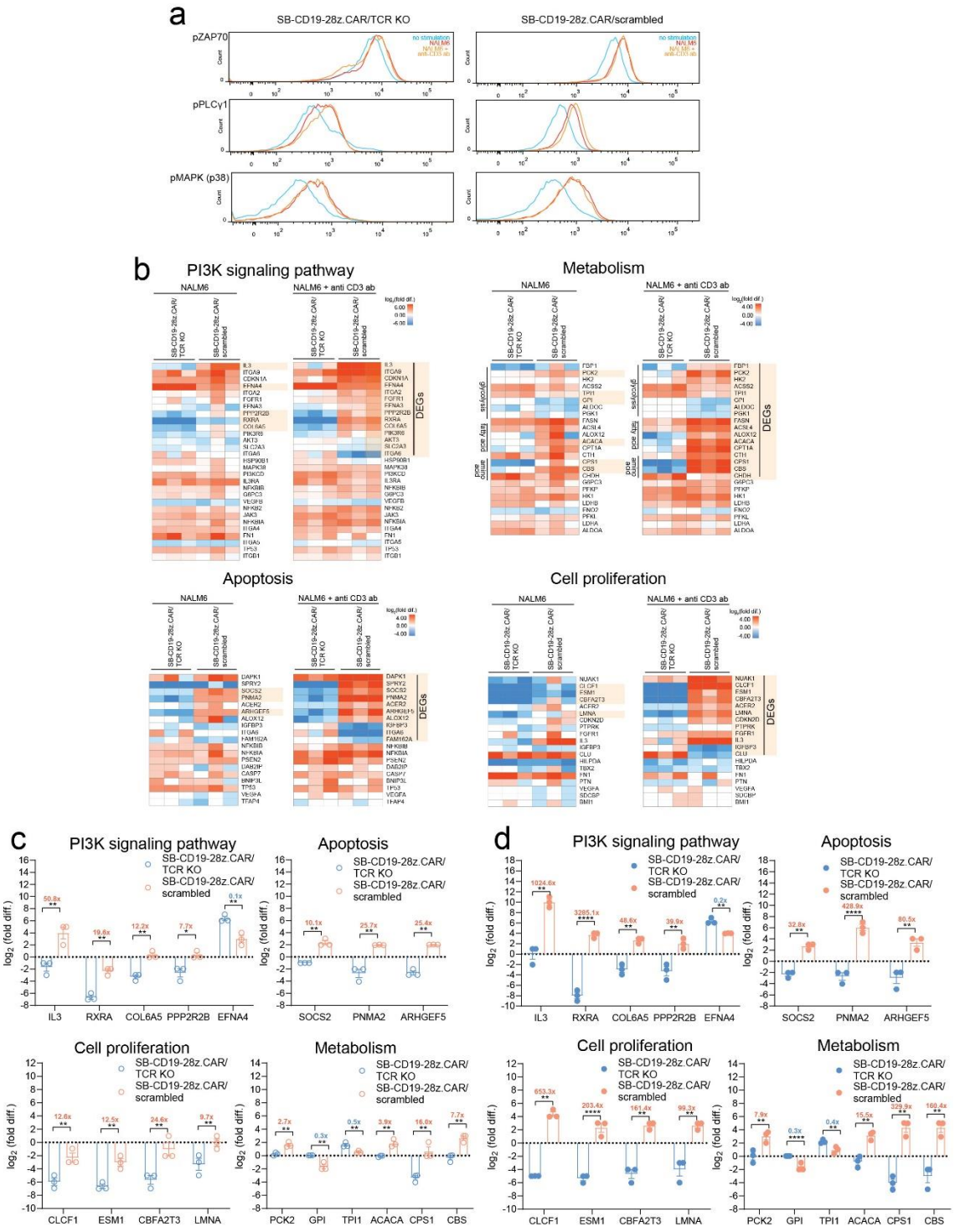

Figure S17: Effects of single CAR stimulation and CAR/endogenous TCR co-stimulation on molecular signature of SB-CD19-28z.CAR/TCR KO and SB-CD19-28zCAR/scrambled T cells. a, Representative flow cytometric plot of ZAP70, PLCγ1, and p38 protein phosphorylation in CAR T cells after 24 hours of stimulation. **b,** Heat map and, **(c-d)**, Quantitative analysis of RNA expression profiling of selected genes associated with PI3K

signaling pathway, apoptosis, metabolism; and cell proliferation in SB-CD19-28z.CAR/TCR KO and SB-CD19-28z.CAR/scrambled T cells at 48 hours post-stimulation by (**c**) CAR-targeting NALM6, or (**d**) CAR/endogenous TCR-targeting NALM6 and anti-CD3. Differentially expressed genes (DEGs) was defined as the genes showing $P<0.05$ for differential expression and labelled in light yellow square. Red and blue indicate upregulation and downregulation of the genes normalized to the values from the resting states, respectively. Data are shown as means ± s.e.m. (n=3 biologically independent donors); Student's t test; n.s., not significant; *$P<0.05$; **$P<0.01$; ***$P<0.001$; ****$P<0.0001$.

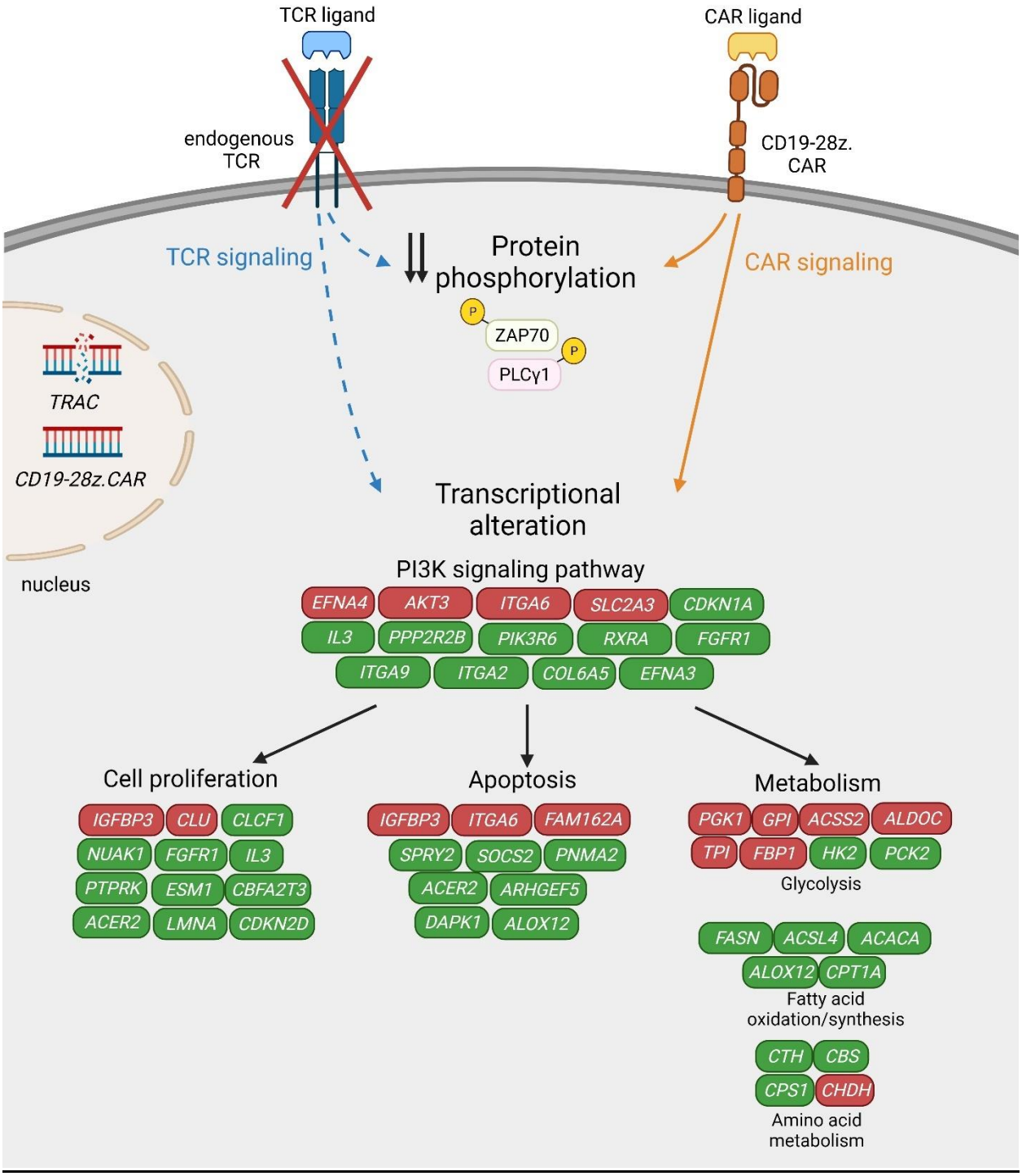

Figure S18: Schematic summary of SB-CD19-28z.CAR/TCR KO T cell molecular profile upon dual CAR and endogenous TCR co-signaling. Despite the presence of TCR and CAR ligands, SB-CD19-28z.CAR/TCR KO T cells fails to activate endogenous TCR due to CRISPR/Cas9-mediated *TRAC* gene disruption (blue dotted arrow), and only CAR signal is transduced to activate the downstream pathways (orange solid arrow). This results in i) reduced tyrosine kinase ZAP70 (ZAP70) and phospholipase C-γ1 (PLCγ1) signaling protein phosphorylation, and ii) transcriptional alteration of PI3K signaling pathway and its downstream cellular processes including cell proliferation, apoptosis and

metabolism compared to SB-CD19-28z.CAR/scrambled T cell. Gene upregulation and downregulation of SB-CD19-28z.CAR/TCR KO T cell versus SB-CD19-28z.CAR/scrambled T cell were in red and green symbols, respectively.

Supplemental references

[1] Kochenderfer JN, Feldman SA, Zhao Y, Xu H, Black MA, Morgan RA, et al. Construction and preclinical evaluation of an anti-CD19 chimeric antigen receptor. J Immunother. 2009;32:689-702.
[2] Mates L, Chuah MK, Belay E, Jerchow B, Manoj N, Acosta-Sanchez A, et al. Molecular evolution of a novel hyperactive Sleeping Beauty transposase enables robust stable gene transfer in vertebrates. Nat Genet. 2009;41:753-61.
[3] Sander JD, Zaback P, Joung JK, Voytas DF, Dobbs D. Zinc Finger Targeter (ZiFiT): an engineered zinc finger/target site design tool. Nucleic Acids Res. 2007;35:W599-605.
[4] Andersch L, Radke J, Klaus A, Schwiebert S, Winkler A, Schumann E, et al. CD171- and GD2-specific CAR-T cells potently target retinoblastoma cells in preclinical in vitro testing. BMC Cancer. 2019;19:895.
[5] Schneider CA, Rasband WS, Eliceiri KW. NIH Image to ImageJ: 25 years of image analysis. Nat Methods. 2012;9:671-5.
[6] Gabriel R, Eckenberg R, Paruzynski A, Bartholomae CC, Nowrouzi A, Arens A, et al. Comprehensive genomic access to vector integration in clinical gene therapy. Nat Med. 2009;15:1431-6.
[7] Paruzynski A, Arens A, Gabriel R, Bartholomae CC, Scholz S, Wang W, et al. Genome-wide high-throughput integrome analyses by nrLAM-PCR and next-generation sequencing. Nat Protoc. 2010;5:1379-95.
[8] Schmidt M, Hoffmann G, Wissler M, Lemke N, Mussig A, Glimm H, et al. Detection and direct genomic sequencing of multiple rare unknown flanking DNA in highly complex samples. Hum Gene Ther. 2001;12:743-9.
[9] Afzal S, Wilkening S, von Kalle C, Schmidt M, Fronza R. GENE-IS: Time-Efficient and Accurate Analysis of Viral Integration Events in Large-Scale Gene Therapy Data. Mol Ther Nucleic Acids. 2017;6:133-9.
[10] Ewing B, Green P. Base-calling of automated sequencer traces using phred. II. Error probabilities. Genome Res. 1998;8:186-94.
[11] Ewing B, Hillier L, Wendl MC, Green P. Base-calling of automated sequencer traces using phred. I. Accuracy assessment. Genome Res. 1998;8:175-85.
[12] Altschul SF, Gish W, Miller W, Myers EW, Lipman DJ. Basic local alignment search tool. J Mol Biol. 1990;215:403-10.
[13] Schroder AR, Shinn P, Chen H, Berry C, Ecker JR, Bushman F. HIV-1 integration in the human genome favors active genes and local hotspots. Cell. 2002;110:521-9.
[14] Wu X, Li Y, Crise B, Burgess SM. Transcription start regions in the human genome are favored targets for MLV integration. Science. 2003;300:1749-51.
[15] Mitchell RS, Beitzel BF, Schroder AR, Shinn P, Chen H, Berry CC, et al. Retroviral DNA integration: ASLV, HIV, and MLV show distinct target site preferences. PLoS Biol. 2004;2:E234.
[16] Wu X, Burgess SM. Integration target site selection for retroviruses and transposable elements. Cell Mol Life Sci. 2004;61:2588-96.
[17] Lewinski MK, Yamashita M, Emerman M, Ciuffi A, Marshall H, Crawford G, et al. Retroviral DNA integration: viral and cellular determinants of target-site selection. PLoS Pathog. 2006;2:e60.
[18] Demeulemeester J, De Rijck J, Gijsbers R, Debyser Z. Retroviral integration: Site matters: Mechanisms and consequences of retroviral integration site selection. Bioessays. 2015;37:1202-14.
[19] Rényi A. On measures of entropy and information. Proceedings of the fourth Berkeley Symposium on Mathematics, Statistics and Probability. 1961.
[20] Afzal S, Gil-Farina I, Gabriel R, Ahmad S, von Kalle C, Schmidt M, et al. Systematic comparative study of computational methods for T-cell receptor sequencing data analysis. Brief Bioinform. 2019;20:222-34.
[21] Alsulami AF, Torres PHM, Moghul I, Arif SM, Chaplin AK, Vedithi SC, et al. COSMIC Cancer Gene Census 3D database: understanding the impacts of mutations on cancer targets. Brief Bioinform. 2021;22.

[22] Recchia A, Bonini C, Magnani Z, Urbinati F, Sartori D, Muraro S, et al. Retroviral vector integration deregulates gene expression but has no consequence on the biology and function of transplanted T cells. Proc Natl Acad Sci U S A. 2006;103:1457-62.
[23] Hargrove PW, Kepes S, Hanawa H, Obenauer JC, Pei D, Cheng C, et al. Globin lentiviral vector insertions can perturb the expression of endogenous genes in beta-thalassemic hematopoietic cells. Mol Ther. 2008;16:525-33.
[24] Kulkarni A, Bangham CRM. HTLV-1: Regulating the Balance Between Proviral Latency and Reactivation. Front Microbiol. 2018;9:449.
[25] Spandidos A, Wang X, Wang H, Seed B. PrimerBank: a resource of human and mouse PCR primer pairs for gene expression detection and quantification. Nucleic Acids Res. 2010;38:D792-9.
[26] Naserian S, Leclerc M, Thiolat A, Pilon C, Le Bret C, Belkacemi Y, et al. Simple, Reproducible, and Efficient Clinical Grading System for Murine Models of Acute Graft-versus-Host Disease. Front Immunol. 2018;9:10.
[27] Lai HY, Chou TY, Tzeng CH, Lee OK. Cytokine profiles in various graft-versus-host disease target organs following hematopoietic stem cell transplantation. Cell Transplant. 2012;21:2033-45.
[28] Westphal S, McGeary A, Rudloff S, Wilke A, Penack O. The Green Tea Catechin Epigallocatechin Gallate Ameliorates Graft-versus-Host Disease. PLoS One. 2017;12:e0169630.